

**Final Report
submitted to the**

**Canadian Nuclear Safety
Commission (CNSC)**

for

**R613.4 Laboratory determination of
sealing material performance**

Contract no.: 87055-14-0228

by

**R.K. Rowe, O.C., FRS, Ph.D., P.Eng
and**

R.W.I. Brachman, Ph.D., P.Eng

**Queen's University
GeoEngineering Centre
Department of Civil Engineering
Kingston, ON K7L 3N6
Canada**

March 1, 2019

Summary

Bentonite is often an important component of the barrier system proposed to isolate radioactive wastes from the biosphere for very long periods of time. There is an extensive data set on the engineering properties of bentonite and bentonite/sand mixtures for pore fluids with deionized water and some data with modest salt content in the pore fluid. However, the pore fluid in one possible geologic setting, for example, the Cobourg formation of the Michigan Basin, may have very high soluble salts (160-360 g/L). The purpose of this Project was to conduct laboratory experiments to measure the hydro-mechanical properties of a natural sodium bentonite and a bentonite/sand mixture at several representative initial densities when exposed to a highly saline pore fluid.

Swelling, permeability, gap sealing, suction, and compression experiments were conducted (at 22°C) on small specimens of compacted bentonite and bentonite/sand mixtures when hydrated with one particular pore fluid, called Model Water. The Model Water was designed to reproduce the multiple constituents and concentrations of the Cobourg limestone pore fluid. The decrease in swell pressure and increase in permeability on Model Water hydration (relative to hydration with deionized water and under-zero-volume increase conditions) are reported with an emphasis on the time required to capture the interactions between the bentonite and Model Water. The ability of the bentonite to swell to close small, intentional gaps when hydrated with Model Water is examined. Suction measurements are reported to gain insight into hydration with Model Water. The compressibility after Model Water hydration is reported. Changes in the exchange complex and capacity of the bentonite after 1 year of Model Water hydration and macro-pore scale images are reported to provide additional insight into the measured engineering properties.

1. Introduction

Queen's University was contracted by the Canadian Nuclear Safety Commission (CNSC) to conduct laboratory experiments to measure the hydro-mechanical properties of a natural sodium bentonite and a bentonite/sand mixture at several representative initial densities when exposed to a highly saline pore fluid as per Contract no. 87055-14-0228, dated January 29, 2015 and the Contract Amendments dated December 22, 2015 and March 1, 2018 – referred to herein as the Project. This is the Final Report documenting methods and reporting results, and corresponds to Deliverable 6.10 from the March 2018 Contract Amendment.

2. Bentonites tested

MX-80 bentonite, a natural sodium bentonite, was obtained from the American Colloid Company. Variability in Swell Index (ASTM D5890) from 14 to 25 mL/2g was detected from the as-supplied material. Swell Index provides a measure of the potency of the clay fraction in terms of volumetric swell in deionized (DI) water per initial 2 g of dry bentonite. This variability is consistent with the range of 12 to 26 mL/2g reported for Free Swell Index by IAEA (2013, p. 83, Table 5.5) from a synthesis of data for “USA, MX-80” materials. The large variation in swell index is consistent with bentonite being a processed and blended product. As noted by Karnland et al. (2006, p. 11), MX-80 produced by the American Colloid Company “is a blend of several natural sodium dominated bentonite horizons, that are mined, dried and milled to millimeter-sized grains”. Consequently, without a strict specification, variations in swell index are to be expected and these can result in different performance that could impact the interpretations of results, particularly when comparing the results from this Project with other published values. To reduce the potential for variability of test specimens in this Project, a 3 kg sample of MX-80 was taken from the as-supplied material and then was well mixed. Based on 15 random specimens from that well-mixed sample, the Swell Index only varied between 19 and 22 mL/2g. It had a mean of 20 mL/2g (Table 1) and a standard deviation of 1 mL/2g. The well-mixed sample, and a similar second 3 kg well-mixed sample, collectively denoted as MX-80-QU-B2 (abbreviated herein as MX-80), were used for all swell pressure, permeability, radial gap swell, suction and compressibility tests.

A second bentonite, denoted as GCL-NWL-QU (abbreviated herein as NWL), was also used for swell pressure, radial gap swell, and suction tests. It was used as an internal standard of known high-quality, montmorillonite-rich, natural Wyoming sodium bentonite. It was obtained from a geosynthetic clay liner (GCL) sample of product NWL provided by Terrafix Geosynthetics (Toronto). It is noted that most GCL specifications require a minimum Swell Index of 24 mL/2g. GCL-NWL-QU had a Swell Index of 26 mL/2g (Table 1).

The mineralogical composition of the MX-80 and NWL materials tested are reported in Table 1. These were obtained from analysis of X-ray diffraction traces as documented in Appendix 1. Based on the available data and analysis conducted (Appendix 1), smectite contents of 83 and 96% were found for MX-80 and NWL, respectively. The MX-80 for this Project (MX-80-QU-B2) had a similar smectite content (83%) as the mean (83.5%) and range (81.1-85.8%) reported by Karnland et al. (2006) for a 2001 sample of Wyoming MX-80 material (denoted as MX-80-WyR1), Table 1.

Soluble cations, bound cations, and the cation exchange capacity of the two bentonites were established following ASTM D7503 (additional details are given in Appendix 1). The resulting cation exchange complex and capacity are reported in Table 2. Comparison of the well-mixed MX-80-QU-B2 with the internal standard GCL-NWL-QU shows that, on average, MX-80 has less exchangeable sodium (62 vs 69%) and more exchangeable calcium (32 vs 24%). These

values are more variable for MX-80 (the coefficient of variation for MX-80 is roughly twice as large as that for NWL), such that the differences in exchangeable sodium and calcium are not statistically significant at a 95% confidence level. The cation exchange capacity of MX-80 is less than that for NWL (64 vs 78 cmol/kg). This difference is statistically significant at 95% confidence level. The higher cation exchange capacity corresponds to the amount and potency of the smectite in GCL-NWL-QU and explains why it has a larger Swell Index than MX-80-QU-B2 (26 vs. 20 mL/2g, respectively; Table 1). Although similar in mineralogy, greater index swell would be expected for MX-80-WyR1 relative MX-80-QU-B2 given its higher cation exchange capacity, higher sodium and lower calcium content (Table 2).

The MX-80-QU-B2 bentonite being tested for the Project has a mineralogy that falls within the published range reported in the literature. It has a lower exchangeable sodium percentage than reported for other MX80 tests although the exchangeable sodium percentage is similar to that in GCL-NWL-QU. The MX-80-QU-B2 bentonite is considered representative of MX-80 that could be delivered to site with the simple specification of “MX-80” and no more specific requirements.

MX-80 / sand mixtures were also tested and were comprised of 70% bentonite and 30% sand, by mass. Silica sand with a mean grain of 0.6 mm (maximum = 1.2 mm, minimum = 0.3 mm) was used.

3. Model water

Constituents and concentrations of the Cobourg limestone of the Michigan Basin, at depths of approximately 700 m, are given in Table 3 based on data reported for boreholes DGR-1 to DGR-6 by NWMO (2011). Thermodynamic modelling with programs PHREEQC (1999) and AQION (2015) were conducted to help design a single, stable solution for testing. The composition of the Model Water (MW) is given in Table 3. The element concentrations of the Model Water match the mean measured concentrations (within 1% of the mean) from DGR-1 to DGR-6 (NWMO 2011) for Cl, Na, K, and Br. Proposed Ca and Mg concentrations are limited to 19% and 27% of the mean measured values, respectively, for model solution stability, but are only less than the mean by 0.5 to 0.6 times the standard deviation (i.e. they are well within the range defined by the Mean – Std dev. in Table 3). Sulphate (SO₄) concentration is limited by solution stability to 0.6 g/L, which is less than the minimum measured value of 4 g/L, Table 3. The discrepancy with sulphate likely arises from greater ion availability due to method of sample preparation (i.e., from ground rock specimens) to obtain the measured values. Observations over two years suggest that the Model Water solution is stable.

Recognizing that only one pore fluid could be examined for the experiments of this Project, Swell Index tests (ASTM D5890) were conducted with the MX-80 bentonite and eight pore fluids to provide some insight into the effects of the pore fluid composition on bentonite swell (Table 4). For reference, swell index for the as-received MX-80 bentonite with deionized water was 21 mL of volumetric swell per 2 g of initial dry bentonite. Identical results were obtained from triplicate experiments. Swell index for the other seven solutions were all much less than with deionized water. Increasing the pore water concentration would be expected to decrease double-layer thickness and hence decrease free swell. The adopted Model Water (Solution 2 in Table 4) had a swell index of 5 mL/2g based on two replicates. For reference, the swell index of natural calcium rich bentonite in deionized water is 7-8 mL/2g. Decreasing pore water concentrations to an intermediate values and the minimum measured values from DGR-1 to DGR-6 (other than SO₄, which was taken as 0.6 g/L for solution stability) only gave swell index values of 6 and 7 mL/2g, respectively (solution 3 and 4 in Table 4). Swell index values of 5-8 mL/2g with single salt

solutions 5-8 (Table 4) suggests that it is the high concentration levels in the solutions that likely reduce the bentonite swell rather than the particular presence of polyvalent cations. Although the swell index results from single salt solutions 5-8 also seems to suggest that a simpler pore water could be a reasonable model to capture the effects of Cobourg formation water on bentonite, the proposed Model Water was used for all subsequent testing, especially to adequately capture potential long-term interlayer clay mineral interactions with constituents (e.g., monovalent potassium with small hydrated radius) from the pore fluid.

4. Swell pressure

Swell pressure measurements were conducted under conditions of zero volume increase for compacted bentonite and bentonite/sand mixtures when hydrated with DI water and Model Water. At the outset of the project in 2015, it was expected that Model Water hydration would lead to lower swell pressures relative to literature values with lower pore fluid concentrations. The purpose of these experiments was to quantify the effects of Model Water hydration on swell pressure of one particular compacted bentonite. The initial focus of the Project, as stipulated by CNSC, was on an MX-80 bentonite at dry densities of 1.61 and 1.41 Mg/m³, and MX-80 bentonite/sand mixtures at dry densities of 1.65 and 1.8 Mg/m³. Swell pressure measurements with DI water hydration were added to provide a comparison with Model Water and to link the particular batch of MX-80 bentonite tested in this project to previous published studies. The Project was subsequently extended to investigate Model Water effects at higher densities and with a second bentonite.

4.1 Method

Soil specimens were first prepared to the target dry density at an initial bentonite gravimetric water content of 11%. Deionized water was used to increase the water content in the bentonite from the as supplied value of approximately 9%. The base, lower porous stone and body of the swell pressure apparatus (Fig. 1) were used to contain the sample during static compaction to provide zero lateral strain conditions. The specimen was compressed using stroke control to a thickness to obtain the target dry density after removal of the compaction pressure. The final thickness was obtained after removal of the compaction pressure with a laser scanner. This final thickness was used to calculate the initial dry density of the specimen. Additional sample preparation details are given in Appendix 2.

Within 15 to 20 minutes following compaction, the top cap, load cell and lid of the swell pressure apparatus were placed and secured to the base with eight, 12.7 mm diameter steel bolts. The initial vertical pressure on the specimen applied by tightening the bolts was recorded as the seating pressure. All swell pressure measurements reported herein include the initial seating pressure, in a manner consistent with swell pressure tests conducted with conventional soil one-dimensional compression equipment.

Once contained within the apparatus, the specimen was then allowed to hydrate with pore fluid introduced at the base of the specimen via a porous stone at a head of 1.5 m. This head was selected following trials conducted with both 0.3 and 1.5 m head, where a larger swell pressure was found with the higher head. Air from the bottom part of the cell and porous stone was initially removed by purging with the pore fluid for that particular experiment. Purging the base was repeated once a month with pore fluid. Another porous stone was placed on top of the soil specimen which was vented to atmospheric pressure. The direction of hydration was from the

bottom of the sample to the top. A load cell was used to measure the force generated during hydration under conditions of zero volume increase with a precision of ± 20 kPa.

Three trial experiments were conducted on MX-80 specimens compacted to an initial dry density of 1.56 Mg/m^3 with deionized water to examine the effectiveness of the new apparatus developed to measure swell pressure. One of these experiments was conducted in a constant volume swell pressure cell with load cell measurements (Fig. 1) and a swell pressure of 2070 kPa was obtained. The other two were conducted in one-dimensional compression cells where the applied pressure on the sample was continually adjusted to maintain the height of the sample essentially constant within ± 0.0025 mm and swell pressures of 2030 and 2350 kPa were obtained. The difference between these two replicates is attributed to experimental variability from subtle differences in soil density for the same nominal density. The overall good agreement between the swell pressures from one-dimensional compression cells and the swell pressure cell provides confidence that the swell pressure cells are performing as designed.

Reproducibility of results from the swell pressure cells with Model Water hydration was examined for MX-80 bentonite at a nominal dry density of 1.6 Mg/m^3 (denoted herein as the reference case). Swell pressure values of 610, 650 and 720 kPa were recorded from three replicate tests after 800-900 h of Model Water hydration. The resulting coefficient of variation of 8% and a maximum difference of less than 20% indicate good reproducibility, where the variability is predominately attributable to differences in actual dry densities of 1.59, 1.60, and 1.61 Mg/m^3 for the three replicates.

4.2 Results

The relative effects of pore water, type of bentonite and dry density on long-term measured swell pressure are shown in Fig. 2. Test details are summarized in Table 5. Detailed results for each test are given in Appendix 3. At a reference density of 1.6 Mg/m^3 , and with DI water hydration, swell pressures of 2300 and 4700 kPa were obtained for the MX-80 and NWL bentonites tested (Fig. 2; Tests 1.1 and NWL1 in Table 5). The lower swell pressure for MX-80 is consistent with having a lower cation exchange capacity relative to the NWL bentonite. When hydrated with Model Water for the same reference density, the long-term swell pressures decreased significantly to just 350 kPa for MX-80 and 1000 kPa for NWL bentonite from interactions between the high concentration Model Water and smectite minerals (Tests 2.3 and NWL2 in Table 5). Swell pressures with Model Water hydration increased as the dry density of the MX-80 samples increased. However, chemical interactions between the Model Water and smectite minerals appear to dominate over density as a swell pressure of just 1250 kPa was measured for MX-80 after 1.4 years of Model Water hydration when initially compacted to the highest dry density examined (1.8 Mg/m^3 ; Test 2.3(j) in Table 5).

The evolution of swell pressure with time is shown in Fig. 3. With DI water, after reaching a peak swell pressure of 2800 kPa with MX-80 at 1.6 Mg/m^3 , there was a progressive decrease in swell pressure with time, reaching a value of 2300 kPa after nearly 3 years of testing. Between 6000 and 25700 h, the average rate of swell pressure decrease was 120 kPa per year. This small, but continual, decrease is not from cation exchange amongst internal constituents of the processed and blended bentonite as the exchangeable sodium and calcium percentages of 70 and 25% measured upon termination of this sample were found to lie within the range of values obtained prior to testing (Table 2). Creep deflections of the steel apparatus leading to a release of vertical pressure are unlikely, as the apparatus was designed to have vertical deflections less than 0.01 mm under 5000 kPa pressure. Creep effects of the load cells are estimated to be the order of ± 20 kPa, based on specifications provided by the manufacturer. The long term reliability of the load cells

was confirmed after termination of this experiment, as there was no discernible difference from the initial calibration. The continual decrease in swell pressure with time is likely due to time dependent compression of the hydrated bentonite (i.e., creep) under the sustained swell pressure.

The peak pressure of 2800 kPa with DI water hydration for the particular MX-80 being tested for this project (MX-80-QU-B2) is consistent with the range of 2000 to 3000 kPa reported by Agus and Schanz (2008) and Herbert et al. (2008) for MX-80 under comparable conditions; but, lower by a factor of 1.3 to 3.6 than values for MX-80 published by Karnland et al. (2006), Liu (2013), Ferrari et al. (2014) and Dixon et al. (2016). The differences between the measured swelling pressure values of MX-80 may be attributed to several factors such as differences in smectite content, cation exchange capacity and exchangeable cation complex of the bentonite, as well as differences from measurement equipment and procedures.

As expected, Model Water hydration resulted in lower swell pressures than with DI water, but it also produced a much different initial response with time. With Model Water hydration, there was an initial rapid increase in swell pressure (more evident with time plotted on a logarithmic scale; Fig. 3b), reaching a peak swell pressure 15 to 30 h after the start of hydration, which was then followed by a continual decrease in pressure with time as the pore fluid interacts with the smectite minerals. A steady pressure trend with time was achieved after around 6000 h in most cases. The experiments conducted for up to 12,000 h showed rates of pressure decrease with time of around 100 kPa per year (Fig. 3, Table 5), similar to that from the long term test with DI water, suggesting most of the chemical interactions with between the pore fluid and smectite minerals have occurred.

Peak swell pressures with Model Water hydration for MX-80 bentonite at a dry density of 1.53 to 1.61 Mg/m³ and initial water content of 11% are summarized in Table 6 for nominally the same test configuration. There appears to be no effect of seating pressure on peak measured pressure. The average peak swell pressure from the five experiments with densities between 1.53 to 1.56 Mg/m³ in Table 6 is 920 kPa (std. dev. = 90 kPa). An additional test conducted with the bentonite at its as-supplied water content of 8.7% (Test 2.3(b), MX-80, $\rho_d=1.52$ Mg/m³, MW), but otherwise the same configuration as for Table 6, showed no significant difference in peak swell pressure (930 kPa). This indicates that the small amount of DI moisture added during the sample compaction stage to bring the initial water content to 11% was not responsible for the early peak swell pressure. Similarly, it was demonstrated by another test that the peak initial swell pressure was not related to restraint against post-compaction specimen rebound. Specifically, in this test a 260-h-long pause was allowed between the time the specimen was restrained in the apparatus and the start of hydration with Model Water, but with otherwise the same conditions as for Table 6. The measured pressure after compaction but prior to hydration was less than 40 kPa, which then quickly increased after introduction of the Model Water. These two additional tests support the attribution of the observed initial peak swell pressure to interactions with the Model Water. Early hydration is dominated by Model Water movement through the interconnected macropores formed by the void space in between the compacted bentonite aggregates. Early hydration is expected to be concentrated on the outer surface of these aggregates. Some rapid hydration with water from the Model Water likely occurs, prior to the chemical interactions that follow shortly thereafter at these same locations around the aggregate perimeters.

While the peak swell pressure was not recorded in Test 2.3 (Table 5), an average peak swell pressure of 1500 kPa was obtained from two replicate tests (Table 6, Tests 2.3(R1) and 2.3(R2)). With MX-80, increasing the dry density from the reference of 1.6 Mg/m³ to an intermediate value of 1.68 Mg/m³ (Test 2.3(i)) increased the initial peak swell pressure with Model Water by a factor

of 1.5; whereas increasing to the highest tested density of 1.82 Mg/m^3 (Test 2.3(j)) increased peak swell by a factor of 1.9 (Table 5). However, both the intermediate and higher density specimens still experienced a rapid decrease in swell pressure within 30 h, followed by continual decreases over the monitoring period from interactions with the Model Water (Fig. 3). The rate of swell pressure decrease appears to be faster at the higher density, most likely because it attained a larger peak swell pressure from initial interactions with the Model Water.

Although the NWL bentonite was of higher quality than the MX-80 tested, as evidence by the much higher swell pressure with DI water, Model Water hydration also had big effect on the swell pressure of the NWL bentonite. The swell pressure of NWL bentonite reduced from around 5000 kPa with DI water to 1000 kPa after Model Water hydration, at a dry density of 1.62 Mg/m^3 (Fig. 3; Tests NWL1 and NWL2 in Table 5). At an intermediate dry density of 1.68 Mg/m^3 (replicate Tests 7.1 and 7.2 with NWL bentonite), the peak swell pressure with Model Water was 1.6 times larger than at 1.62 Mg/m^3 , but had only slightly larger long-term swell pressure of 1070 kPa (Fig. 3; Tests NWL2 and 7.2 in Table 5). Here, pore water effects dominate even more so over density effects in terms of long-term swell pressure. While the peak swell pressure with Model Water at the highest density tested of 1.82 Mg/m^3 reached nearly 3600 kPa, there is insufficient data at the time of writing to establish the long-term swell pressures for the high density configuration (Fig. 3; Test 7.3 in Table 5), although the trend with time in Fig. 3b tends to suggest that it may approach a similar value as in the intermediate density case.

No anomalies were evident from visual inspection of the samples upon termination all tests. Load cells calibration was checked after termination of all long-term tests. No change from the initial calibration was found, indicating reliable long-term measurement of swell pressure.

One case with a higher initial water content (Test 2.3k; gravimetric water content = 20%, initial degree of saturation $\approx 90\%$) was conducted to investigate the extent to which prehydration with DI water would alleviate the chemical interactions of MX-80 with the Model Water. This sample was first allowed 4 days of conditioning time with the added DI moisture prior to compaction to allow for bentonite hydration. After being compacted to an intermediate dry density of 1.67 Mg/m^3 , a period of 495 h was allowed to further allow for bentonite hydration. The swell pressure remained below 200 kPa for this period (Fig. 4). Model water was introduced after 495 hours, immediately resulting in a peak swell pressure of 2160 kPa. The peak pressure, and subsequent decrease in swell pressure with time was similar to that obtained at the water content of 11% (initial degree of saturation $\approx 50\%$) used for most of the other swell pressure tests (Fig. 3). Thus, bentonite prehydration intended to attain a crystalline layer of water in closest proximity to the clay mineral surface did not alleviate the Model Water interaction effects.

Swell pressure for other configurations with MX-80 bentonite at dry densities less than 1.6 Mg/m^3 are reported in Table 7. All of these samples started at a water content of 11%. Similar trends with Model Water hydration causing a reduction in swell pressure as were observed at dry densities of 1.55 to 1.56 Mg/m^3 (Table 6) were observed at the lower density of 1.42 to 1.44 Mg/m^3 (Table 7). There was little difference between DI water and Model Water hydration at a dry density of 1.42 to 1.45 Mg/m^3 and these measured values were less than 400 kPa.

MX-80/SP sand-bentonite mixture configuration swell pressures are also summarized in Table 7. Test 6.1 was monitored for 17,100 h (1.95 y) and the swell pressure has remained stable at a value of 340 kPa up to 10,000 h (Appendix 3).

Fig. 5 is a summary plot of: (a) peak swell pressures and (b) last measured swell pressures measured with DI water and Model Water for the particular MX-80 and NWL bentonites and MX-80/SP mixture tested.

The bentonite results from this Project are compared with data reported by Dixon et al. (2016) for another MX-80 bentonite in Fig. 6. Rather than just dry density, swell pressures in Fig. 6 are plotted against the effective smectite dry density in an attempt to account for the amount of swelling clay mineral in the bentonite. Dixon et al. (2016) used a montmorillonite percentage of 80% for their calculations, based on a range of values between 79 and 95% they reported, whereas swelling clay percentages of 83 and 96% were used for the particular MX-80 and NWL bentonites (Table 1). As previously mentioned, with DI water hydration, swell pressures for the MX-80 bentonite testing in this Project are 1.3 to 2.9 times smaller than the values reported by Dixon et al. (2016). Differences in the mineralogy, exchange complex and exchange capacity of the MX-80 bentonites likely account for most of the difference (the exchange complex was not reported by Dixon et al. (2016)). This highlights that MX-80 is not necessarily a consistent material and careful reporting of mineralogy and exchange capacity and complex is important when comparing results.

The swell pressure data with Model Water hydration from this Project tends to lie within in the lower range of swell pressures reported by Dixon et al. (2016) for the SR-Sh 335 g/L solution (Fig. 6). Two puzzling observations based on the data set for the 335-350 g/L solution are: i) other than one data point around 1.6 Mg/m³, the swell pressures are larger than the data set for the 335 g/L solution, and ii) the overlap with the DI hydration data set at 1.42 Mg/m³ is unexpected based on the results from this project. The publication forum for the paper by Dixon et al. (2016) likely limited the ability to provide specific details on the equipment and procedures used, as well as the composition of the hydration fluids that are needed to fully compare the results.

5. Permeability

The hydraulic conductivity of MX-80 bentonite and bentonite / sand mixtures (70/30%, by mass) when permeated with Model Water were measured from permeation experiments. Reference tests were also conducted for hydration with DI water. The configurations tested are summarized in Table 8. As hydraulic conductivity is a function of the porous medium, permeant, and temperature, reference to hydraulic conductivity herein either refers to permeation of the soil specimen with DI water or Model Water at 22°C.

5.1 Method

The apparatus used for the permeation experiments is shown in Fig. 7. The soil specimen was 38 mm diameter and 10 mm high. Following the same procedure as the swell pressure tests, the moisture content was increased from the as supplied water content to 11% using deionized water and then the specimens were compacted under zero lateral displacement conditions (detailed procedure given in Appendix 2). Once the lid of the apparatus was connected to the base, the specimen was then hydrated and permeated with DI water or Model Water under zero volume increase conditions (i.e., the effective stresses in the soil specimen will result from soil swelling under constant volume conditions). With porous stones on the top and bottom of the soil specimen, the bottom boundary was connected to a constant fluid pressure of 15 kPa and the top boundary has zero fluid pressure (i.e., zero back pressure). The direction of hydration and flow was from the bottom of the sample to the top. The bottom porous stones and ports were flushed with permeant prior to the start of hydration / permeation.

For Tests 1-4 and 7-9, a pressure control panel (ELE Tri Flex 2) was being used to apply the constant fluid pressure (i.e., the hydraulic driving force) and to measure the volume of fluid that passed into the specimen from the start of hydration. Tests 5 and 6 were first allowed to hydrate with Model Water for just over one year where the fluid pressure was applied using a

column of water, and then were connected to the pressure control panel to more precisely measure inflow volumes. In all permeation tests, outflow volume was first collected and measured by mass to evaluate when steady state flow conditions were attained. Steady state conditions were then verified, and final values of hydraulic conductivity were attained for Tests 3-6 by directly measuring the outflow volume with the control panel. Reported values of hydraulic conductivity were obtained using the falling head, rising tail water method (ASTM D5084, Method C). These values were verified by computing hydraulic conductivity based on measured inflow and outflow volumes.

For Tests 3 and 4 with Model Water, the electrical conductivity of the effluent concentration was monitored (using YSI Model 30 conductivity probe) to provide an indication of when chemical steady state conditions were reached relative to the influent. Electrical conductivity measurements provide an index of the total ion concentration in the effluent. More detailed chemical analysis was conducted for Tests 4-6 with Model Water (using Inductively Coupled Plasma Mass Spectrometry, ICP-MS) to confirm the results provided by the conductivity probe and provide additional evidence of chemical steady state between the influent and effluent. The ICP-MS results provided concentrations of major cations (Na, Ca, Mg, and K). Given the high concentrations in the Model Water, the collected effluent was diluted with DI water by volume ratios of 1:200 and 1:10 to permit measurement with the conductivity probe and ICP-MS, respectively.

5.2 Results

Fig. 8 shows the cumulative volume of DI water flowing into the MX-80 and MX-80/SP specimens. Early values provide a measure of the amount of DI water that goes to specimen hydration. No fluid has appeared to-date on the outlet side in these tests despite permeation for 1.5 years, and hence steady state flow conditions may not have been reached. Inflow rates are very small for both configurations such that the possibility evaporation may be impacting the lack of outflow can not be excluded despite it being in a rigid steel and essentially closed system (Figure 7). Based on inflow alone, both configurations are tending to hydraulic conductivities with respect to DI water around 8×10^{-13} m/s for MX-80 (Test 1) and 1×10^{-12} m/s for MX-80/SP (Test 2), Table 8.

Tests 3-6 with Model Water reached steady state flow conditions as shown by very small (< 4%) differences between incremental inflow and outflow volumes (Table 8). The termination criteria from ASTM D 5084 (Method C) were met in all Model Water cases as more than four values of hydraulic conductivity were obtained over an interval of time in which the ratio of inflow to outflow rate was between 0.75 and 1.25, and the hydraulic conductivity was steady. Entire flow records for these tests are given in Appendix 4. Chemical steady-state conditions, in terms of measurable influent and effluent concentrations, were also attained. Effluent concentrations of Na, Ca, Mg, and K, were within the range of uncertainty around the mean influent concentrations (at the 95% confidence level), based on five influent measurements (Appendix 4). These chemical steady state conditions apply to the macropores between bentonite aggregate where flow is predominantly occurring. The possibility that there are ongoing mineral level interactions with the Model Water can not be excluded but, if they are, they were undetectable by monitoring the effluent concentrations given the very high concentrations in the Model Water and small mass of bentonite tested.

Inflow hydraulic conductivities with respect to Model Water are plotted in Figs 9 and 10 for the MX-80 and MX-80/SP configurations tested. Tests 5a and 5b show that an additional 140-220 days of exposure to Model Water caused no significant increases in hydraulic conductivity

relative to Test 3a (Fig. 9). Based on these three tests, the hydraulic conductivity ranges between 2×10^{-11} and 5×10^{-11} m/s (Fig. 11a), with an average of 4×10^{-11} m/s. Based on the available data, the hydraulic conductivity to Model Water was at least 50 times larger than that for DI water for MX-80 at a dry density of 1.60 to 1.62 Mg/m³ (Fig. 11a). The Model Water appears to have a larger effect on the MX-80/SP mixture, as the hydraulic conductivity to Model Water is around 4000 times larger for DI water at a dry density of 1.63 to 1.67 Mg/m³ (Fig. 11b).

6. Chemical interaction with bentonite

Soluble and bound cations were measured (as per ASTM D7503) for bentonite specimens obtained upon termination of Swell Pressure Tests 2.3, 2.3(i), and 7.2 (Table 5), and Permeability Tests 5a and 5b (Table 8), representing between 9000 to 12,900 h of exposure to Model Water, to investigate exchangeable cation after Model Water hydration. Comparison of MX-80 natural with MW hydration values in Table 2 shows that upon MW hydration, there was a decrease in exchangeable sodium (from 62 to 25%, on average), mostly arising from an increase in exchangeable potassium (from 3 to 29%) from the Model Water and some increase in exchangeable magnesium (from 3 to 12%) also from the Model Water. These changes are statistically significant at a 95% confidence level. There was no statistically significant change in exchangeable calcium after Model Water hydration. Similar changes in exchange complex were found for the one long-term test with NWL bentonite examined.

The increased concentrations of Na, K, Ca and Mg from the Model Water (relative to the as-received bentonite with DI water hydration) and exchange of some natural monovalent sodium with divalent magnesium from the Model Water would be expected to decrease double-layer thickness as per Modified Guoy-Chapman theory (Mitchell and Soga 2005). Conceptually, inter-particle repulsions and the amount of bound water both decrease as double-layer thickness decreases which would be expected to contribute to the lower swell pressure and higher permeability measured with Model Water relative to DI water. Although both monovalent, displacement of natural sodium with smaller hydrated radius potassium may be hypothesized to also lead to internal ('c-axis') contraction from potassium fitting within the ditrigonal cavities (i.e., hexagonal 'holes') in the silicate sheets of the smectite minerals (e.g., see Rowe et al. 2004). However, in the current study, any such contraction does not appear to have had a major, if any, component due to irreversible potassium fixation, as any decrease in the cation exchange capacity of MX-80 (on average from 64 to 54 cmol/kg; Table 2) was modest and may largely also be explained by variability based on the measurements made. This assessment is supported by the observation that although the smectite peak in x-ray diffraction traces was altered after either Model Water hydration or potassium treatment (relative to an air-dried natural specimen) its position still returned to expected values from swelling after glycol treatment (see Appendix 1, Fig. A1-4). Thus the available data provides no clear evidence of a significant change in clay mineralogy upon Model Water hydration over the 1-year timeframe and room temperature conditions examined.

7. Radial gap sealing

These experiments were conducted to evaluate if compacted bentonite samples can swell to close an intentional radial gap around the perimeter of the sample (i.e., a technological void) while under vertical restraint with Model Water hydration for MX-80, NWL and MX-80/SP specimens.

7.1 Method

Soil specimens with diameter of 36.1 mm were contained within 38 mm diameter test cells. This created an initial annular void with thickness of 0.95 mm (5% of the specimen radius) between the outside perimeter of the specimen and the inside surface of the apparatus. The thickness (axial extent) of the cylindrical sample (Table 9) was not allowed to increase during hydration, but rather any swelling had to occur radially upon hydration.

The soil specimens were first prepared to the target dry density (Table 9) at an initial bentonite gravimetric water content of 11%, following the procedures detailed for the swell pressure tests. Again, deionized water was used to increase the water content in the bentonite from the as supplied value of approximately 9% to the desired 11%. A removable sleeve (outside diameter = 38 mm, inside diameter = 36.1 mm) was placed inside the apparatus prior to specimen compaction, and removed after specimen compaction to create the annular void.

Once the apparatus was secured, the specimen was allowed to hydrate with pore fluid introduced at the base of the specimen via a porous stone with a head of 1.5 m. Air from the bottom part of the cell and porous stone was initially removed by purging with the Model Water for 1 minute. Another porous stone was placed on top of the soil specimen which was vented to atmospheric pressure where outflow volume was measured. Hydration was from the bottom of the sample up, but unlike all the other swell pressure and permeation experiments, there could also be some radial hydration from Model Water in the radial gap. Additional sample preparation details are given in Appendix 2.

7.2 Results

For the cylinder made from MX-80/SP at $\rho_d=1.66 \text{ Mg/m}^3$ (Test 1), the radial gap did not entirely seal. This is shown by the very high initial flow rates measured in Test 1 (Fig. 12). For reference, flow rates from permeation Test 4a (i.e., the same soil configuration, but without the radial gap) are also plotted in Fig. 12. After 350 days, the apparatus in Test 1 was opened to visually inspect the top and bottom of the specimen. A gap of approximately 1 mm wide was visible around nearly the entire perimeter of the bottom of the specimen, and at several locations around the perimeter of the top of the specimen (Fig. 13). After visual inspection, this specimen was then permeated with Model Water (using the same equipment and method as the permeability tests) for 30 more days where the flow rate through the apparatus was found to be nearly twice as large than the same soil configuration but without the radial gap (permeation Test 6b). The final diameter of the specimen was 37.0 mm at the top, 36.5 mm at mid-height, and 36.2 mm at the bottom, based on three measurements of diameter at each height made with calipers.

There is evidence to suggest that the radial gap sealed initially in Tests 2-4 for intermediate and high density MX-80 and high density NWL configurations (Table 9). Upon introduction of Model Water at the bottom of the specimen, fluid started coming out of the top of the apparatus for the first 10-20 seconds. Flow then gradually decreased over the next minute until it essentially stopped (i.e., was not measurable with this apparatus). Outflow was next detected after 5 days in Test 4 (MX-80; $\rho_d=1.66 \text{ Mg/m}^3$), 480 days in Test 2 (MX-80/SP; $\rho_d=1.8 \text{ Mg/m}^3$), and after 20 days in Test 3 (NWL; $\rho_d=1.8 \text{ Mg/m}^3$). Overall, flow rates remained low as the samples hydrated (Fig. 14). At the time of writing, steady state flow conditions had not been attained for Tests 2-4 despite hydration for up to 600 days in Test 2. The radial gap specimens require additional time to attain steady state flow conditions as they are twice as thick as the swell pressure and permeability specimens. As such, values of bulk hydraulic conductivity to Model Water of the

radial gap specimens cannot yet be obtained. However, three additional permeation tests (without a radial gap, as per Section 5) were conducted for the same soil and density configurations as radial gap Tests 2-4 to allow comparison of flow rates. They are denoted as permeability Tests 7-9 in Table 8 and results to-date are given in Fig. 15. The flow rate through intermediate density MX-80 sample that had a radial gap (radial gap Test 4) is presently 60% of that in the permeation test without a radial gap (Test 9a; Table 9). It appears that volumetric swell even with Model Water is sufficient to initially close the radial gap and maintain it closed for the test duration. The fact that flow is lower with the radial gap sample may be due to (i) sample variability, as evidenced by the difference in hydraulic conductivity to Model Water obtained for replicate permeation in Tests 3a, 5a, and 5b (Table 8), and/or (ii) the fact that neither tests had yet reached a steady state but the test with the radial gap has been running more than three as long as the permeability test. The flow rate from the high density MX-80 radial gap test is only 1.25 times larger than the comparable permeation test (Table 9). Flow through the high density NWL radial gap test is low, but it is around 5 times larger than through the comparable MX-80 radial gap test (Fig. 14, Table 9) and also 5 times larger than the comparable NWL permeation test; however, care is needed in interpreting these results since neither tests had yet reached a steady state but the test with the radial gap has been running twice as long as the permeability test. Sealing of the gap can be confirmed upon termination of the test.

8. Suction

8.1 Method

In these experiments, soil specimens were first prepared to their target water content by adding test pore fluid (either DI water or Model Water) to the as-supplied bentonite water content of approximately 9%. The specimen was sealed and allowed to recondition for 1 h after addition of pore fluid. The specimen was then statically compacted (at a rate of 0.05 mm/min) under conditions of zero radial strain to its target dry density. After compaction, the 36 mm diameter by 4 mm high specimen was placed in a sealed plastic container (38.5 mm diam.) and allowed to rest for 1 h under zero vertical and radial stress. A dew point potentiometer device, also known as a water activity meter (Gee et al. 1992; Brye 2003), was then used to measure the total suction. Model WP4C from Decagon Devices, which uses the chilled mirror hygrometer technique (ASTM-D6836) was used in its precise mode at a temperature of 22°C. After the suction measurement, the water content of the specimen was measured by oven drying at 105°C.

There may be some water remaining in the specimen after oven drying (i.e., in the form of bound water and some water associated with the salts that remain from the Model Water). To account for the effect of salt from the Model Water, two gravimetric water contents are reported. The first is the *measured water content* and is taken as the wet mass of the specimen immediately after the suction measurement minus the mass of the specimen after oven drying, which is then divided by the mass of the specimen after oven drying. Included in the oven dried mass is any remaining water and the mass of salt from the added Model Water. The second is a *calculated water content* which is obtained by calculating the total mass of water in the wet specimen divided by the calculated mass of soil solids (see Appendix 5 for the specific details and assumptions). Unless otherwise noted, the reported water contents correspond to measured values.

8.2 Results

Measurements of total suction for MX-80 after being compacted to an initial dry density of 1.61 Mg/m³ are plotted in Fig. 16 against the measured gravimetric water content of the individual

specimens prepared at different water contents to create a wetting-path along the water retention curve for free swell conditions. At the as-supplied water content of around 9%, a total suction of 86 MPa was measured. In this high suction and low water content range, water uptake is mainly controlled by the physiochemical properties of the smectite clay minerals (Gatabin et al., 2016) which is comprised of matric suction and possibly some osmotic suction from salts naturally present in the as-supplied bentonite. Increasing the water content with DI water decreased the measured total suctions. For comparison, Seiphoori et al. (2014) conducted free-swell and constant-volume water retention tests on MX-80 and reported no significant difference in measured suctions between those cases, nor between the level of compaction (for initial dry densities they tested from approx. 1.5 to 1.8 Mg/m³) for their constant-volume conditions. Although not for identical experimental conditions, the particular test procedures and MX-80 bentonite being used for this Project produced comparable results as the free-swell values obtained by Seiphoori et al. (2014) as shown in Fig. 16.

Measured values of total suction and measured values of gravimetric water content with Model Water for the three configurations required by the Contract are plotted in Fig. 17. There was no significant difference between the measured values for initial compaction levels of 1.50 and 1.65 Mg/m³ of the MX-80/SP mixtures. For measured gravimetric water contents less than 15%, the bentonite content impacted the measured suction, with greater water potential being measured for the pure MX-80 configuration relative to the 70% bentonite in the MX-80/SP mixture. Fig. 18 shows that the results for the three cases are essentially the same if all of the measured water after oven drying is assumed to be associated with the bentonite, and not the sand.

Comparison of results with deionized and Model Water for MX-80 specimens initially compacted to $\rho_d=1.61 \text{ Mg/m}^3$ in Fig. 19 shows the effect of Model Water on the measured suctions and water content. The highest suction for each data sets correspond to the case of no added moisture to the bentonite (data points highlighted in Fig. 19). The difference in the two suctions of 86 MPa and 97 MPa measured at the as-supplied water content of the bentonite ($8.6 \pm 1\%$) provides some indication of the reproducibility of the sample preparation and measurement technique. By increasing the water content of the bentonite specimen by adding Model Water, the salt concentration in the specimen increases and hence the osmotic component of suction increases, which explains the increasing difference between the suctions for the DI water and Model Water results with increasing water content. As the specimens prepared with Model Water approach saturation, the measured suctions tend towards a total suction of 45 MPa for the three Model Water cases in Fig. 19; this value is dominated by osmotic suction.

The measured suctions for MX-80 and Model Water from Fig. 19 are plotted again in Fig. 20, but this time the corresponding calculated water content (intended to account for the presence of salts in the oven dried specimens) is also shown. The adjustment from measured to calculated water content does not alter the suction measurement, only the water content associated with each suction measurement, and the difference between the calculated and measured water contents increases as the measured water content increased (i.e., as the amount of Model Water added to the as-supplied bentonite increased). Since measured suctions for the specimens prepared with Model Water approaches a limiting value of 45 MPa, uncertainty in the water content adjustment has little practical effect on the shape of the wetting path. Fig. 21 is a summary of results when plotted against the calculated water content.

Results from two additional experimental configurations are plotted in Fig. 22 to investigate whether the use of a different bentonite in preparing the deionized and Model Water specimens would affect the measured suctions. Despite the difference in mineralogy (Table 1),

no significant difference was found between the suction measurements for the MX-80 bentonite being tested for the Project and NWL bentonite, for both pore fluids tested. The comparison with DI water is similar to the observation by Tang and Cui (2010) that changes in MX-80 mineralogy had no clear impact on water retention behaviour. There is even less difference between the particular MX-80 bentonite being tested for the Project and NWL bentonite when prepared with Model Water most likely because osmotic suctions from the high salt concentration in the Model Water are dominating the measured value of total suction.

9. Compressibility

9.1 Method

Soil specimens were initially mixed with the test pore fluid (either deionized or Model Water) from the as-supplied bentonite water content and then prepared to its initial dry density at a target initial degree of saturation of 90%. Consequently, the bentonite is exposed to Model Water prior to compaction and application of stress. The specimens were compacted and then loaded within the one-dimensional compression tests cells developed for this project (Fig. 23). Porous stones that were saturated with the test pore fluid were placed on the top and bottom of the soil specimen to provide two-way hydration and drainage conditions. The first stage of the experiment was to allow the soil specimen to swell with the pore fluid under an applied vertical pressure of 100 kPa. Incremental load steps, where the magnitude of the load increment doubled for each successive increment, were applied up to maximum applied vertical pressure of 12 MPa. A period of 7 days (± 1 day) was adopted as the duration for the first stage and all subsequent load increments. The change in specimen height was recorded with a very precise dial gauge to ± 0.0025 mm.

9.2 Results

Measured values of incremental vertical displacement for each load increment are plotted versus time in Figs 24–29 for the one-dimensional compression tests. The vertical displacement reported for the first 100 kPa increment is relative to the height of the specimen following removal of the compaction stress. Downward vertical displacements (i.e., specimen compression) are reported as negative values.

Comparison of results for the first 100 kPa load increment for all completed tests shows that only the specimens with deionized water increased their volume (Figs 24 & 27), while those prepared with Model Water either did not swell or compressed slightly under the 100 kPa pressure (Figs 25, 26, 28 & 29). The vertical strain, ε_v , for the first load increment (where ε_v = the change in height of the specimen, ΔH , divided by the original height of the specimen, H_0) is summarized in Table 10. The lack of swelling for the specimens prepared with Model Water is consistent with the measurements of low swell pressures under constant volume conditions with Model Water.

Vertical displacement measurements for each completed test have been compiled and plotted as vertical strain (ε_v) and void ratio (e) versus applied pressure (p) in Figs 30–35. In the plots of vertical strain, the zero point is taken as the height of the specimen after removal of the compaction stress and the calculated initial void ratio (e_0) at this time is indicated in each of the plots. The initial void ratio was calculated based on the initial dry mass of soil, the initial height of the specimen and specific gravity values of 2.75 and 2.705 for the MX-80 and MX-80/SP specimens, respectively.

10. Imaging

The purpose of this task was to gain insight into the pore structure of the compacted bentonite specimens after DI water and Model Water hydration to enhance the understanding of the measured swell pressures and permeabilities. Microstructure imaging with an environmental scanning electron microscope (ESEM) has been completed for the six original test configurations listed in Table 11 after 272 days hydration with either DI water or Model Water.

10.1 Method

Sample preparation and hydration procedures largely followed those used to prepare specimens for swell pressures measurement. The soil specimen is 38 mm diameter and 10 mm high. The specimens were compacted under zero lateral displacement conditions at a gravimetric water content of 11% and deionized water was used to increase the water content from the as supplied water content to 11%. Once the lid of the apparatus was connected to the base, the specimen was then hydrated and permeated with DI water or Model Water under zero volume increase conditions (i.e., the effective stresses in the soil specimen will result from soil swelling under constant volume conditions). With porous stones on the top and bottom of the soil specimen, the bottom boundary specimens was connected to a constant fluid pressure of 15 kPa and the top boundary has zero fluid pressure (i.e., zero back pressure).

After 272 days of hydration, the specimens were removed from the apparatus for visual inspection. Photographs were taken of the bottom and top surfaces of the specimen. Measurements of final mass and thickness were made. Specimens were then sealed within a bag and stored in a refrigerator (at 4°C) prior to ESEM imaging. Approximately 15 to 20 minutes elapsed between when the apparatus was opened and the specimen was placed in the refrigerator. Specimen storage time in the refrigerator varied from one day to one week, depending on the availability of ESEM equipment.

The FEI-MLA Quanta 650 FEG-ESEM with energy dispersive spectroscopy (EDS) and fast X-ray analysis housed in the Department of Geological Sciences and Geological Engineering at Queen's University was used. The specimens were frozen with liquid nitrogen prior to taking images. Images were taken when chamber pressure comes into equilibrium. The images taken immediately after defrosting of liquid nitrogen from the surface of a specimen are reported.

10.2 Results

Images of the bottom surface of the 38-mm-diameter specimens after 272 days hydration are given in Fig. 36. Selected ESEM images for each of these specimens are given in Fig. 37 at with magnifications factors of either 250 or 300 to allow pore scale observations. For reference, the field of view in Fig. 37 is around 0.9 mm wide.

Comparison of the MX-80 specimens in Figs 37a and b show that in addition to formation of salt crystals (likely after termination of the test), the grains of bentonite and inter-grain macropores are more distinct after MW hydration than for DI water at a comparable initial dry density (1.63-1.64 Mg/m³). More prominent inter-grain macropores are visible around bentonite grain for the lower density MX-80 specimen in Fig. 37c (1.42 Mg/m³).

For the MX-80/SP specimens, inter-grain macropores are visible within the pore space between sand particles after MW hydration (Fig. 37e) relative to the more massive structure with DI hydration (Fig. 37d). The surface pattern visible in Figs 37e and f are most likely impressions from fibres of the filter paper used to separate the specimen from the porous stone.

The pore scale images in Fig. 37 are useful to better understand the hydraulic conductivities with respect to DI water and Model Water reported in Section 5.

11. Conclusions

Swelling, permeability, gap sealing, suction, and compression experiments were conducted on small specimens of compacted bentonite and bentonite/sand mixtures when hydrated with one particular pore fluid, called Model Water, at 22°C. Model Water is a stable, high-salt-concentration solution that was designed to reproduce the constituents and concentrations of the pore water in the Cobourg limestone of the Michigan Basin, at depths of approximately 700 m based on data reported for boreholes DGR-1 to DGR-6 by NWMO (2011). The Model Water has a total dissolved solids of 333 g/L, with main constituents of chloride (197 g/L), potassium (41 g/L), sodium (60 g/L), calcium (22 g/L) and magnesium (11 g/L), and a pH of 8.2. An MX-80 bentonite, a second natural sodium bentonite NWL, and MX-80 / sand mixtures (70% bentonite and 30% sand, by mass) were examined. The particular MX-80 bentonite tested (MX-80-QU-B2) is representative of MX-80 that could be obtained based on the simple specification of “MX-80” and no additional specific requirements other than it swell index exceed 19 mL/2g (MX-80 samples that were below 19 mL/2g were excluded from this study). The mineralogy of the tested MX-80-QU-B2 was within the published range reported for other MX-80 bentonites, but had a lower exchangeable sodium percentage.

Based on the data obtained for the particular Model Water, bentonites, procedures and conditions examined, the following conclusions were reached.

1. Swell pressure. Model Water hydration had a dominant effect on the swell pressure measured under zero-volume-increase and one-dimensional (bottom-up) hydration conditions. Interactions between the Model Water and bentonite decreased the swell pressure of MX-80 by a factor of eight (8) relative to DI water, from a peak of 2800 kPa with DI water to 350 kPa after 1 year with Model Water at a reference dry density of 1.6 Mg/m³. Swell pressures with Model Water hydration increased as the dry density of the MX-80 samples increased. However, chemical interactions between the Model Water and smectite minerals appear to dominate over density as a swell pressure of just 1250 kPa was measured for MX-80 after 1.4 years of Model Water hydration when initially compacted to the highest dry density of 1.8 Mg/m³ examined.

2. Permeability. Despite interactions between the Model Water and MX-80 bentonite, low hydraulic conductivity with an average of 4×10^{-11} m/s was measured after 1-1.7 years of permeation with Model Water at a dry density of 1.6 Mg/m³ (again, under zero-volume-increase and one-dimensional hydration conditions). However, MX-80/SP mixtures tested at a dry density of 1.63 to 1.67 Mg/m³ were unable to attain a low hydraulic conductivity with values tending to 4×10^{-9} m/s after 1 year permeation with Model Water.

3. Model Water interactions. Model water effects appear very soon (within 10-30 hours) after the start of hydration. At this point, these initial interactions were limited to the outer surface of bentonite aggregates, as Model Water movement mostly occurs through the interconnected macropores formed by the void space in between the aggregates. However, interactions continued over the 1 year or testing as Model Water constituents penetrated the aggregates and interacted with the smectitic agglomerate particles within the aggregates. These interactions were slow and likely dominated by diffusion which would control the time scale for measurement. At least 1 year

of testing was required provide a reasonable indication of Model Water effects for the mass of specimens tested. Monitoring these tests for longer periods of time would be required to confirm that this time scale is sufficient to capture any additional effects from interlayer clay mineral interactions with constituents from the pore fluid. The natural sodium percentage of the smectitic clay minerals decreased from 62 to 25% following 1-1.7 years of interaction with the Model Water. The decrease sodium occurred from cation exchange and was mostly replaced by potassium and some magnesium from the Model Water; there was essentially no change in exchangeable calcium.

4. Radial gap sealing. Despite initial interactions between the Model Water, MX-80 compacted to 1.8 Mg/m^3 was able to volumetrically swell to initially seal an intentional 0.95 mm radial gap (equal to 5% of the specimen radius) around the perimeter of the sample, while otherwise under vertical restraint and subject to Model Water hydration. It maintained this seal for the 600 day monitoring period with a flow rate only 25% greater than that of a similar sample without an initial radial gap. MX-80 compacted to 1.65 Mg/m^3 also volumetrically swelled to initially seal a 0.95 mm radial gap and maintained the seal for 290 days of testing. In contrast, a MX-80/SP sample (1.66 Mg/m^3) was unable to seal the 0.95 mm radial gap, either initially, nor after 1 year hydration with Model Water.

5. Suction. Initial total suctions around 90 MPa were measured for the MX-80 bentonite at its as supplied gravimetric water content of 9% when compacted to 1.61 Mg/m^3 . This corresponds to the initial water content adopted for the swelling, permeability, and gap sealing experiments. Wetting-path suction measurements for MX-80 specimens prehydrated with Model Water and compaction to 1.61 Mg/m^3 showed subsequent decreases in suction with increasing water content. Total suction values decreased to 45 MPa at Model Water saturation, which were dominated by osmotic suction. For measured gravimetric water contents less than 15%, the bentonite content impacted the measured suction, with greater water potential being measured for the pure MX-80 configuration relative to the 70% bentonite in the MX-80/SP mixture.

6. Compression. The compressibility of MX-80 and MX-80/SP was quantified for specimens prehydrated with Model Water that were allowed to initially swell under 100 kPa of vertical stress. Rather than swell, the MX-80 sample compacted to 1.57 Mg/m^3 experienced vertical compression of 0.3% of its height under the initial 100 kPa pressure. The compressibility was similar for Model Water and DI water MX-80 specimens beyond 1000 kPa.

References

- Agus, S.S., & Schanz, T. 2008. A method for predicting swelling pressure of compacted bentonites. *Acta Geotechnica*, 3: 125–137.
- ASTM D5890. Test Method for Swell Index of Clay Mineral Component of Geosynthetic Clay Liners, American Society for Testing and Materials.
- ASTM D7503. Test Method for Measuring the Exchangeable Complex and Cation Exchange Capacity of Inorganic Fine-Grained Soils, American Society for Testing and Materials.
- Brye, K. R. 2003. Long-term effects of cultivation on particle size and water-retention characteristics determined using wetting curves. *Soil Science*, 168(7): 459–468.
- Dixon, D.A., Man, A., Stone, J., Rimal, S., Siemens, G., Abootalebi, P., & Birch, K. 2016. Backfilling and sealing materials for a deep geological repository, 3rd Canadian Conference on Nuclear Waste Management, Decommissioning and Environmental Restoration, Ottawa, ON, Canada, September 11-14, 2016, 10 pp.
- Ferrari, A., Seiphoori, A., Rüedi, J., & Laloui, L. 2014. Shot-clay MX-80 bentonite: An assessment of the hydro-mechanical behaviour. *Engineering Geology*, 173: 10–18.
- Gatabin, C., Talandier, J., Collin, F., Charlier, R., & Dieudonné, A. C. 2016. Competing effects of volume change and water uptake on the water retention behaviour of a compacted MX-80 bentonite/sand mixture. *Applied Clay Science*, 121: 57–62.
- Gee, G. W., Campbell, M. D., Campbell, G. S., & Campbell, J. H. 1992. Rapid measurement of low soil water potentials using a water activity meter. *Soil Science Society of America Journal*, 56(4): 1068–1070.
- Herbert, H., Kasbohm, J., Sprenger, H., Fernández, A., & Reichelt, C. 2008. Swelling pressures of MX-80 bentonite in solutions of different ionic strength. *Physics and Chemistry of the Earth*, 33: S327–S342.
- IAEA. 2013. Characterization of swelling clays as components of the engineered barriers system for geological repositories. International Atomic Energy Agency, IAEA-TECDOC-1718, Vienna, Austria.
- Karland O., Olsson, S., & Nilsson, U. 2006. Mineralogy and sealing properties of various bentonites and smectite-rich clay materials. Swedish Nuclear Fuel and Waste Management, Technical Report TR-06-30, Stockholm, Sweden.
- Liu, L., 2013. Prediction of swelling pressures of different types of bentonite in dilute solutions. *Colloids and Surfaces A: Physicochem. Eng. Aspects*, 434: 303–318.
- NWMO 2011. Hydrogeological Modelling Report NWMO DGR-TR-2011-16, by: J.F. Sykes, S.D. Normani, and Y. Yin, March 2011.
- Mitchell, J.K., and Soga, K. 2005. *Fundamentals of Soil Behavior*, 3rd Edition, Wiley & Sons, New York, 592 p.
- Rowe, R.K., Quigley, R.M., Brachman, R.W.I., and Booker, J.R. 2004. *Barrier Systems for Waste Disposal Facilities*, Taylor & Francis / Spon, London, U.K., 579 p.
- Seiphoori, A., Ferrari, A., & Laloui, L. 2014. Water retention behaviour and microstructural evolution of MX-80 bentonite during wet and dry cycles. *Géotechnique*, 64(9): 721–734.
- Tang, A. M., & Cui, Y. J. 2010. Experimental study on hydro-mechanical coupling behaviours of highly compacted expansive clay. *J. Rock Mech. and Geotechnical Eng.*, 2(1): 39–43.
- Wang, Q. 2012. Hydro-mechanical behaviour of bentonite-based materials used for high-level radioactive waste disposal, Ph.D. Thesis, Université Paris-Est, France, 192 p.
- Wang, Q., Tang, A.M., Cui, Y., Delage, P., & Gatmiri, B. 2012. Experimental study on the swelling behaviour of bentonite/claystone mixture. *Engineering Geology*, 124: 59–66.

Table 1. Semi-quantitative mineralogy (% of total material) from XRD. MX-80-WyR1 results from Karnland et al. (2006, p. Table 5.5) and are the mean results from three XRD traces.

Bentonite	Swell index (mL/2g)	Smectite	Feldspar	Mica	Quartz	Cristobalite	Zeolite
MX-80-QU-B2	20	83	7	1	3	2	4
GCL-NWL-QU	26	96	2	–	2	–	–
MX-80-WyR1	NR	83.5	0.7 ^a / 2.9 ^b	2.8	2.8	0.4	–

NR = not reported

^a orthoclase

^b plagioclase

Table 2. Cation exchange complex and capacity for natural and Model Water (MW) hydrated samples of MX-80 and NWL bentonites.

			MX-80 natural	NWL natural	MX-80- WyR1 natural ^a	MX-80 after MW hydration	NWL after MW hydration
No. of samples			4	5	<i>b</i>	4	1
Exchange complex (mole fraction)							
	Na	Mean	0.62	0.69	0.75	0.25	0.27
		Std dev.	0.08	0.05	0.03	0.02	-
		Min.	0.54	0.63	0.72	0.22	-
		Max.	0.71	0.77	0.77	0.26	-
	K	Mean	0.03	0.02	0.02	0.29	0.30
		Std dev.	0.02	0.01	0.00	0.04	-
		Min.	0.01	0.01	0.02	0.26	-
		Max.	0.05	0.04	0.02	0.34	-
	Ca	Mean	0.32	0.24	0.16	0.35	0.29
		Std dev.	0.11	0.04	0.02	0.03	-
		Min.	0.20	0.19	0.15	0.32	-
		Max.	0.43	0.28	0.18	0.38	-
	Mg	Mean	0.03	0.05	0.07	0.11	0.14
		Std dev.	0.02	0.03	0.01	0.01	-
		Min.	0.01	0.01	0.06	0.10	-
		Max.	0.05	0.08	0.08	0.12	-
Exchange capacity (cmol/kg)		Mean	64	78	75	54	52
		Std dev.	4	5	1	6	-
		Min.	60	72	74	48	-
		Max.	69	86	76	62	-

Note: Ammonium acetate replacement method following ASTM D7503 used to obtain values for natural and model water hydrated samples of MX-80 and NWL bentonites.

^a from Karnland et al. (2006).

^b Exchangeable mole fraction: No. of samples=3 (p. 24, Table 3.3); Exchange capacity: No. of samples=5 (p. 22, Table 3.1).

Table 3. Summary of pore water data measured at DGR-1 to DGR-6 from NWMO (2011) and proposed Model Water.

Item	Unit	Measured values from DGR-1 to DGR-6						Proposed Model Water
		Max.	Min.	Mean	Std dev.	Mean + Std dev.	Mean – Std dev.	
Cl	g/L	257	92	195	35	230	161	197
Na	g/L	74	29	60	11	71	48	60
Ca	g/L	45	2	27	11	38	16	22
K	g/L	63	25	41	18	59	24	41
Mg	g/L	35	5	15	7	22	7	11
SO ₄	g/L	13	4	9	4	13	4	0.6
Br	g/L	4	1	2	1	3	1	2
TDS	g/L	364	161	280	47	327	233	333
pH	pH	8.2	8.1	8.2	0.0	8.2	8.1	8.2

Notes:

TDS = total dissolved solids

Std dev. = Standard deviation

Table 4. Effect of pore fluid composition on Swell Index (SI) of MX-80 bentonite.

Solution	Cl	Na	Ca	K	Mg	SO ₄	Br	TDS	pH	I	RMD	SI
	g/L	g/L	g/L	g/L	g/L	g/L	g/L	g/L	-	mM	M ^{1/2}	mL/2g
1. Deionized water for control	-	0.0015	0.0001	0.0004	-	-	-	0.002	8.2	0.043	0.05	21 (n=3)
2. Proposed model water	197	60	22	41	11	0.6	2	333	8.2	6600	3.7	5 (n=2)
3. Intermediate concentration solution	145	45	12	33	8	0.6	2	244	8	4700	3.5	6
4. Minimum measured concentrations ^a	84	29	2	25	5	0.6	1	155	8.2	2800	3.8	7
5. NaCl solution	237	153	-	-	-	-	-	390	8.2	6600	-	7
6. CaCl ₂ solution	157	-	88	-	-	-	-	245	8.2	6600	-	7
7. KCl solution	235	-	-	260	-	-	-	495	8.2	6600	-	5
8. MgCl ₂ solution	156	-	-	-	54	-	-	210	8.2	6600	-	8

Notes:

TDS = total dissolved solids

I = ionic strength

RMD = ratio of monovalent to divalent species = $M_M / M_D^{1/2}$

where: M_M = total molarity of monovalent cations and M_D = total molarity of polyvalent cations

n = number of replicates

^a other than Cl and SO₄

Table 5. Peak and long-term swell pressures for MX-80 and NWL bentonites. Initial water content = 11%.

Test	Bentonite	Dry density (Mg/m ³)	Fluid	Compaction pressure (kPa)	Seating pressure (kPa)	Peak swell pressure (kPa)	Last recorded swell pressure (kPa)	Time to last recorded swell pressure (h)	Rate of change		
									From (h)	To (h)	Rate (kPa/yr)
1.3	MX-80	1.61	DI	11000	40	2810	2260	25700	6000	25700	-120
2.3	MX-80	1.60	MW	9220	350	> 800*	350	9000	6000	9000	-200
2.3(a4)	MX-80	1.53	MW	9340	20	860	370	8400	4000	8400	0
2.3(i)	MX-80	1.68	MW	16290	160	2330	750	12320	4000	12000	-80
2.3(j)	MX-80	1.82	MW	-	40	2780	1250	12470	10000	12500	-110
NWL1	NWL	1.62	DI	13510	320	5040	5030	1110	200	1100	-30
NWL2	NWL	1.62	MW	-	290	1420	1020	4090	3500	4090	-260
7.1	NWL	1.69	MW	16630	190	2370	1220	2150	1500	2150	-540
7.2	NWL	1.68	MW	17460	20	2220	1070	12920	6000	13000	-90
7.3	NWL	1.82	MW	-	80	3584	2285	4610	2500	4600	-300

* in this very early test the peak values was not recorded

Table 6. Swell pressure with model water hydration of MX-80 bentonite compacted to 1.53-1.61 Mg/m³ with an initial water content of 11%.

Test	Dry density (Mg/m ³)	Compaction pressure (kPa)	Seating pressure (kPa)	Peak swell pressure (kPa)	Last recorded swell pressure (kPa)	Time to last recorded swell pressure (h)	Relative seating pressure
2.3(a1)	1.53	10390	280	920	420	770	High
2.3(d)	1.55	9640	230	820	370	460	High
2.3(c)	1.56	10130	150	1050	430	340	Intermediate
2.3(a3)	1.53	10500	20	940	450	290	Low
2.3(a4)	1.53	9340	20	860	375	8430	Low
2.3(R1)	1.61	12470	90	1540	690	2090	Low
2.3(R2)	1.59	12320	30	1420	610	890	Low

Table 7. Swell pressure for other MX-80 bentonite and MX-80/SP sand-bentonite mixture configurations. Initial water content = 11%.

Test	Soil	Dry density (Mg/m ³)	Hydration fluid	Seating pressure (kPa)	Peak swell pressure (kPa)	Last recorded swell pressure (kPa)	Time to last recorded swell pressure (h)
1.1	MX-80	1.45	DI	30	350	340	1290
1.2	MX-80	1.56	DI	40	2070	2030	1470
2.1	MX-80	1.44	MW	60	150	140	1290
3.2	MX-80	1.42	MW	110	360	160	2400
4.1	MX-80/SP	1.35	DI	10	120	120	270
4.2	MX-80/SP	1.65	DI	190	980	870	10820
5.1	MX-80/SP	1.64	MW	70	260	80	2880
6.1	MX-80/SP	1.80	MW	200	800	340	21147

Table 8. Summary of permeation experiments.

Test	Soil	Dry density (Mg/m ³)	Permeant	Duration of permeation (days)	Incremental flow rate for last recorded flow			Hydraulic conductivity to permeant, k (m/s)	Range reported k averaged over (days)
					Inflow (mL/day)	Outflow (mL/day)	% Difference		
1	MX-80	1.61	DI	935	0.01	n.d.	-	^a 7.8x10 ⁻¹³	600-935
2	MX-80/SP	1.66	DI	885	0.03	n.d.	-	^a 1.1x10 ⁻¹²	606-885
3a	MX-80	1.61	MW	387	0.50	0.50	0	2.1x10 ⁻¹¹	290-387
3b	MX-80	1.55	MW	384	1.76	1.78	1.4	6.3x10 ⁻¹¹	327-384
5a	MX-80	1.60	MW	471 ^b /611	1.10	1.08	1.4	4.6x10 ⁻¹¹	531-611
5b	MX-80	1.60	MW	399 ^b /524	1.11	1.15	3.5	4.4x10 ⁻¹¹	445-524
4a	MX-80/SP	1.63	MW	96	129	129	0	5.5x10 ⁻⁹	87-96
4b	MX-80/SP	1.63	MW	208	36	35.6	1	4.0x10 ⁻⁹	195-208
6a	MX-80/SP	1.63	MW	477 ^b /487	44.4	43.8	1.4	4.1x10 ⁻⁹	478-487
6b	MX-80/SP	1.67	MW	408 ^b /422	36.2	36.6	1.0	3.5x10 ⁻⁹	408-422
7a*	MX-80	1.80	MW	545	0.04	0.03	25	1.8x10 ⁻¹²	400-545
8a*	NWL	1.80	MW	190	0.03	n.d.	-	1.1x10 ⁻¹²	120-190
9a*	MX-80	1.65	MW	190	0.50	0.52	4	1.4x10 ⁻¹¹	110-190

^a These values are based on rate of inflow. This is a rate of water uptake rather than not a hydraulic conductivity. The real k values can not be obtained until there is equilibrium between inflow and outflow. After 900 days no outflow has been observed.

^b Hydration time prior to permeation measurement.

*Average flow rate are calculated considering last 3 recorded values; not yet at steady state.

n.d. = not detected.

Inflow head = 1.5 m, except for Tests 4b, 6a and 6b where inflow head = 0.4 m.

Table 9. Experiments conducted to assess sealing of intentional 0.95 mm radial gap around 36.1 mm diameter specimen with Model Water hydration.

Radial Gap Test	Soil	Dry density (Mg/m ³)	Thickness (mm)	Inflow (mL/day)	Outflow (mL/day)	Time over which in/outflow obtained (days)	% diff. between inflow and outflow	Radial Gap flow / Perm. test flow (-)
1	MX-80/SP	1.66	20	70	71	350-380	1.4	2
4	MX-80	1.65	22.1	0.27*	0.20*	245-290	30	0.6
2	MX-80	1.8	20	0.05	0.03	500-600	25	1.25
3	NWL	1.8	22.1	0.19*	0.14*	200-380	25	5

* not yet measured with volumetric burette; measured with graduated cylinder.

Table 10. One-dimensional compression tests.

Test	Material	Initial dry density (Mg/m ³)	Pore fluid	Vertical strain ϵ_v after initial 100 kPa load increment (%)
1b	MX-80	1.58	DI	24
2b	MX-80	1.57	MW	-0.2
3b	MX-80	1.42	MW	-0.6
4b	MX-80 / SP	1.64	DI	23
5b	MX-80 / SP	1.65	MW	-3
6b	MX-80 / SP	1.75	MW	-0.6

Table 11. Imaging configurations.

Soil	MX-80	MX-80	MX-80	MX-80/SP	MX-80/SP	MX-80/SP
Dry density (Mg/m ³)	1.41	1.61	1.61	1.65	1.65	1.8
Pore fluid	MW	MW	DI	MW	DI	MW

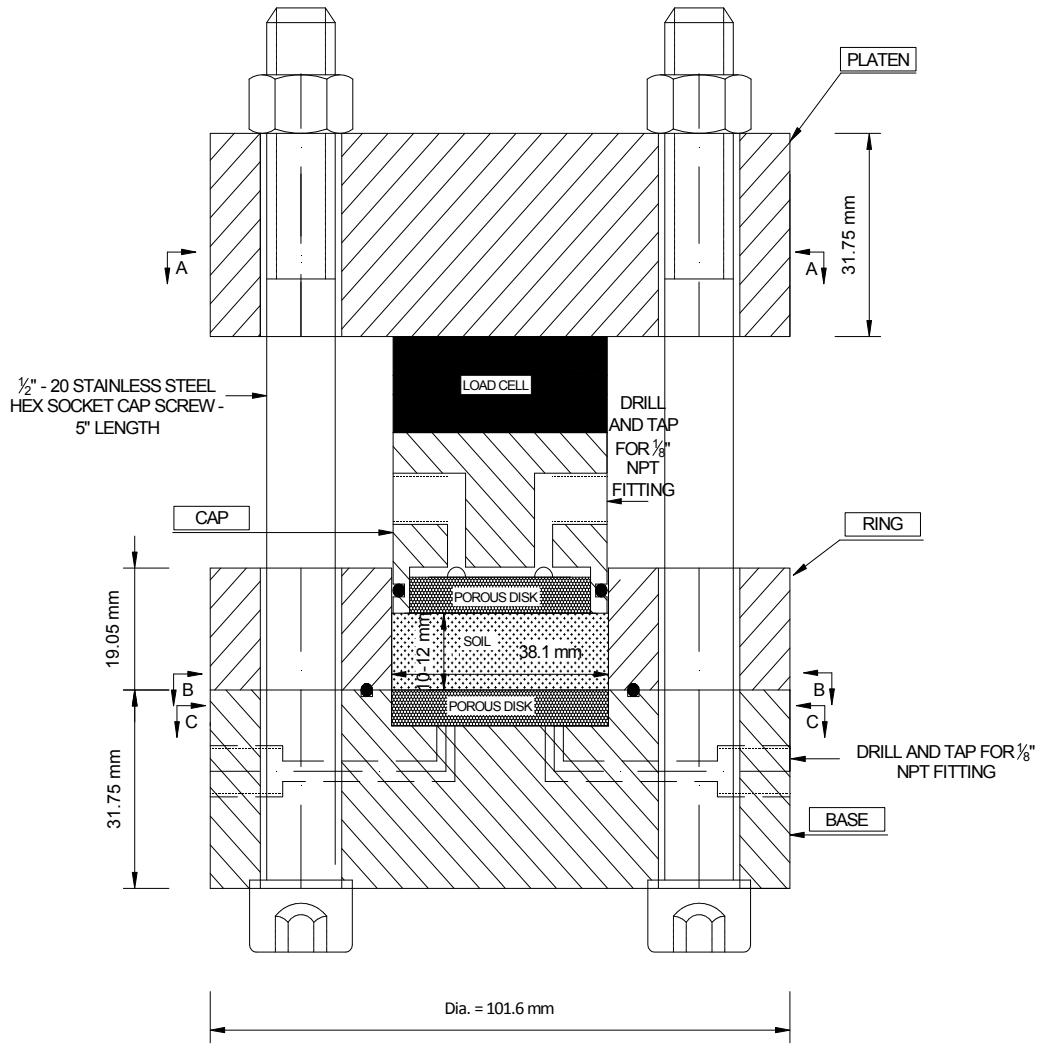


Figure 1. Constant volume swell pressure apparatus.

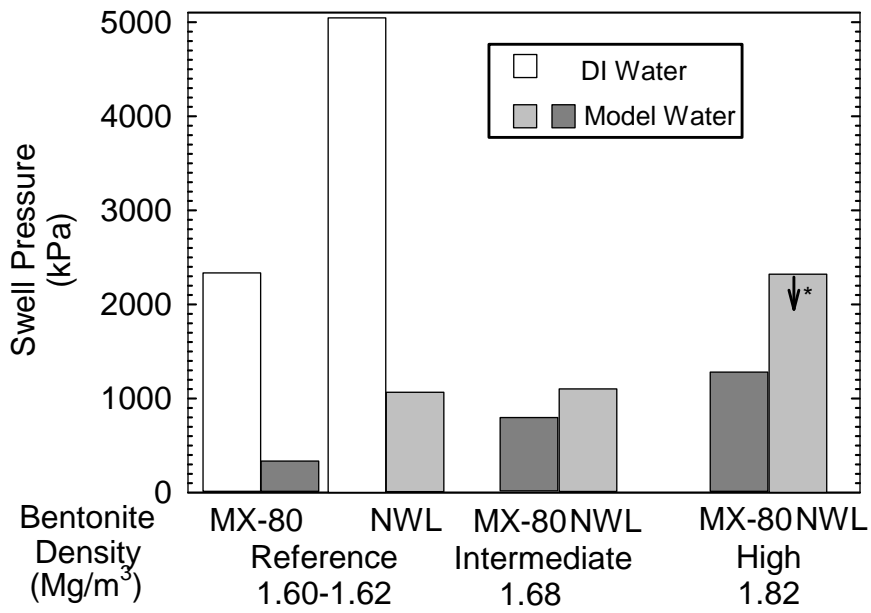


Figure 2. Summary of principal results showing effect of pore water, bentonite, and density on last measured swell pressure.

Note: * Not yet at steady rate of decrease

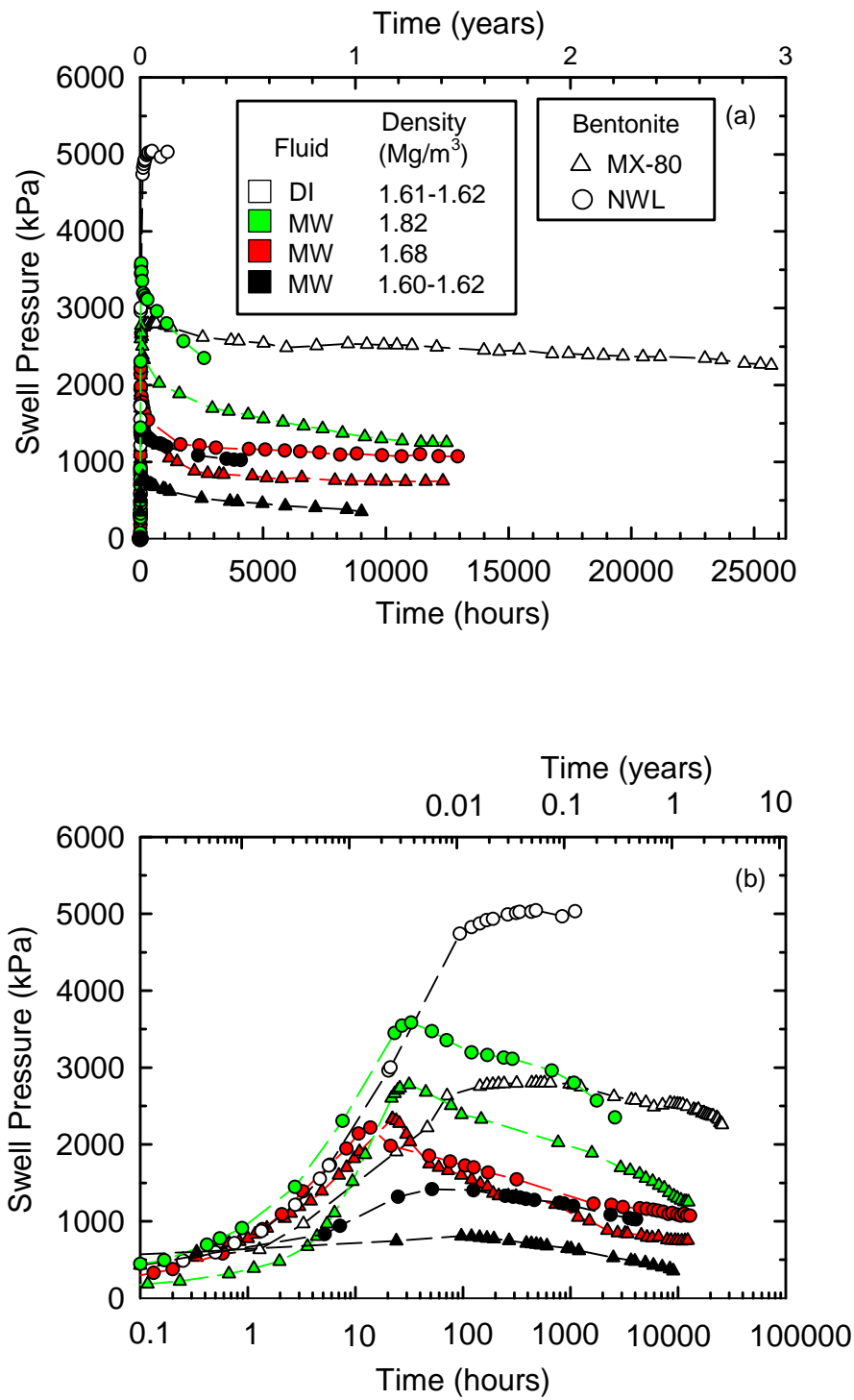


Figure 3. Swell pressure for MX-80 and NWL bentonites plotted versus: (a) time, and (b) logarithm of time.

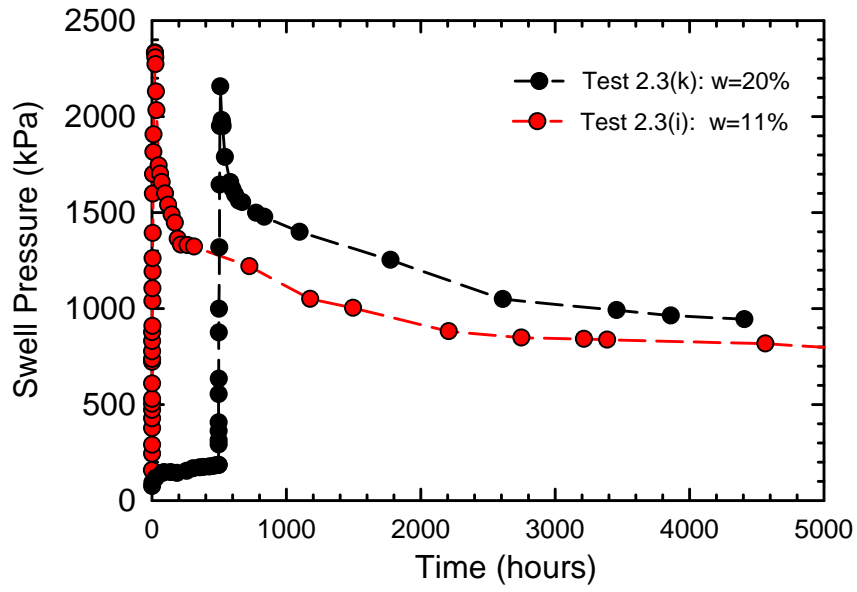


Figure 4. Effect of initial water content on swell pressure for MX-80 at intermediate dry density of 1.68 Mg/m^3 .

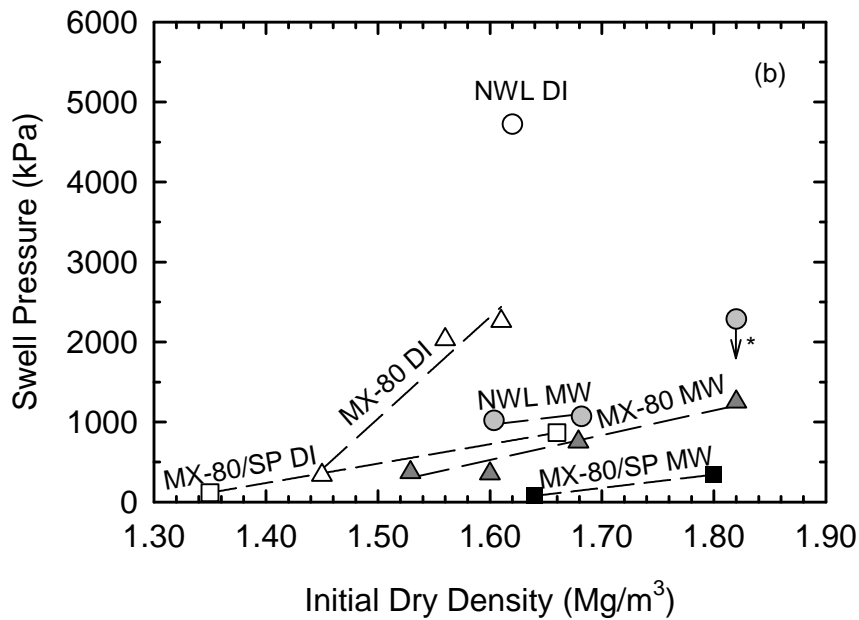
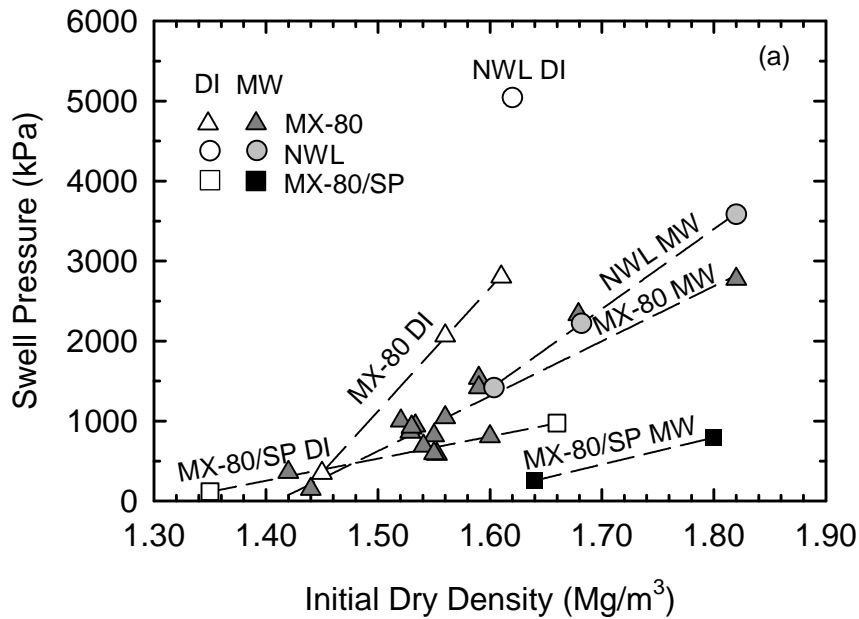


Figure 5. Peak (a) and last measured (b) swell pressure vs dry density.
 Note: * Not yet at steady rate of decrease

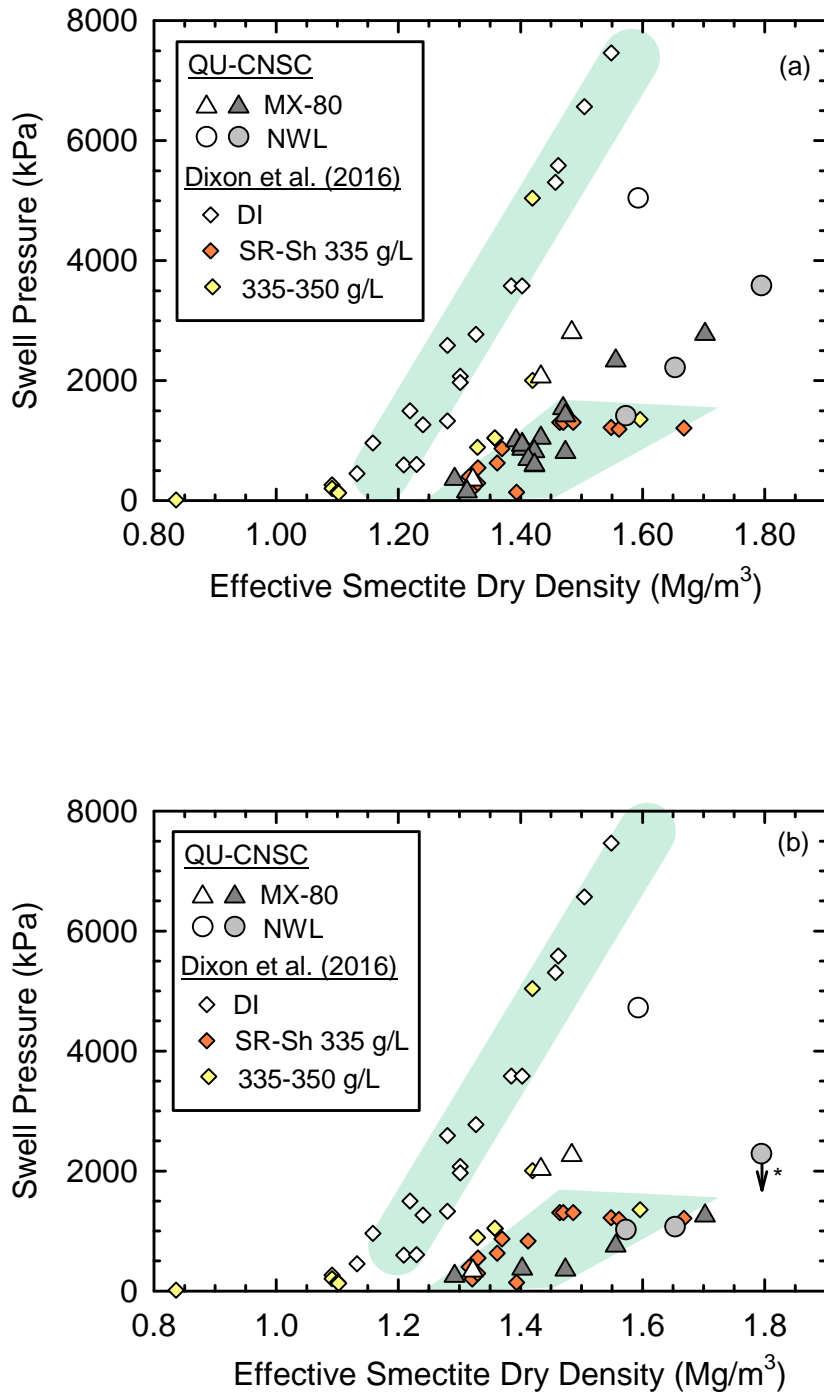


Figure 6. Comparison of peak (a) and last measured (b) swell pressures with the data from Dixon et al.(2016). Note: * Not yet at steady rate of decrease

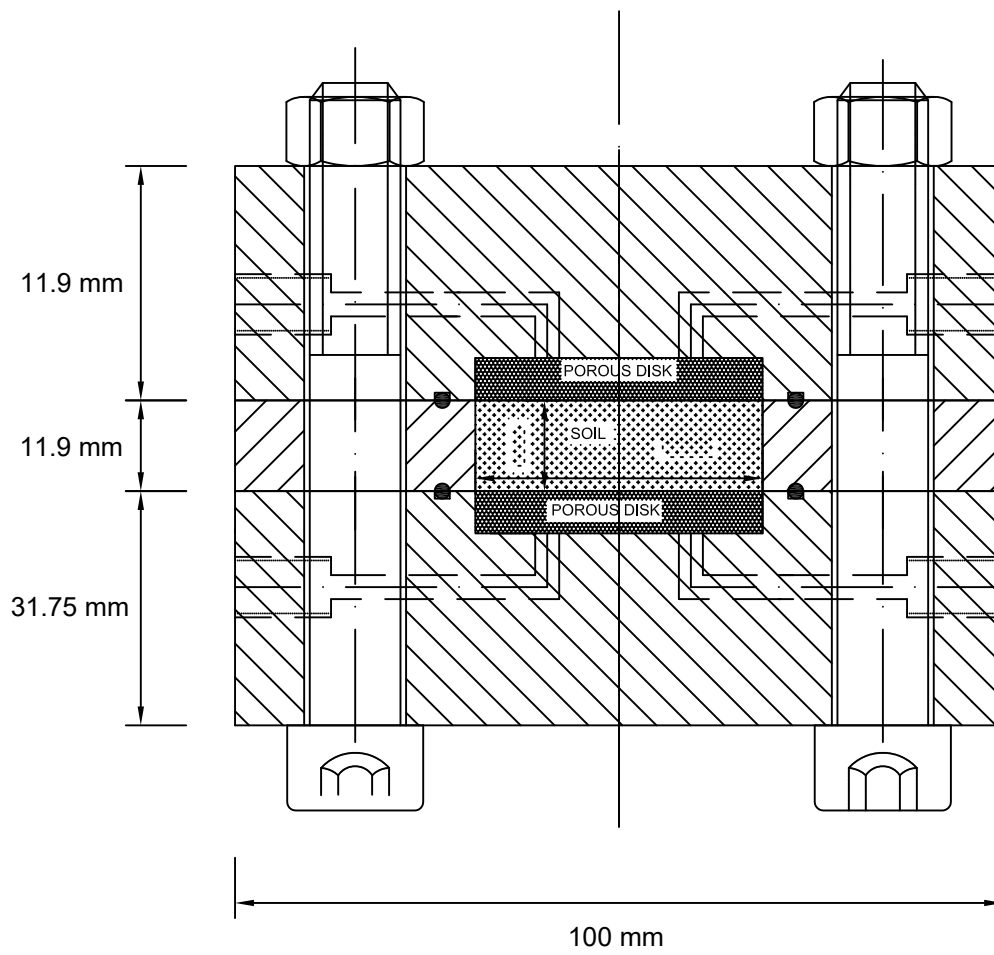


Figure 7. Cross-section showing apparatus used for permeation experiments.

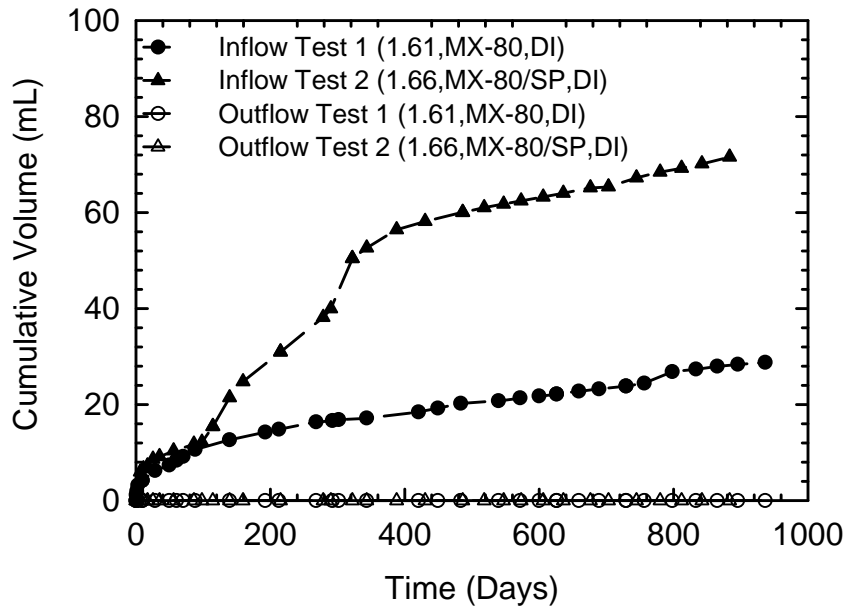


Figure 8. Cumulative inflow and outflow volume measured for on-going permeation test for MX-80 and MX-80/SP samples compacted at different dry density permeated with distilled water.

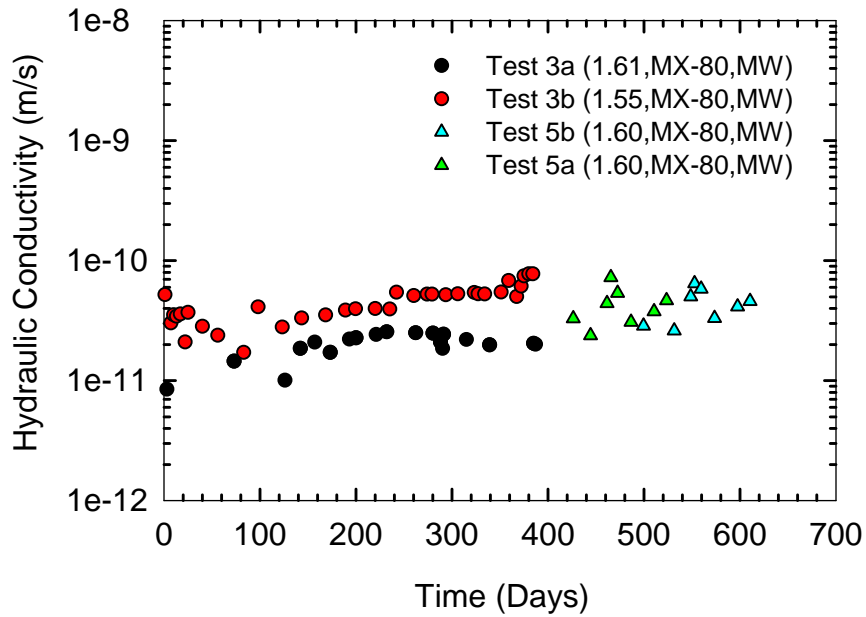


Figure 9. Calculated hydraulic conductivity with respect to Model Water based on inflow falling head in Tests 3a, 3b, 5a and 5b with MX-80. Note: Permeation measurements for Tests 5a and 5b started 1-year after hydration initiated.

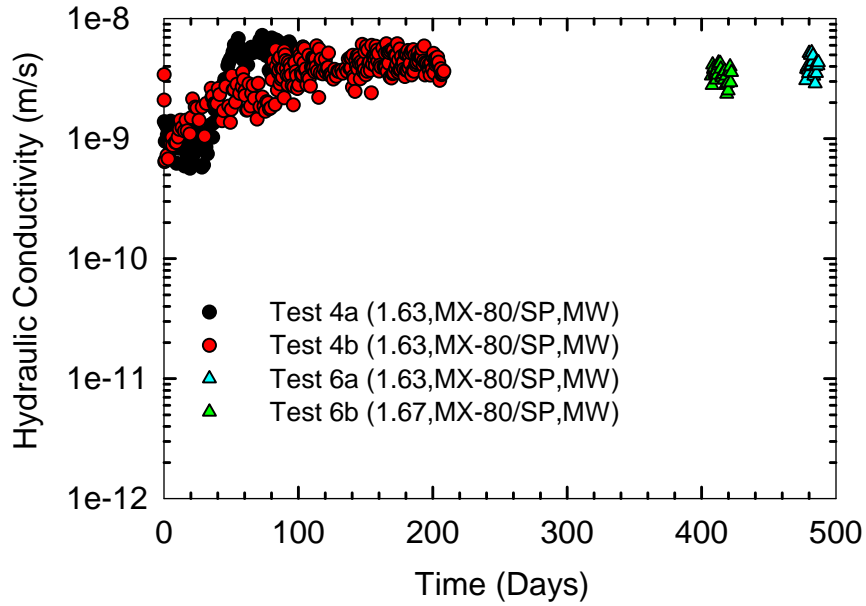


Figure 10. Calculated hydraulic conductivity with respect to Model Water based on inflow falling head in Tests 4a, 4b, 6a and 6b with MX-80/SP. Note: Permeation measurements for Tests 6a and 6b started 1-year after hydration initiated.

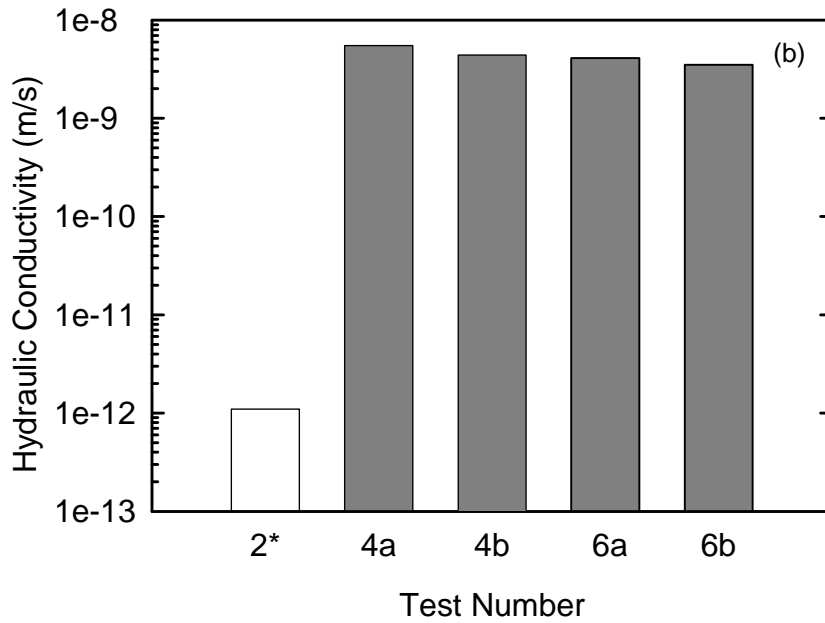
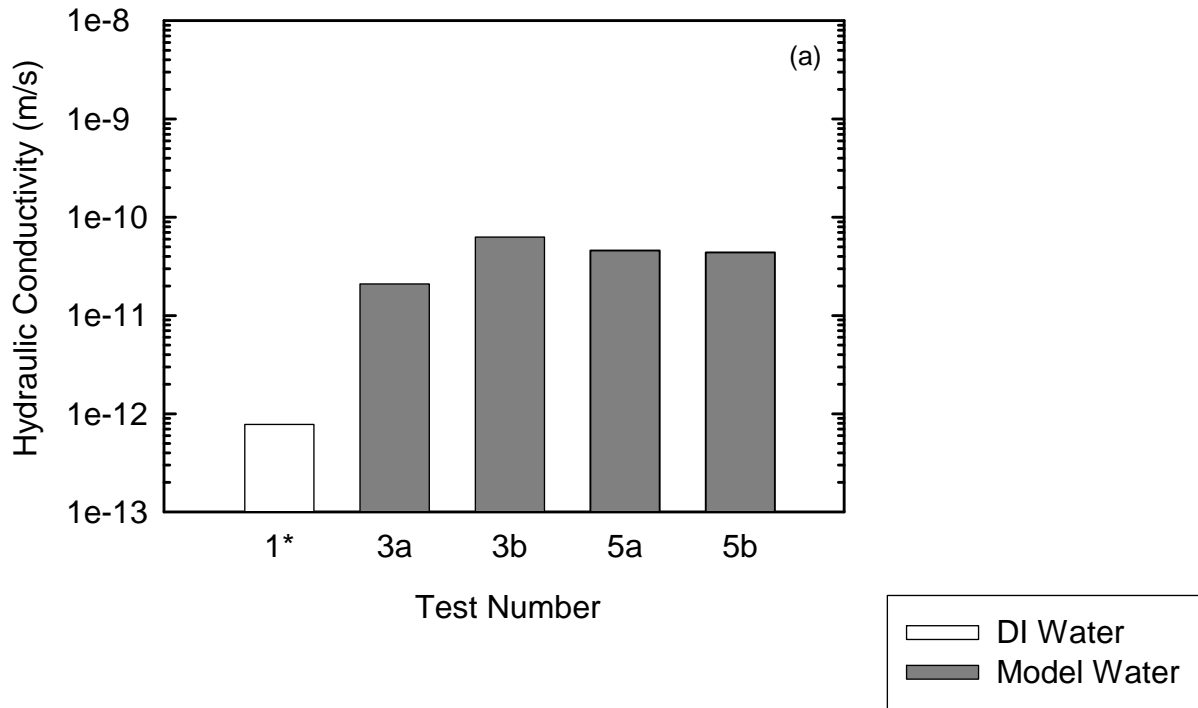


Figure 11. Hydraulic conductivities with respect to DI or Model Water for: (a) MX-80 & NWL (d=1.60 to 1.80 Mg/m³), and (b) MX-80/SP (d=1.63 to 1.67 Mg/m³). Note: Values for DI water may be smaller than reported since steady state conditions have not yet been attained.

Note: * Test running

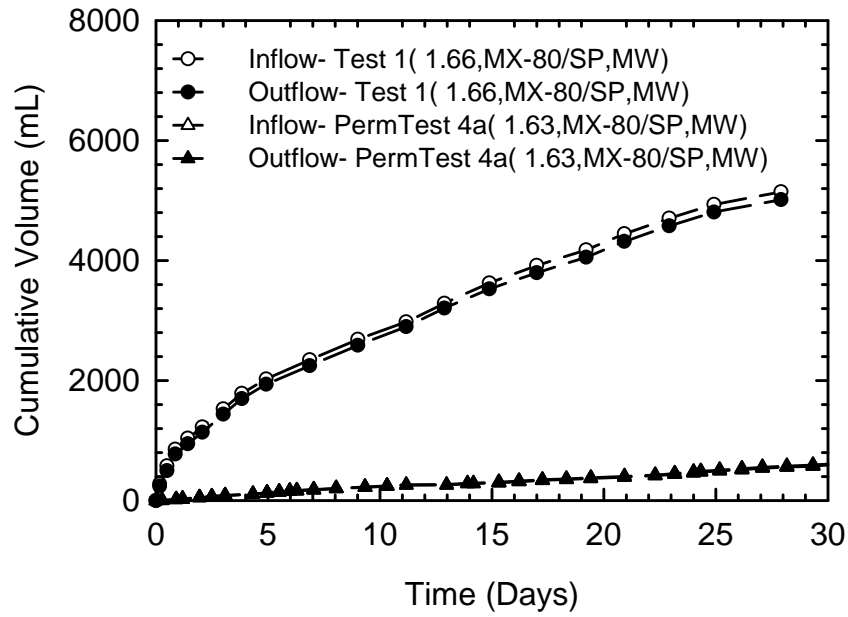


Figure 12. Cumulative flow for radial gap swell Test 1 and permeation Test 4a with MX-80/SP with Model Water hydration.

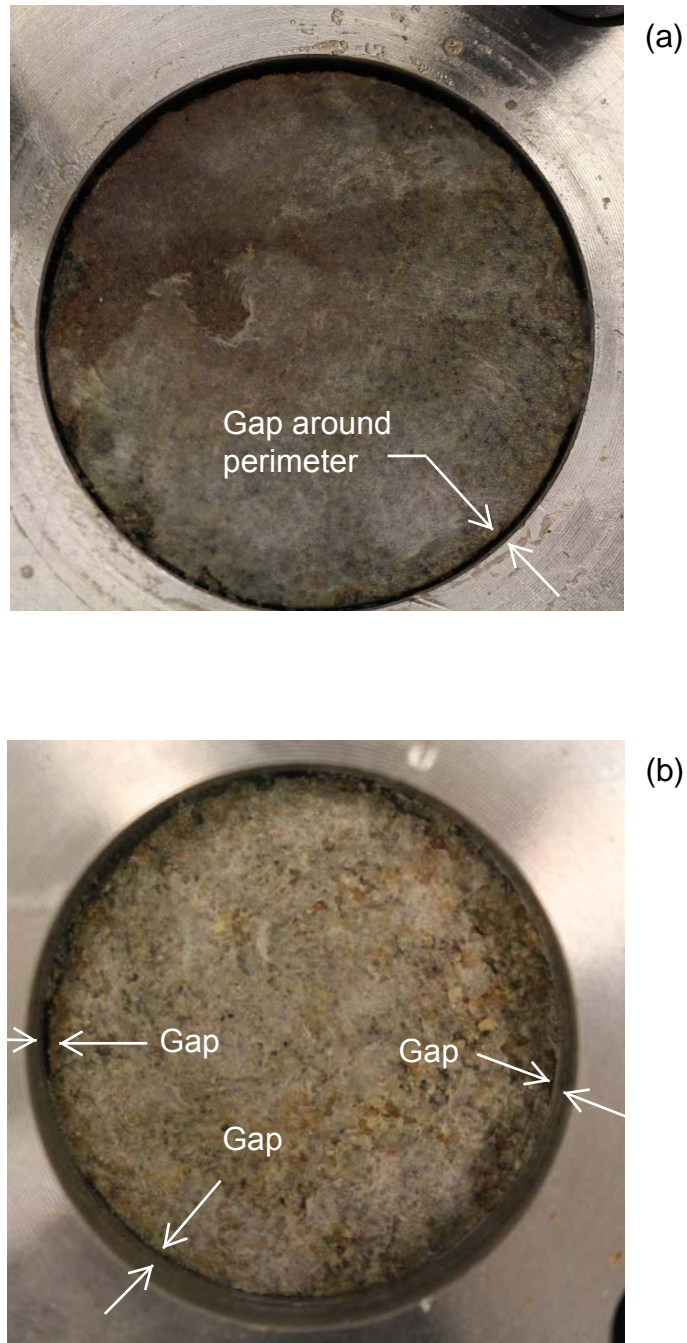


Figure 13. Photographs of a) bottom and b) top MX-80/SP surface 350 days after Model Water hydration in radial gap seal Test 1. Inside diameter of test cell = 38 mm.

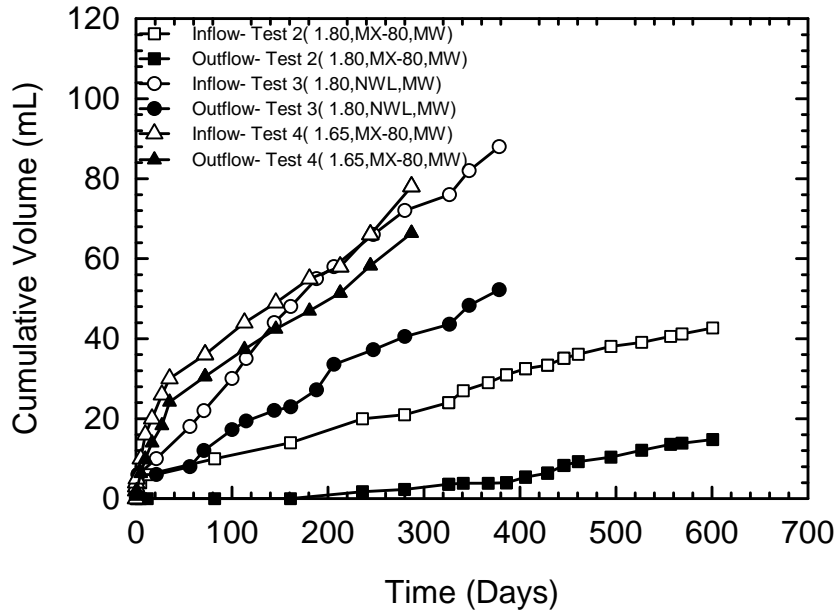


Figure 14. Cumulative flow for radial gap swell Test 2, Test 3 & Test4 with MX-80 & NWL bentonite with Model Water hydration.

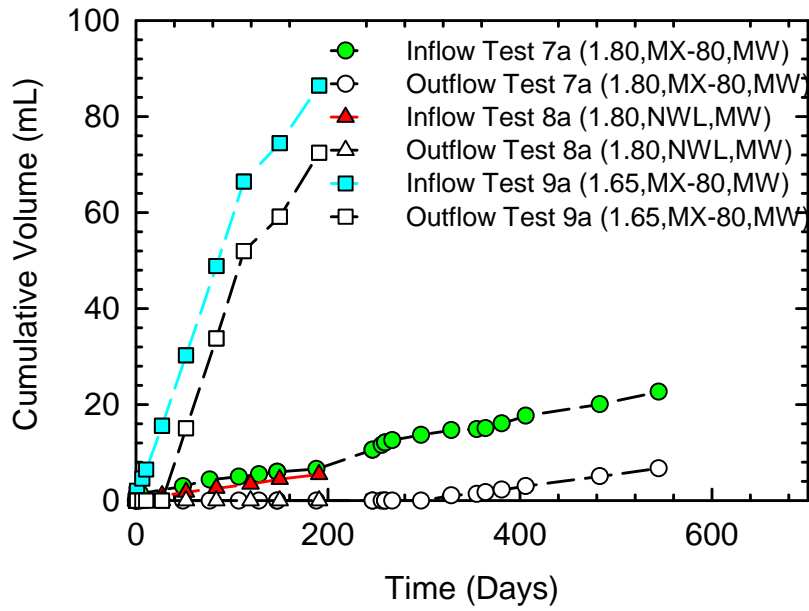


Figure 15. Cumulative inflow and outflow volume measured for on-going permeation test for MX-80 & NWL samples compacted at different dry density permeated with model water

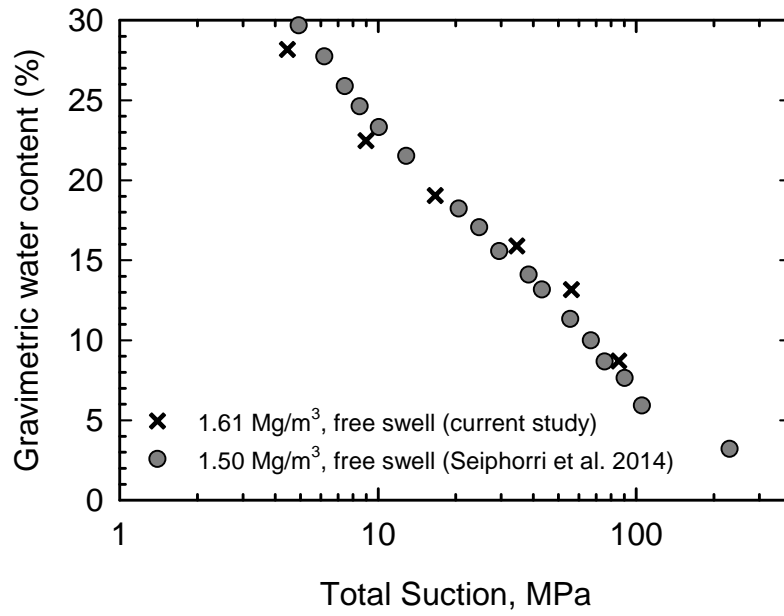


Figure 16. MX-80 free swell DI water wetting path suction measurements from current study and literature value.

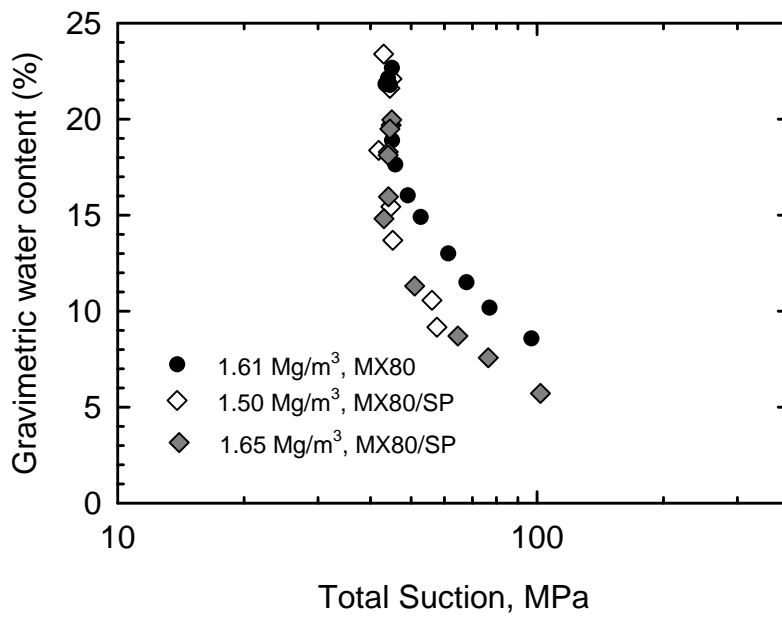


Figure 17. Free swell model water wetting path suction measurements.

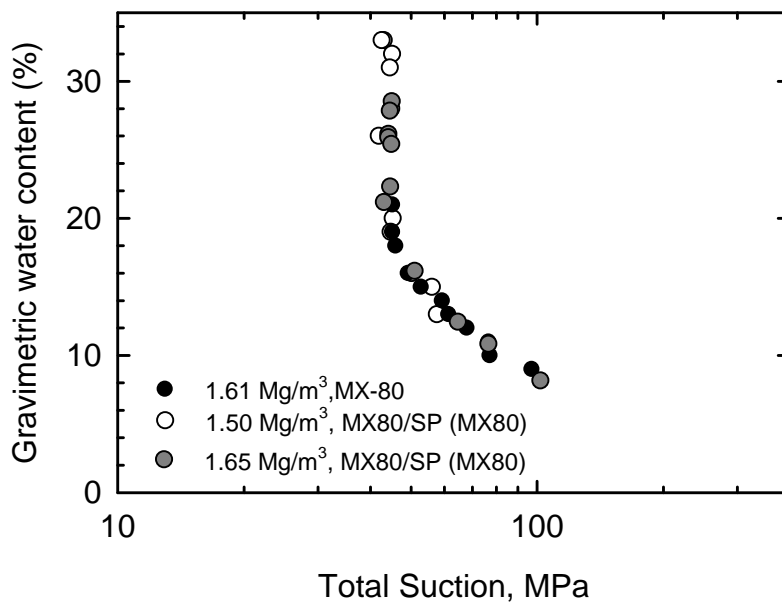


Figure 18. Comparison of three configurations with model water assuming all measured water is attributed to the bentonite.

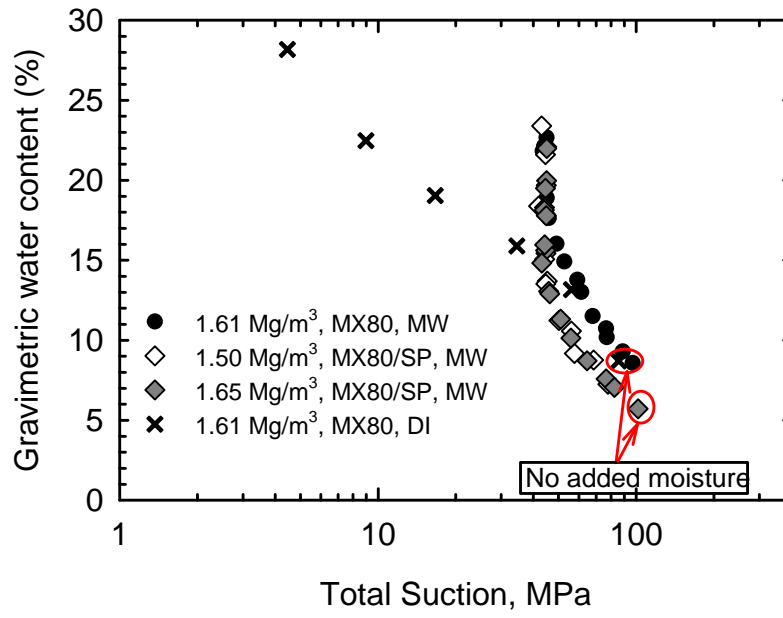


Figure 19. Free swell model water wetting path suction measurement and reference case with DI water.

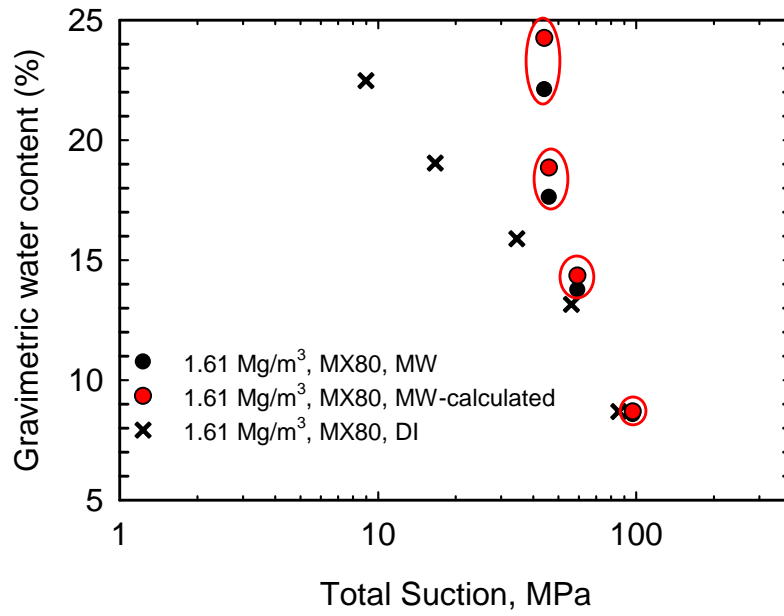


Figure 20. Comparison of measured and calculated water content for MX-80 compacted to 1.61 Mg/m³ with model water

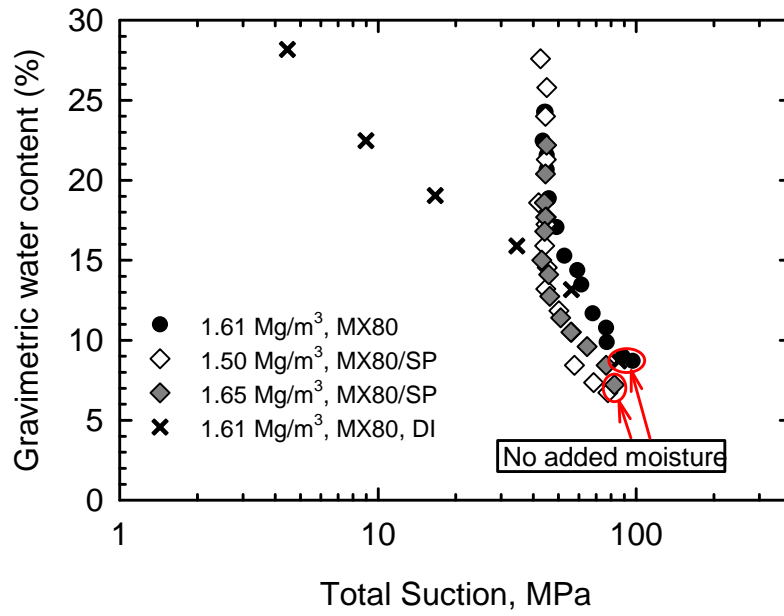


Figure 21. Free swell model water wetting path suction measurements in terms of calculated water content

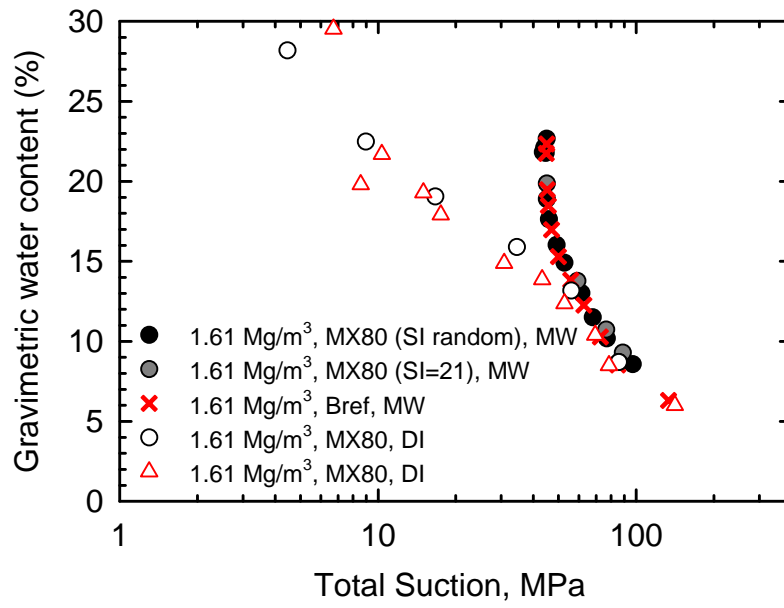


Figure 22. The impact of the mineralogy measured suctions.

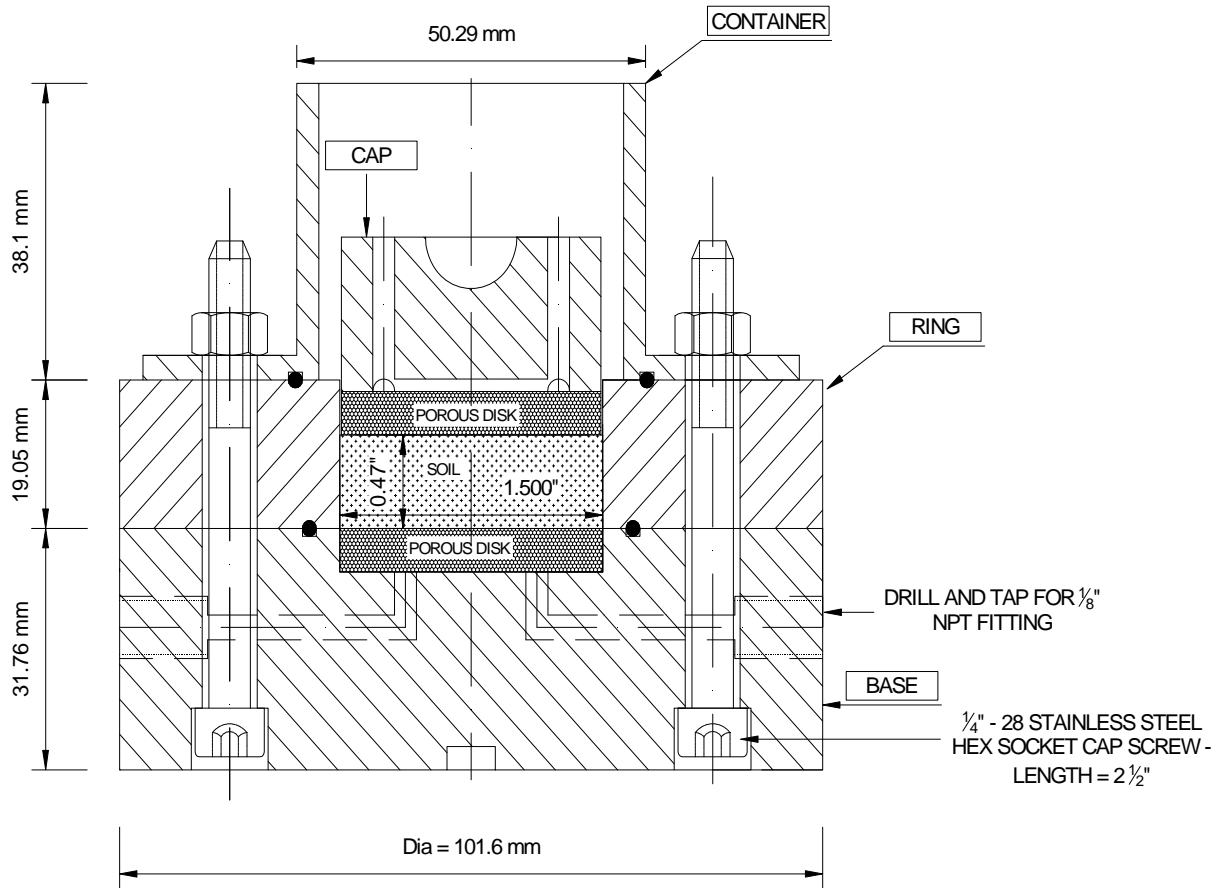


Figure 25. Cross-section through apparatus used for one-dimensional compression experiments.

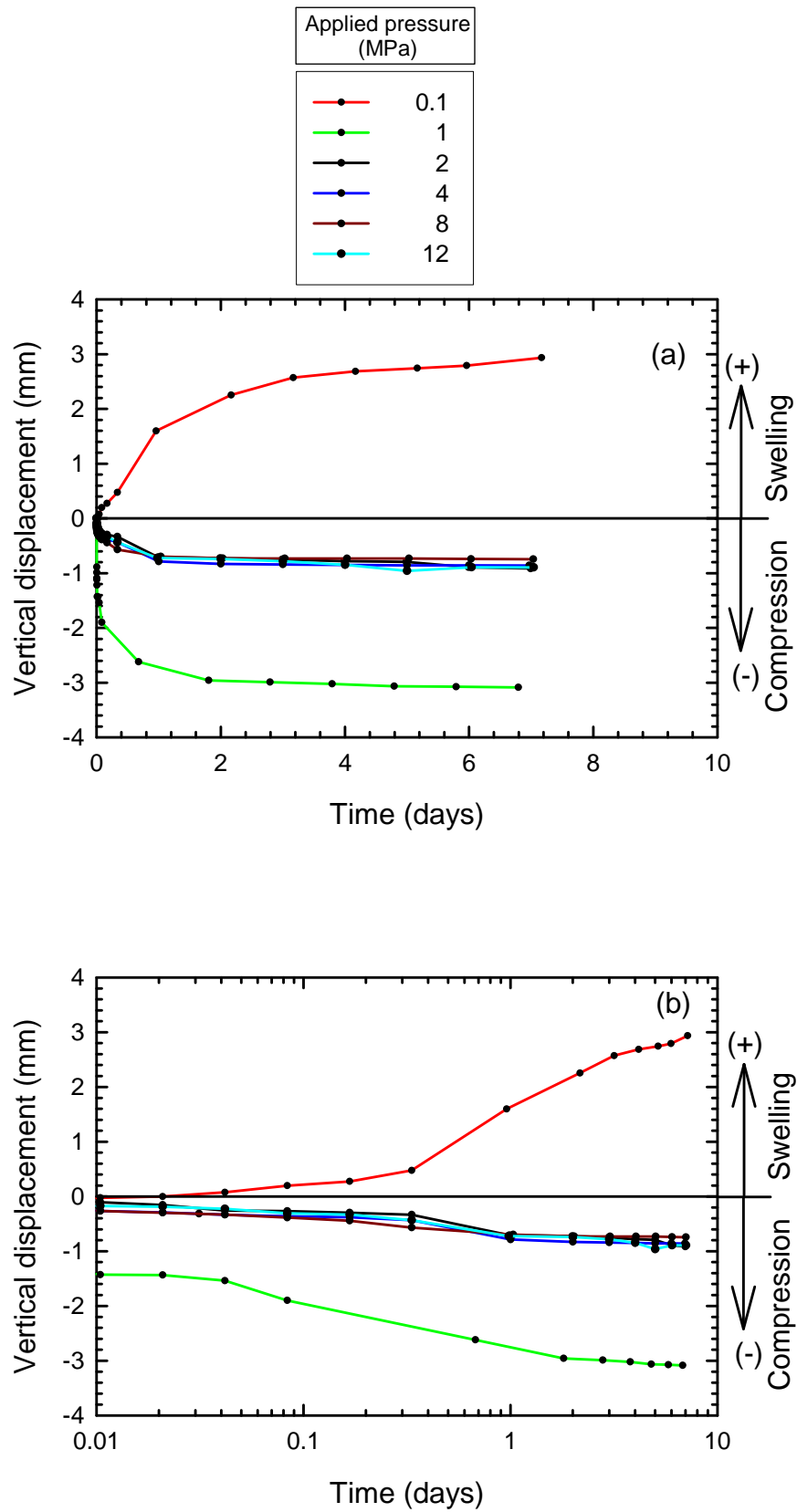


Figure 26. (a) Time and (b) log time versus measured vertical displacement for each load increment on MX-80 initially compacted to an initial dry density of 1.58 Mg/m³ with DI water

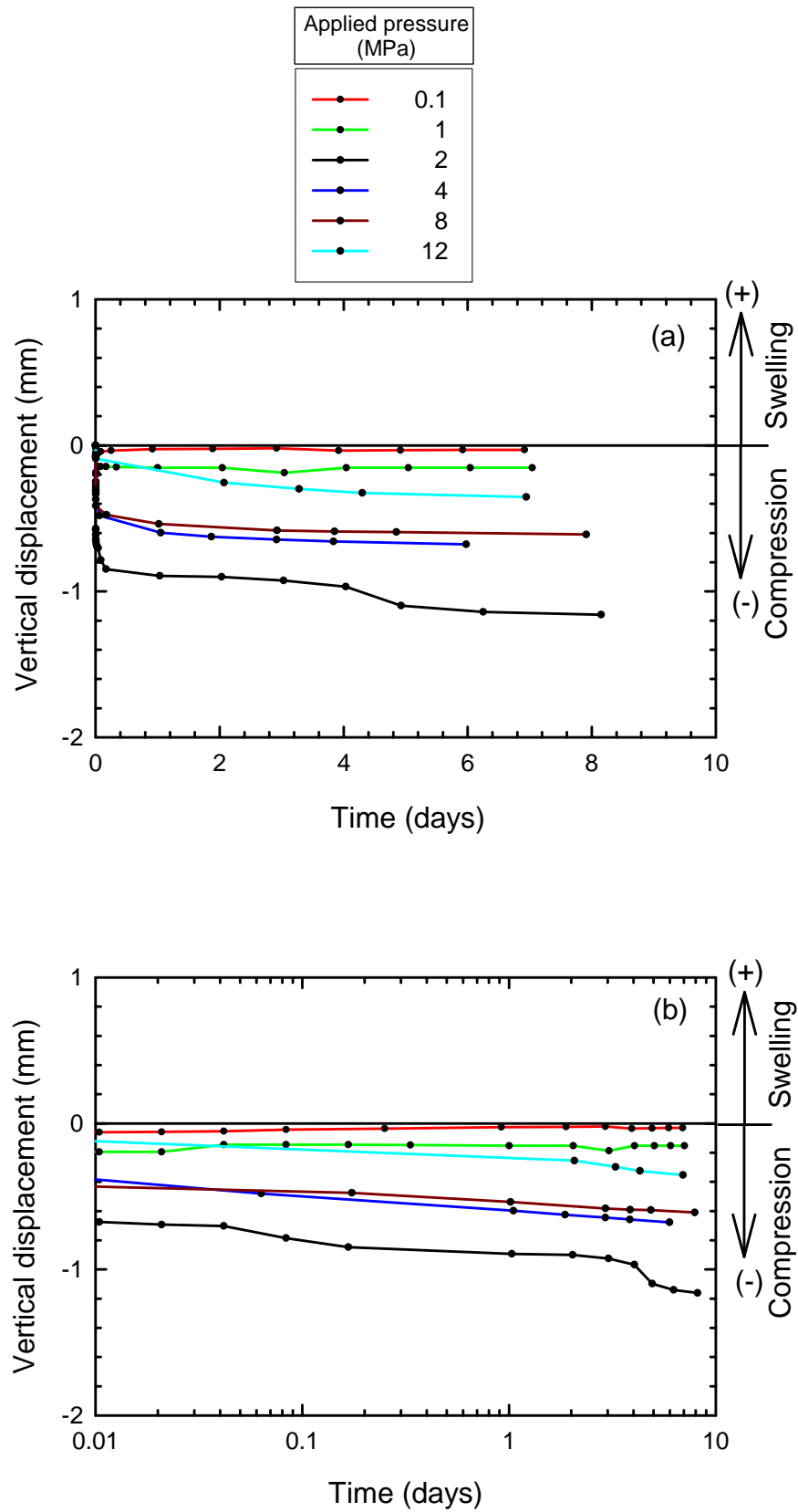


Figure 27. (a) Time and (b) log time versus measured vertical displacement for each load increment on MX-80 initially compacted to an initial dry density of 1.57 Mg/m^3 with model water

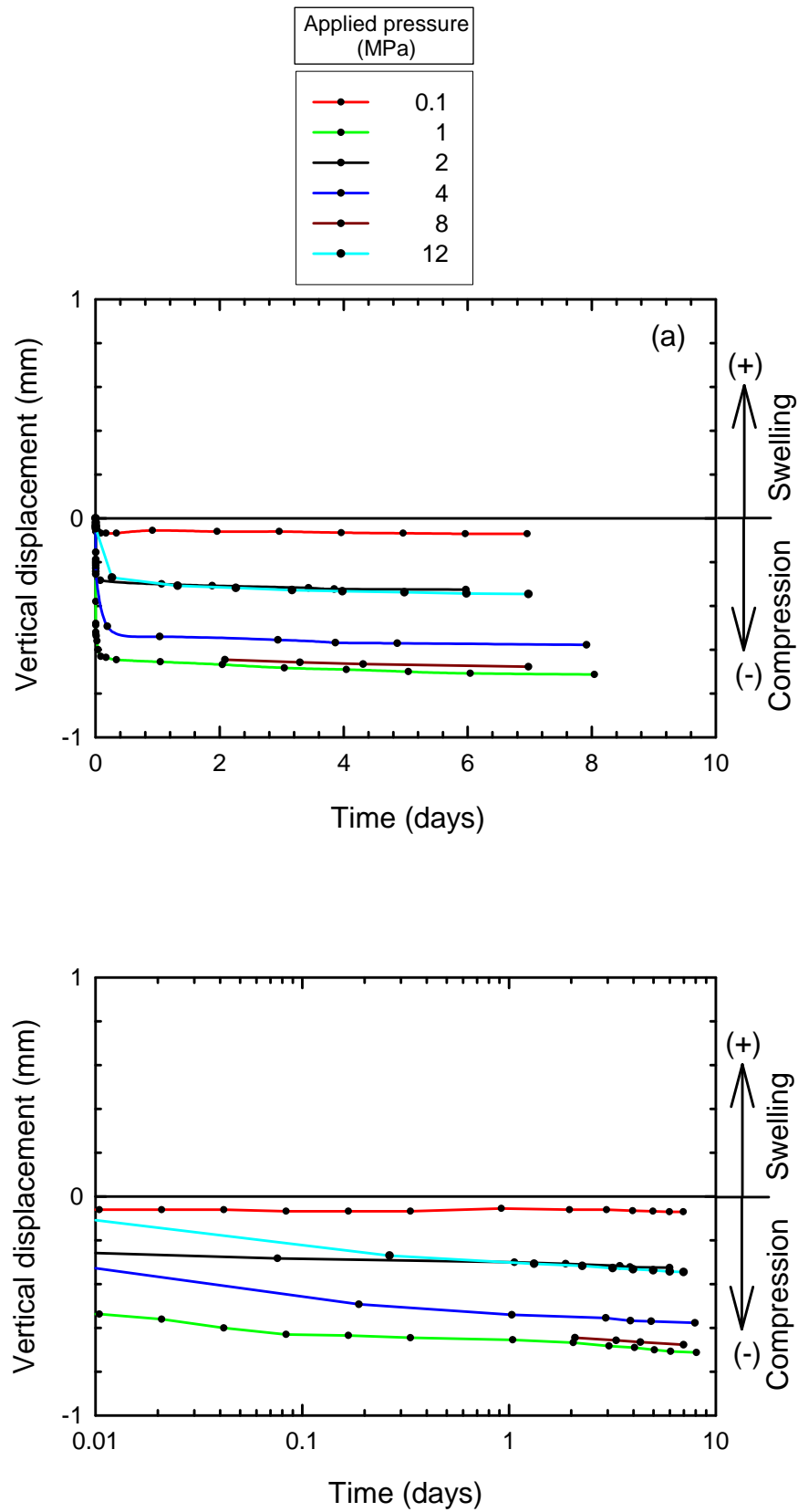


Figure 28. (a) Time and (b) log time versus measured vertical displacement for each load increment on MX-80 initially compacted to an initial dry density of 1.42 Mg/m³ with model water

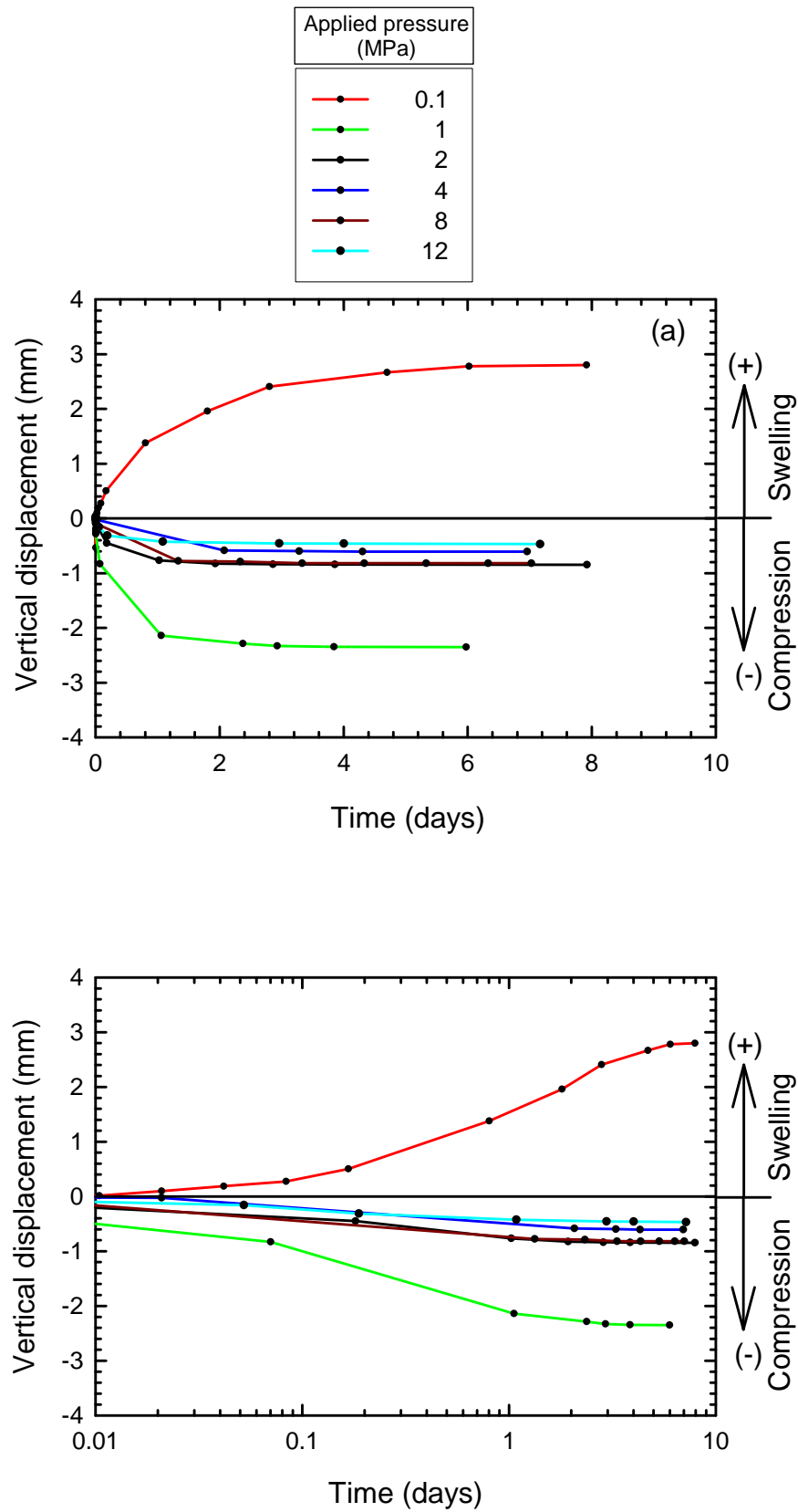


Figure 29. (a) Time and (b) log time versus measure vertical displacement for each load increment on MX-80/SP initially compacted to an initial dry density of 1.64 Mg/m^3 with DI water

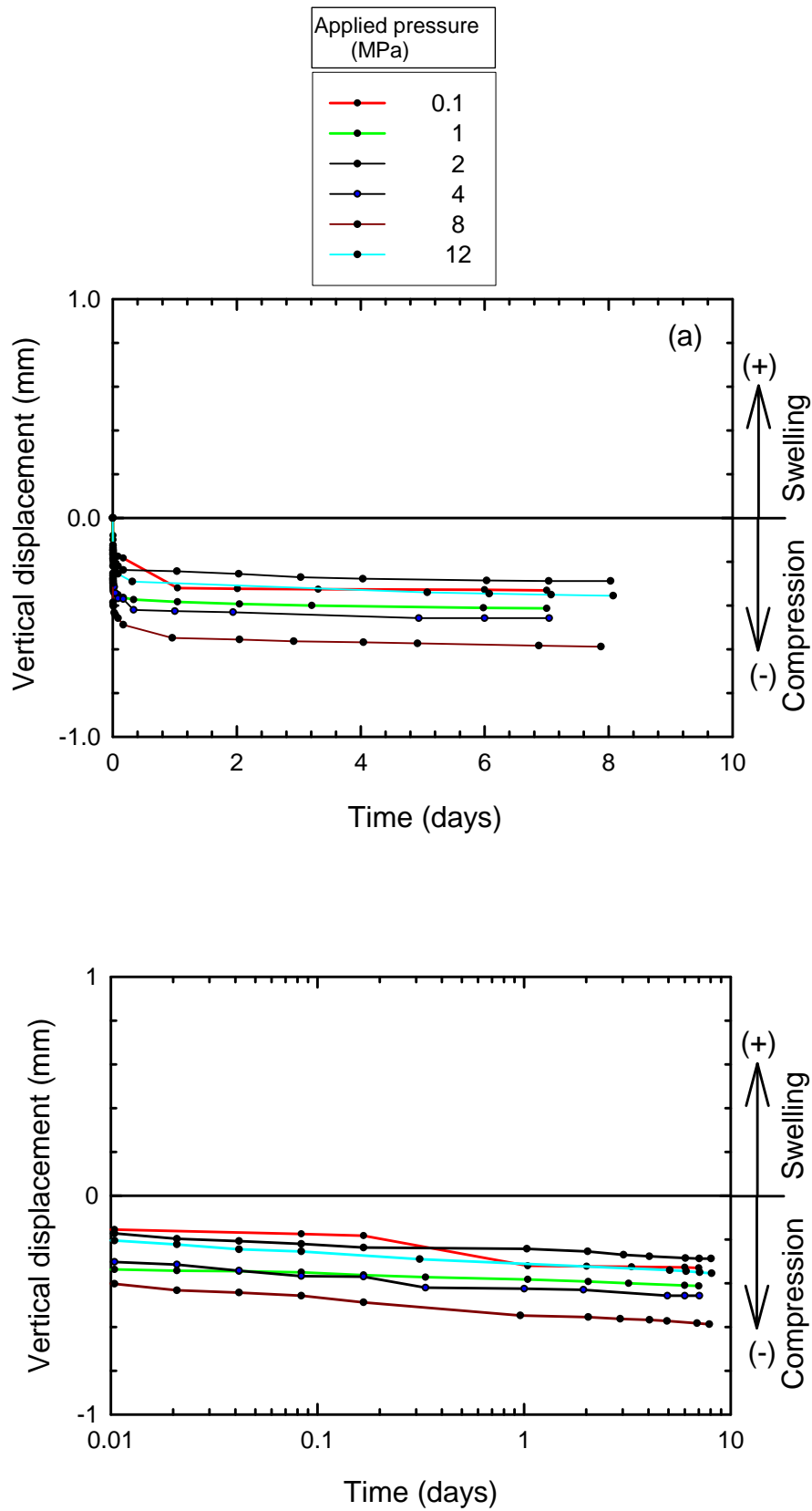


Figure 2: . (a) Time and (b) log time versus measured vertical displacement for each load increment on MX-80/SP initially compacted to an initial dry density of 1.65 Mg/m^3 with model water

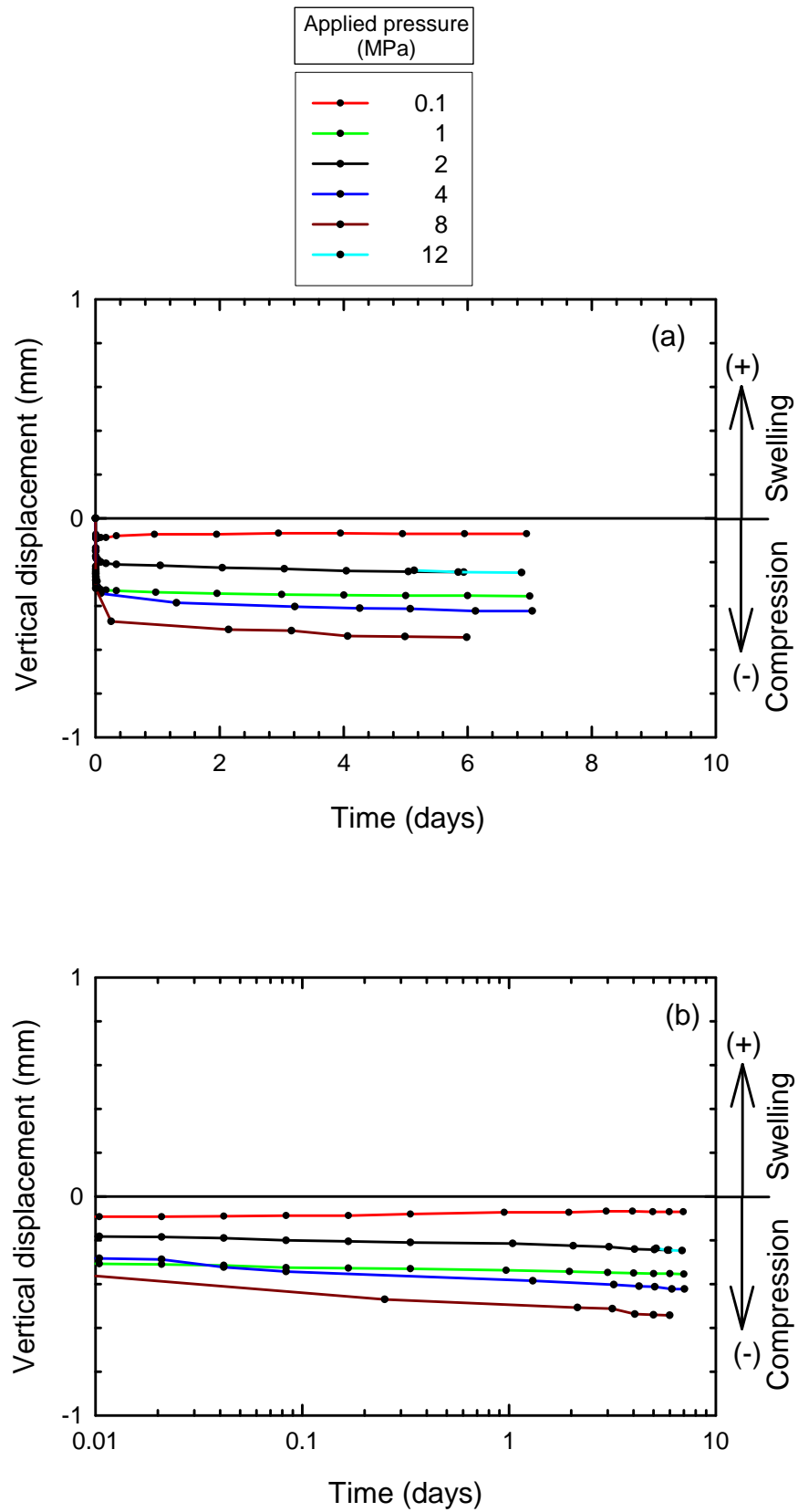


Figure 2; . (a) Time and (b) log time versus measured vertical displacement for each load increment on MX-80/SP initially compacted to an initial dry density of 1.75 Mg/m^3 with model water

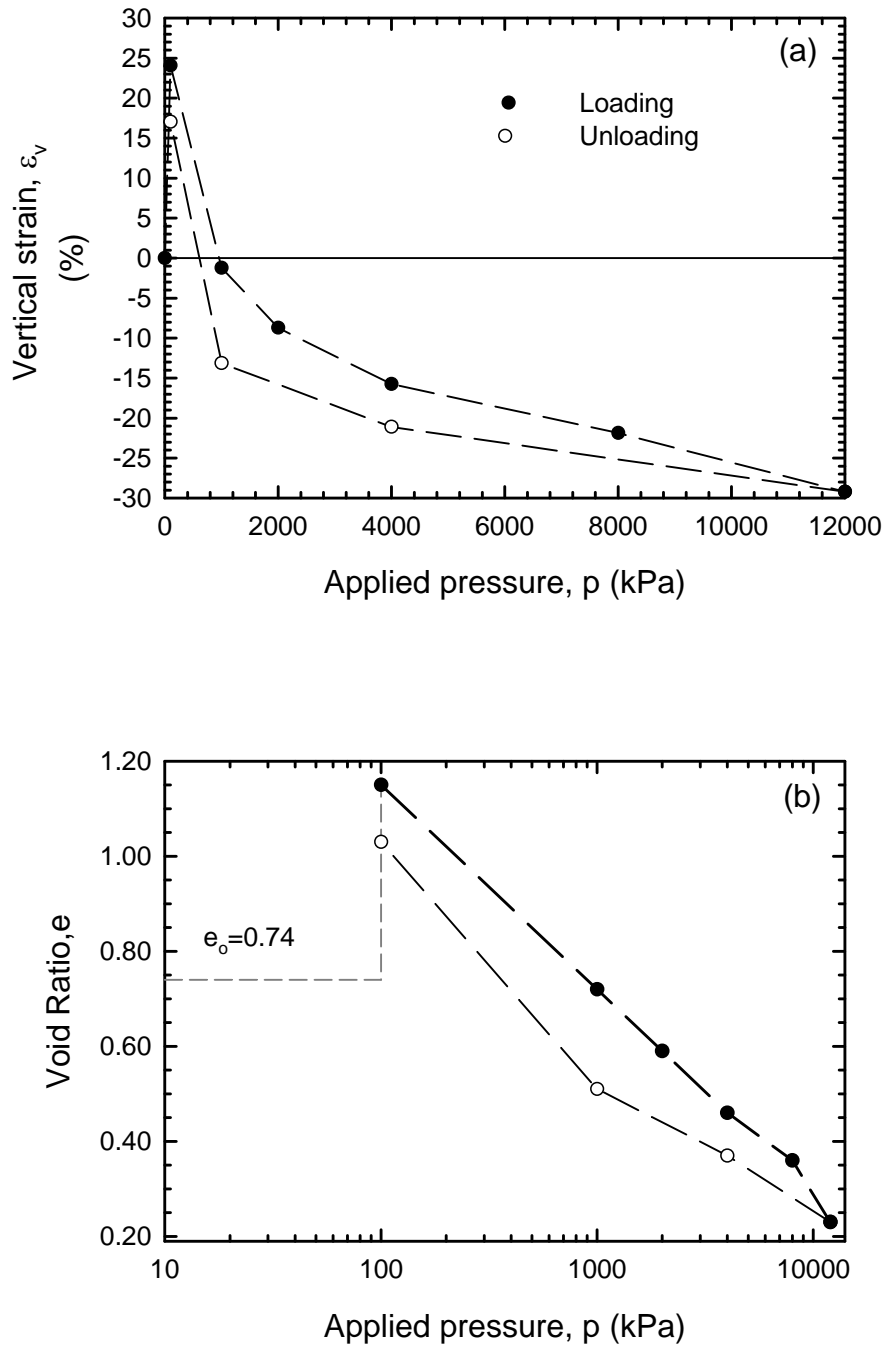


Figure 52. (a) Vertical strain and (b) void ratio versus applied pressure on MX-80 initially compacted to an initial dry density of 1.58 Mg/m^3 with DI water

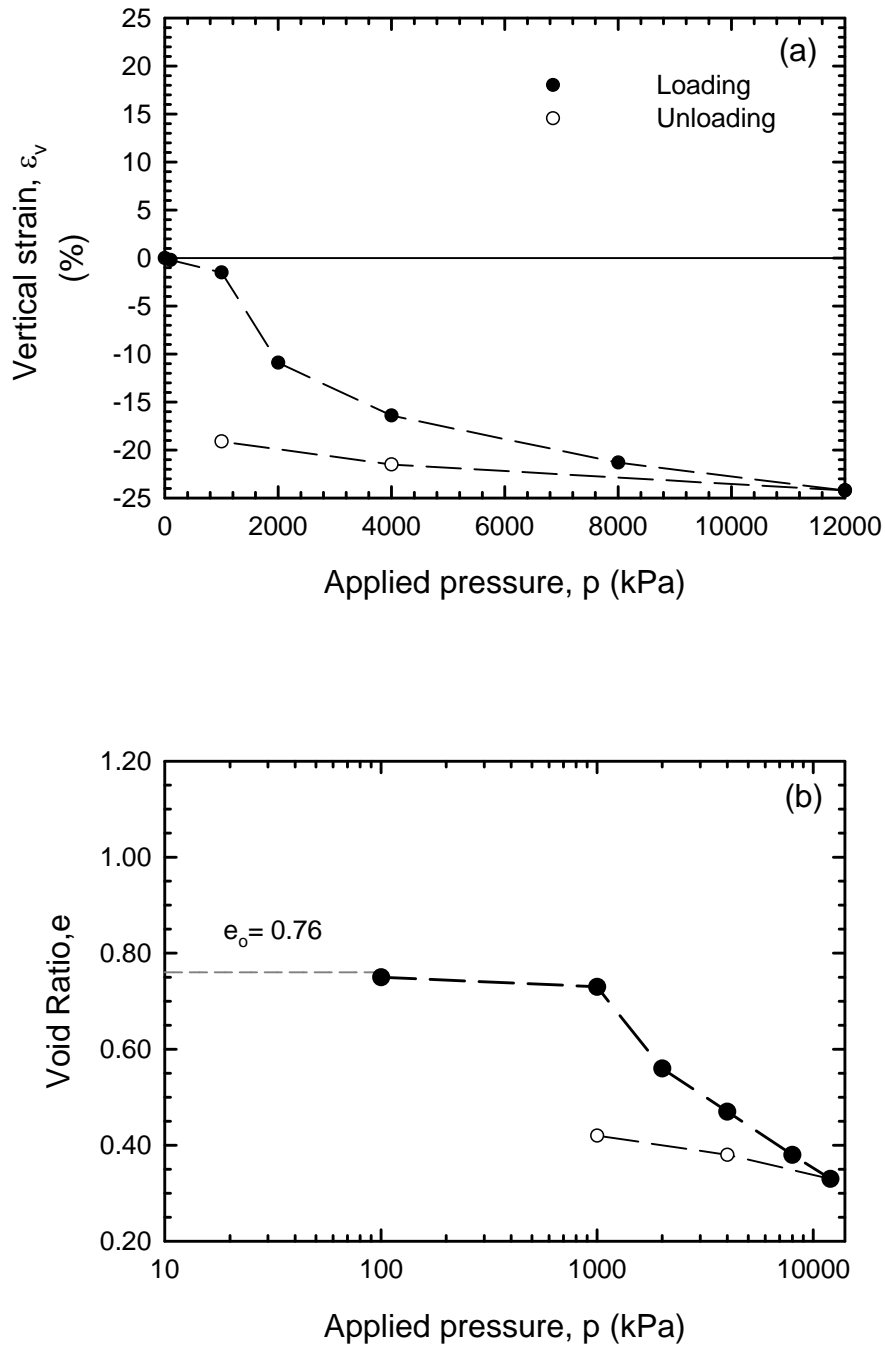


Figure 53. (a) Vertical strain and (b) void ratio versus applied pressure on MX-80 initially compacted to an initial dry density of 1.57 Mg/m^3 with model water

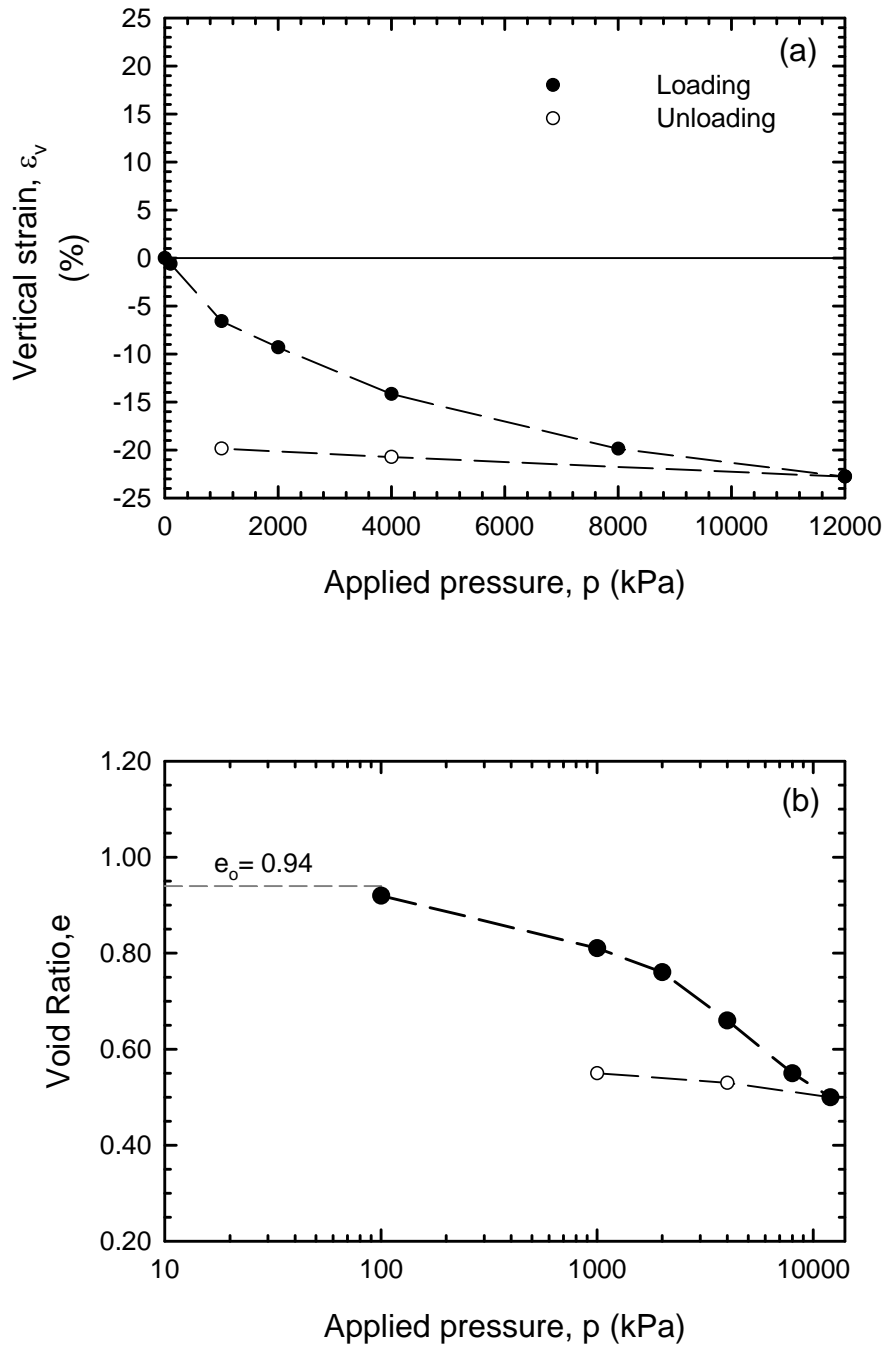


Figure 54. (a) Vertical strain and (b) void ratio versus applied pressure on MX-80 initially compacted to an initial dry density of 1.42 Mg/m^3 with model water

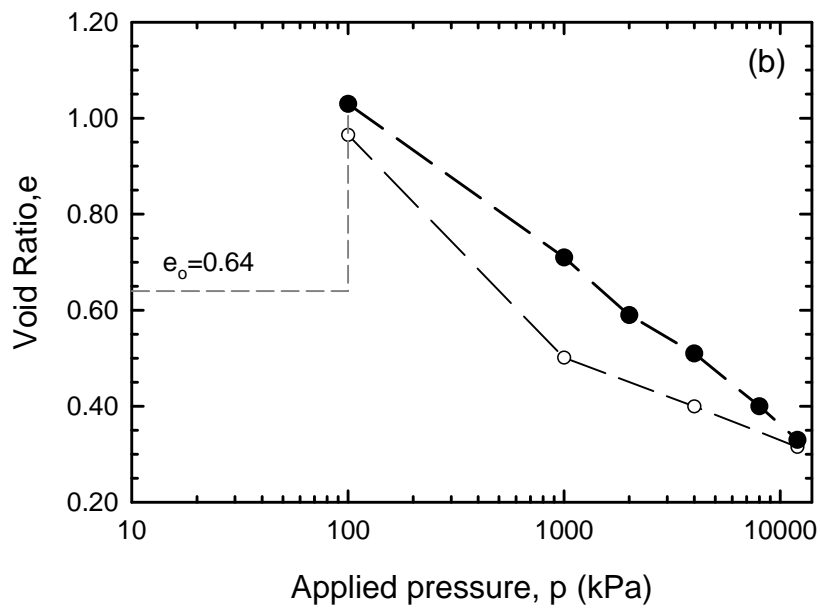
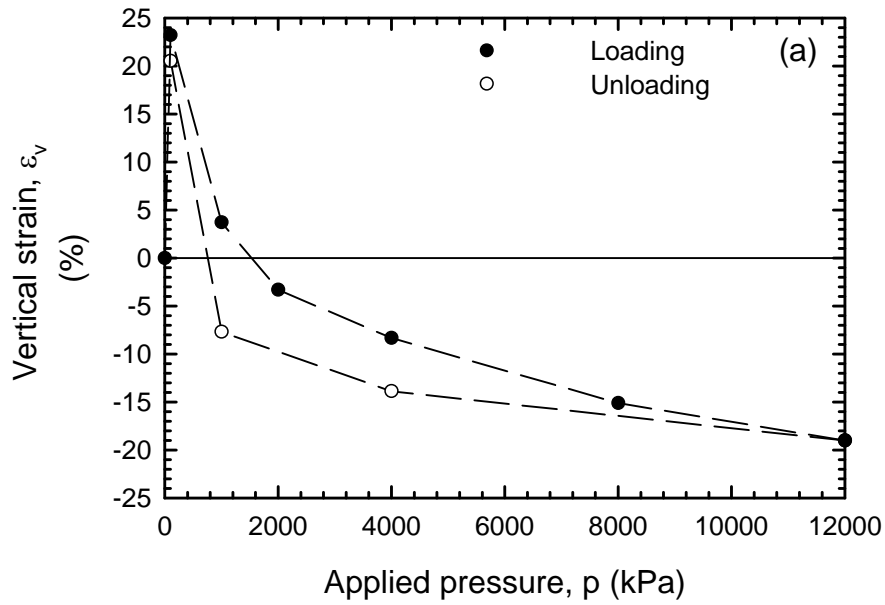


Figure 35. (a) Vertical strain and (b) void ratio versus applied pressure on MX-80/SP initially compacted to an initial dry density of 1.64 Mg/m^3 with DI water

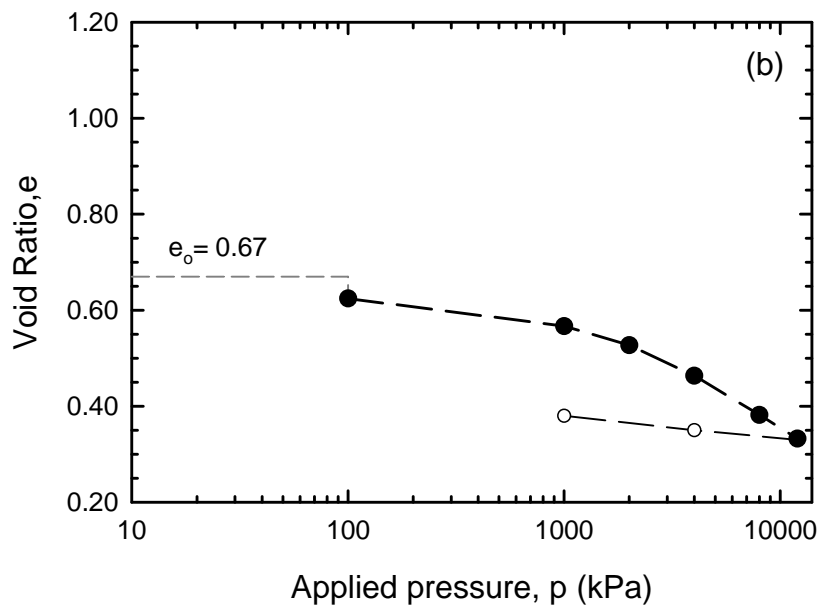
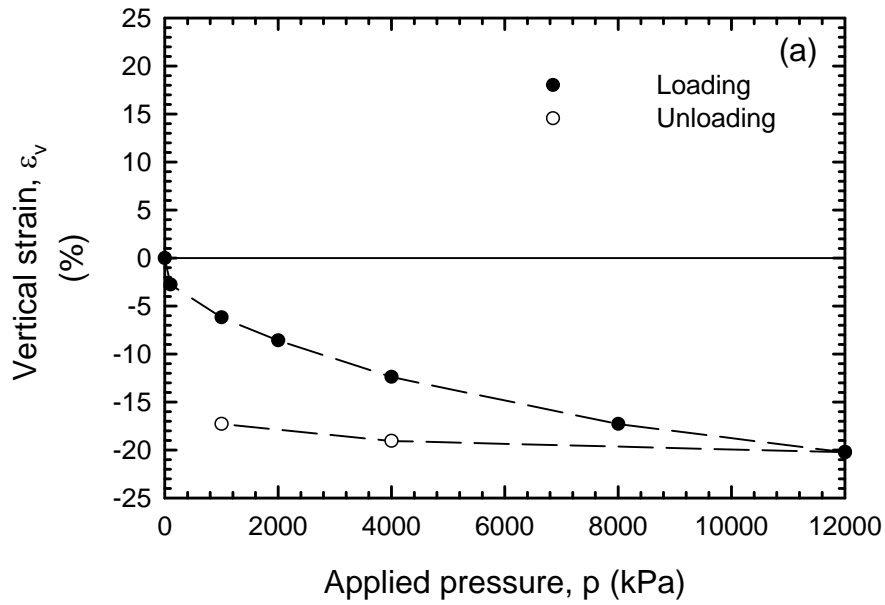


Figure 36. (a) Vertical strain and (b) void ratio versus applied pressure on MX-80/SP initially compacted to an initial dry density of 1.65 Mg/m^3 with model water

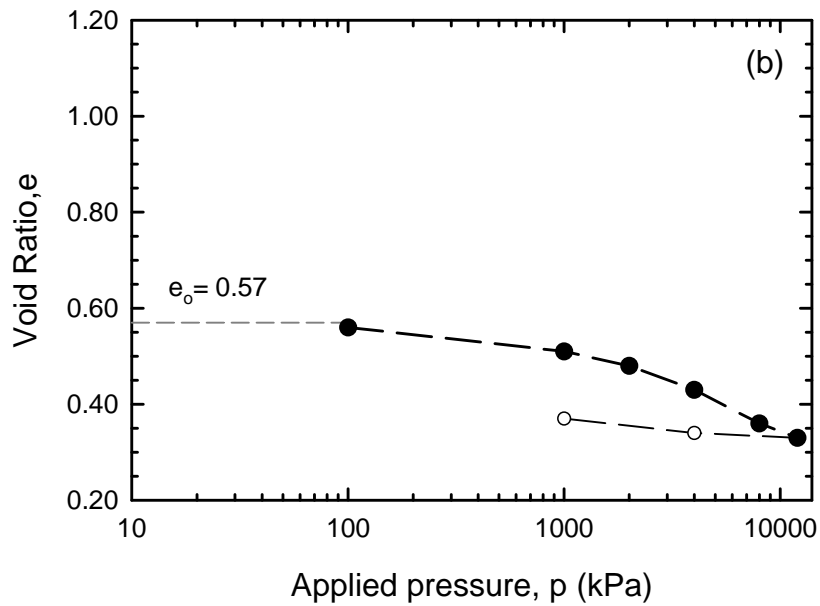
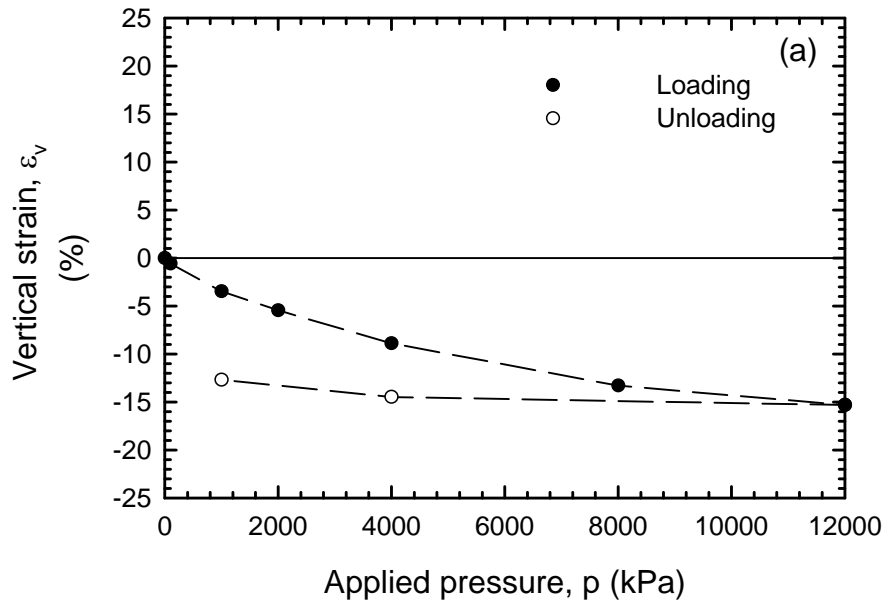
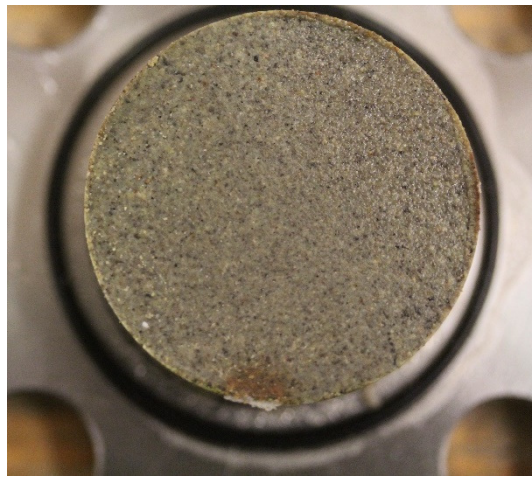


Figure 37. (a) Vertical strain and (b) void ratio versus applied pressure on MX-80/SP initially compacted to an initial dry density of 1.75 Mg/m^3 with model water



a) Specimen 1.3 (1.64, MX-80, DI)



b) Specimen 2.1 (1.63, MX-80, MW)

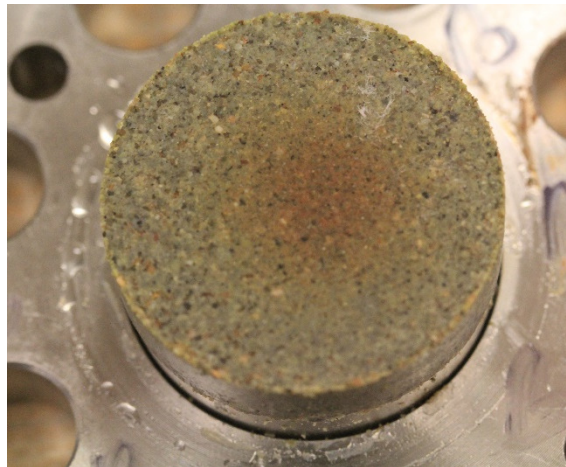


c) Specimen 3.1 (1.42, MX-80, MW)

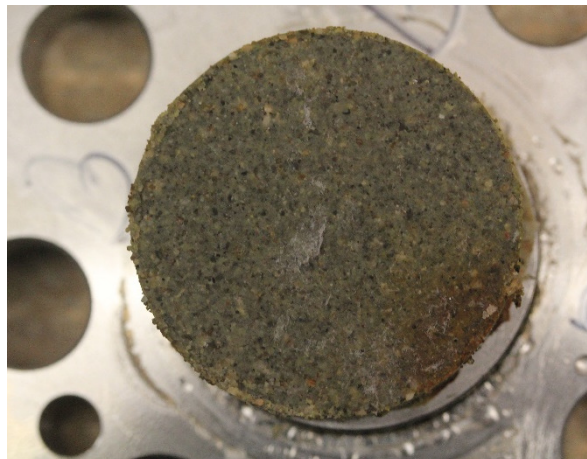
Figure 38. Photographs showing bottom of 38 mm diam. specimens.



d) Specimen 4.1 (1.65, MX-80/SP, DI)

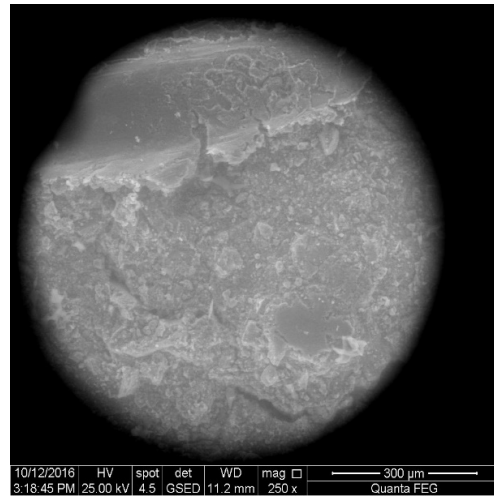


e) Specimen 5.1 (1.67, MX-80/SP, MW)



f) Specimen 6.1 (1.79, MX-80/SP, MW)

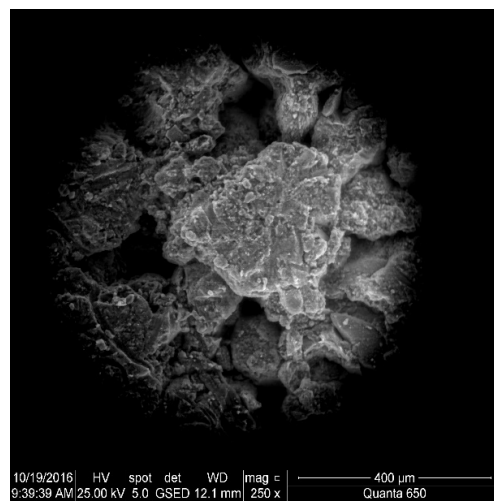
Figure 38. continued.



a) Specimen 1.3 (1.64, MX-80, DI)

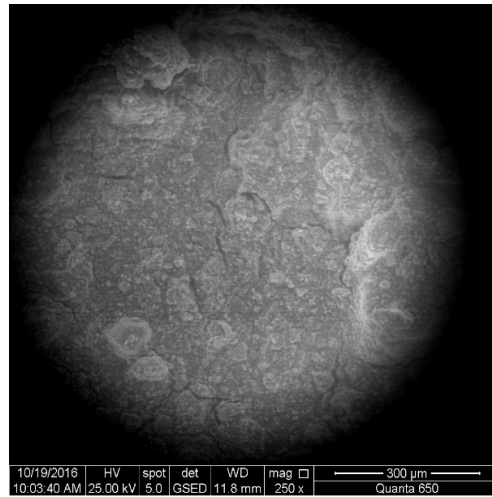


b) Specimen 2.1 (1.63, MX-80, MW)

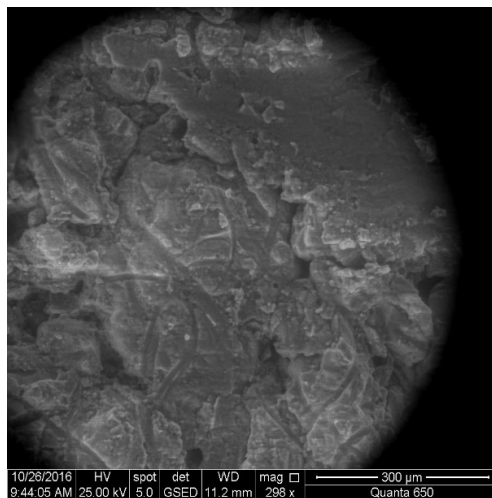


c) Specimen 3.1 (1.42, MX-80, MW)

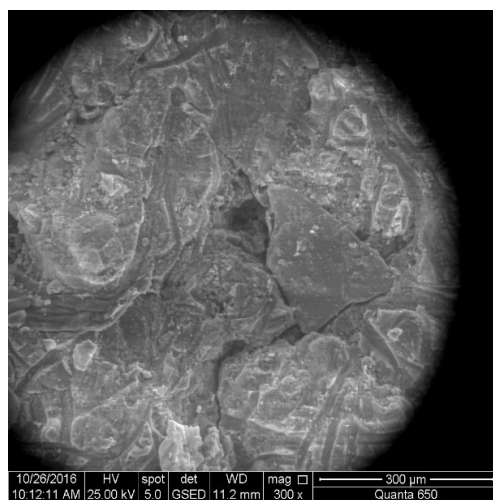
Figure 39. ESEM images.



d) Specimen 4.1 (1.65, MX-80/SP, DI)



e) Specimen 5.1 (1.67, MX-80/SP, MW)



f) Specimen 6.1 (1.79, MX-80/SP, MW)

Figure 39. continued.

Appendix 1. Bentonite evaluation

A1.1 Obtaining Bentonite

On three occasions samples of “MX-80 bentonite” were requested from CETCO, a subsidiary of the American Colloid Company. “MX-80 bentonite ... similar to the ones used in the SEALEX project” was the extent of the description of the material to be tested for this project as detailed by CNSC in the Request for Proposal (87055-14-0228). The adopted approach was to request what was specified by CNSC (MX-80 bentonite) and then quantify the material that was provided for testing. This was considered the best approach in the absence of a specification other than its classification as “MX-80” since this is the bentonite likely to be used for any specific project in the absence of a more definitive specification.

A1.3 Bentonites

Four bentonites are discussed in this Appendix and are described below.

MX-80-QU-B1: This is the first batch of MX-80 obtained by Queen’s. It was used only for assessing the effect of model water composition on Swell Index (Table 4). Since the initial dry granule size did not match that reported by Wang (2012), a second batch of bentonite was requested. However, since Swell Index measures potency of the clay fraction and not grain size (crushing required as part of procedure) the results obtained with MX-80-QU-B1 for the model water composition study are considered valid.

MX-80-QU-B2: This is the second batch of MX-80 obtained by Queen’s. It is the MX-80 bentonite used for all swell pressure, permeation, radial gap sealing, one-dimensional compression, and zero-restraint wetting-path suction measurements experiments.

MX-80-QU-B3: This is the third batch of bentonite obtained by Queen’s. It was used to assess MX-80 bentonite variation.

GCL-NWL-QU: This material is used as an internal standard of known high-quality, montmorillonite-rich, natural Wyoming sodium bentonite. It was obtained from a GCL sample of product NWL provided by Terrafix (Toronto).

MX-80-WyR1m: This material serves as a comparison to high-quality data reported in the literature. This is a Wyoming MX-80 material obtained in 2001 and reported by Karnland et al. (2006). It is used to compare MX-80-QU-B2 with previously reported values for MX-80. “R1m” was used by Karnland et al. (2006) to identify this value as the calculate mean of three diffractograms (WyR1a, WyR1b and WyR1c).

A1.4 Swell Index

Table A1-1 provides a summary of the Swell Index tests conducted as per ASTM D5890 on the three batches of MX-80 obtained for this project. Swell Index provides a measure of the potency of the clay fraction volumetric swell in deionized water per initial 2 g of dry bentonite.

There was no statistically significant difference between the Swell Index of the three batches tested (B1-B3). Thus Batch 2 (MX-80-QU-B2) used for testing does not appear to be anomalous when requesting MX-80 without a more detailed specification on mineralogy and exchange complex.

The Swell Index values ranging from 14 to 25 mL/2g in Table A1-1 is not inconsistent with the range of 12 to 26 mL/2g reported for Free Swell Index by IAEA (2013, p. 83, Table 5.5) from a synthesis of data for “USA, MX-80” materials. The large variation in swell index is consistent with bentonite being a processed and blended product. As noted by Karland et al. (2006, p. 11), MX-80 produced by the American Colloid Company “is a blend of several natural sodium dominated bentonite horizons, that are mined, dried and milled to millimeter-sized grains”. Consequently, variations in swell index are to be expected.

In an attempt to reduce the potential variability of test specimens obtained from Batch 2, a 3 kg sample was taken from Batch 2 and then was well mixed. Based on 15 random specimens from that well-mixed sample, the Swell Index only varied between 19 and 22 mL/2g and had a mean of 20 mL/2g a standard deviation of 1 mL/2g. It appears that obtaining test specimens from larger well-mixed samples can reduce the potential for obtaining low swell index samples.

A1.5 X-ray Diffraction for mineral identification

Fig. A1-1 shows X-ray diffraction (XRD) traces (air dried, random orientation) on two specimens of MX-80-QU-B2. The first was obtained from a 3 kg mixed sample with SI=20 mL/2g (std dev.=1 mL/2g, n=15) prior to obtaining the 0.2 g specimen for analysis. The second was obtained from a 20 g sample with SI=16 mL/2g (n=1). This low SI specimen was intentionally selected to examine whether mineralogy could explain the observed variations in Swell Index. It was obtained by selecting the lowest SI value sample from 10 random 20-g-samples from Batch 2. An XRD trace on the internal montmorillonite standard (GCL-NWL-QU) is given in Fig. A1-2.

These results were obtained with a Panalytical X’Pert Pro MPD diffractometer fitted with an X’Celerator high speed strip detector and K-beta filtered Co radiation ($\lambda=1.79 \text{ \AA}$). The bentonite was ground to a powder finer than 75 μm in diameter; a portion of the powder was mounted with methanol as a thin oriented smear on glass disk. Samples were scanned from 4 to 70 degrees 2θ using a count time of 10 seconds/degree at 0.02 degree increments and a sample rotation of 2 seconds per revolution. PANalytical HighScore Pro software was used for phase identification; the software compares the peak positions and peak intensities to data in the large ICDD (International Centre of Diffraction Data) PDF2+ database of known phases. In addition, a semi-quantitative determination of the percentage of the major minerals in the bentonite samples was performed using integrated peak areas and reference intensity ratio factors. The results were given in Table 1.

The predominant feature at $2\theta=8.3$ degrees (interlayer spacing =1.2 nm) in Fig. A1-1 is the primary smectite peak. Secondary smectite peaks appear at 23 and 33 degrees. Based on the available data and analysis with the PANalytical HighScore Pro software, the smectite phase was identified as beidellite (very similar to montmorillonite, but with its charge deficiency predominantly in the tetrahedral layers). Additional preferred-orientation XRD testing with different treatments would be required to better identify the smectite mineral present. The deduced smectite content for the MX-80-QU-B2 specimen with SI =20 mL/2g was 83%.

In contrast to Fig. A1-1, the trace for the internal standard GCL-NWL-QU showed a strong montmorillonite peak at 2θ of 7.6 degrees (1.4 nm), Fig. A1-2, indicative of a very high-quality (96%) montmorillonite specimen.

In order to compare with MX-80-WyR1 results from Karnland et al. (2006), the XRD traces for MX-80-QU-B2 and GCL-NWL-QU are replotted in Fig. A1-3 for copper radiation. The specimen from the well-mixed sample of MX-80-QU-B2 (with SI=20 mL/2g, std dev.=1 mL/2g, n=15) had a similar smectite content (83%) as the mean (83.5%) and range (81.1-85.8%) reported by Karnland et al. (2006) for a 2001 sample of Wyoming MX-80 material (denoted as MX-80-WyR1).

The location of the smectite peak around 2θ of 7.3 degrees (interlayer spacing =1.2 nm) for XM-80-WyR1m in Fig. A1-3c is not the typical “textbook” montmorillonite peak like that for GCL-NWL-QU (Fig. 3b), but is much more similar to the MX-80-QU-B2 sample. While Karnland et al. (2006) identified their smectite component “generally ... as montmorillonite”, but only “... since this is the database mineral used for the quantifications. However, in order to be more precise some of the minerals should be termed beidellite according to the calculated structural formulas.” Thus the possible interpretation that the smectite phase of MX-80-QU-B2 could be dominated by beidellite is not inconsistent with Karnland et al. (2006).

A1.6 Exchange Capacity and Complex

Soluble cations, bound cations, and the cation exchange capacity of bentonite were established following ASTM D7503-10. A bentonite solid mass of 2 g was used to measure the soluble cations and 10 grams of bentonite solids was used to measure the bound cations and cation exchange capacity. The extracts from the soluble cations and bound cation tests were analyzed chemically using ICP-MS. Ammonia was measured in the extract from the cation exchange capacity test using an autoanalyzer to quantify the nitrogen in the extract and then calculate the cation exchange capacity. Results for MX-80-QU-B2 and GCL-NWL-QU were reported in Table 2.

A1.7 X-ray Diffraction for after Model Water hydration and potassium treatment

Fig. A1-4 shows preferred oriented X-ray diffraction (XRD) traces used to investigate possible changes in mineralogy after Model Water hydration or alteration of the smectite peak upon treatment with potassium chloride. Soil samples were first ground to be finer than 75 μm . A 0.2 g portion of the air dried powder was mounted on a glass slide with methanol. For each case after obtaining the air dried trace, the specimen was allowed to swell with ethylene glycol vapor treatment for 48 ± 6 hours at 25 ± 2 °C prior to obtaining a second trace to principally observe the response of the primary smectite peak.

For reference, Fig. A1-4a shows the air dried smectite peak of a natural (as-received) sample of MX-80-QU-B2 at $2\theta=8.2$ degrees (interlayer spacing =1.26 nm) moving to $2\theta=6.1$ degrees (1.67 nm) after glycolation. The increased interlayer spacing (decreased 2θ position) is from swelling of the clay mineral. The air dried and glycol interlayer spacings are within the range listed for smectite by Mitchell and Soga (2005).

The effect of potassium treatment on a natural sample of MX-80-QU-B2 is shown by Fig. A1-4b. The treatment involved free swell hydration of 100 g of MX-80 bentonite in 1 litre of KCl solution that had the same potassium concentration as the Model Water (41 g/L) for one month at room temperature. Upon air drying, the resulting clay mineral peak was more diffuse than the natural trace and centred near $2\theta=9$ degrees (1.2 nm). Similarly, the traces obtained

after 1 year of Model Water hydration are shown in Figs A1-4c and A1-4d. These traces were obtained on soil specimens obtained upon termination of Swell Pressure Tests 2.3 and 2.3(a4) (details given in Table 4). Diffuse primary clay mineral peaks near $2\theta=10$ degrees (1.0 nm) were obtained for both Model Water hydrated traces upon air drying. For both the KCl treated and MW hydrated cases, the increased 2θ position may be an indication of 'c-axis' contraction from interactions with hydrated potassium at the clay mineral surface, particularly near the ditrigonal cavities ('hexagonal holes') in the silica sheets. Rowe et al. (2004) detail a similar sort of interaction of potassium with clay mineral vermiculite. However, these traces were intentionally conducted on potassium treated and MW hydrated specimens where the residual KCl or Model Water was not washed out of the specimen (e.g., to avoid the potential of losing soil solids). Additional research (beyond the scope of this project) would be useful here with validation of enhanced sample preparation techniques to investigate potential mineralogical changes after relatively high concentration (41 g/L) KCl treatment, or relatively high concentration (see Table 3) Model Water hydration. Upon glycolation of the potassium treated (Fig. A1-4b) and MW hydrated specimens (Figs A1-4c and A1-4d), the clay primary mineral peak shifted to $2\theta=6.1$ degrees (1.67 nm). That the clay still swells much like the natural sample suggests no permanent fixing of interlayer potassium.

Table A1-1. ASTM D5890 Swell Index, SI, values (mL/2g) from three batches of MX-80 obtained by Queen's University.

Batch	Mean	Std dev.	Max.	Min.	No. of tests
MX-80-QU-B1	21	2	21	20	3
MX-80-QU-B2	19	2	25	14	33
MX-80-QU-B2*	20	1	22	19	15
MX-80-QU-B3	18	1	19	17	5

* subset of Batch 2 where a 3 kg sample was mixed prior to obtaining specimens for testing

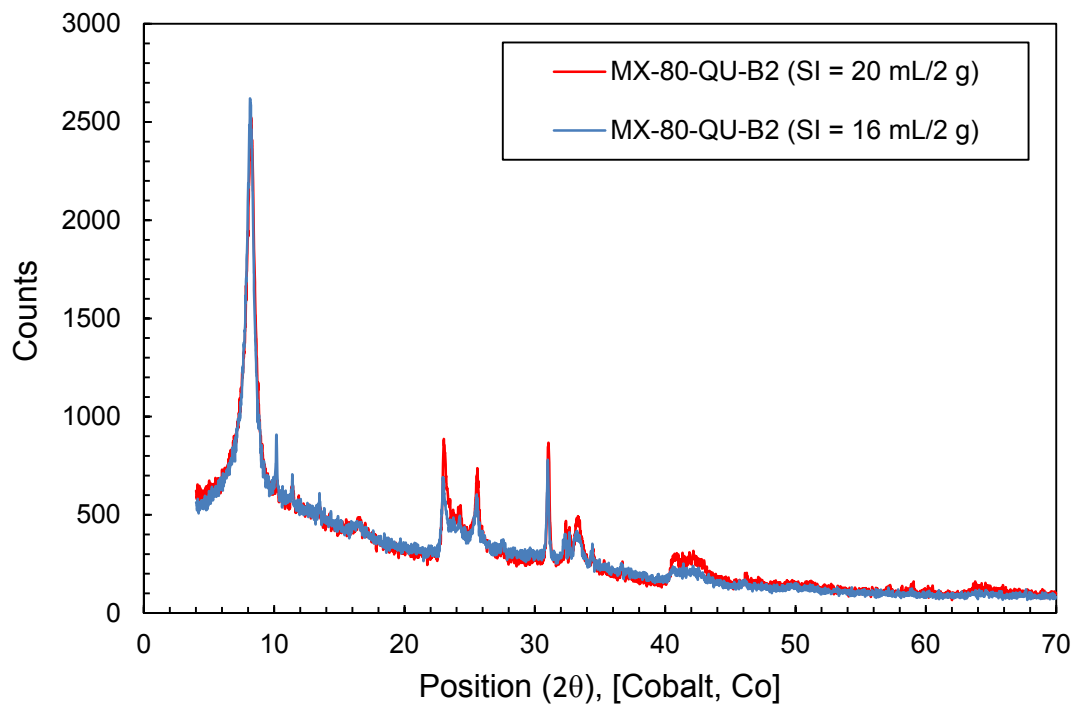


Fig. A1-1. XRD of MX-80-QU-B2 bentonite for two specimens; one with a swell index (SI) = 20 mL/2 g and the other one has a SI = 16 mL/2 g using K-beta filtered Co radiation ($\lambda=1.79 \text{ \AA}$). Position in degrees.

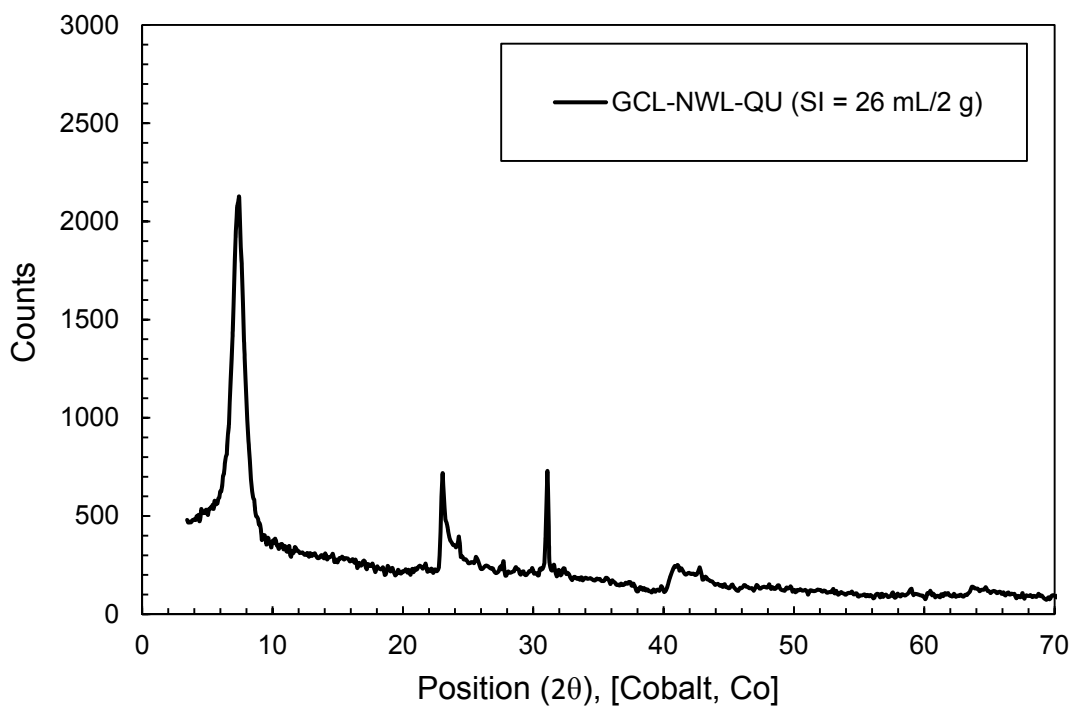


Fig. A1-2. XRD of GCL-NWL-QU bentonite using K-beta filtered Co radiation ($\lambda=1.79 \text{ \AA}$). Position in degrees.

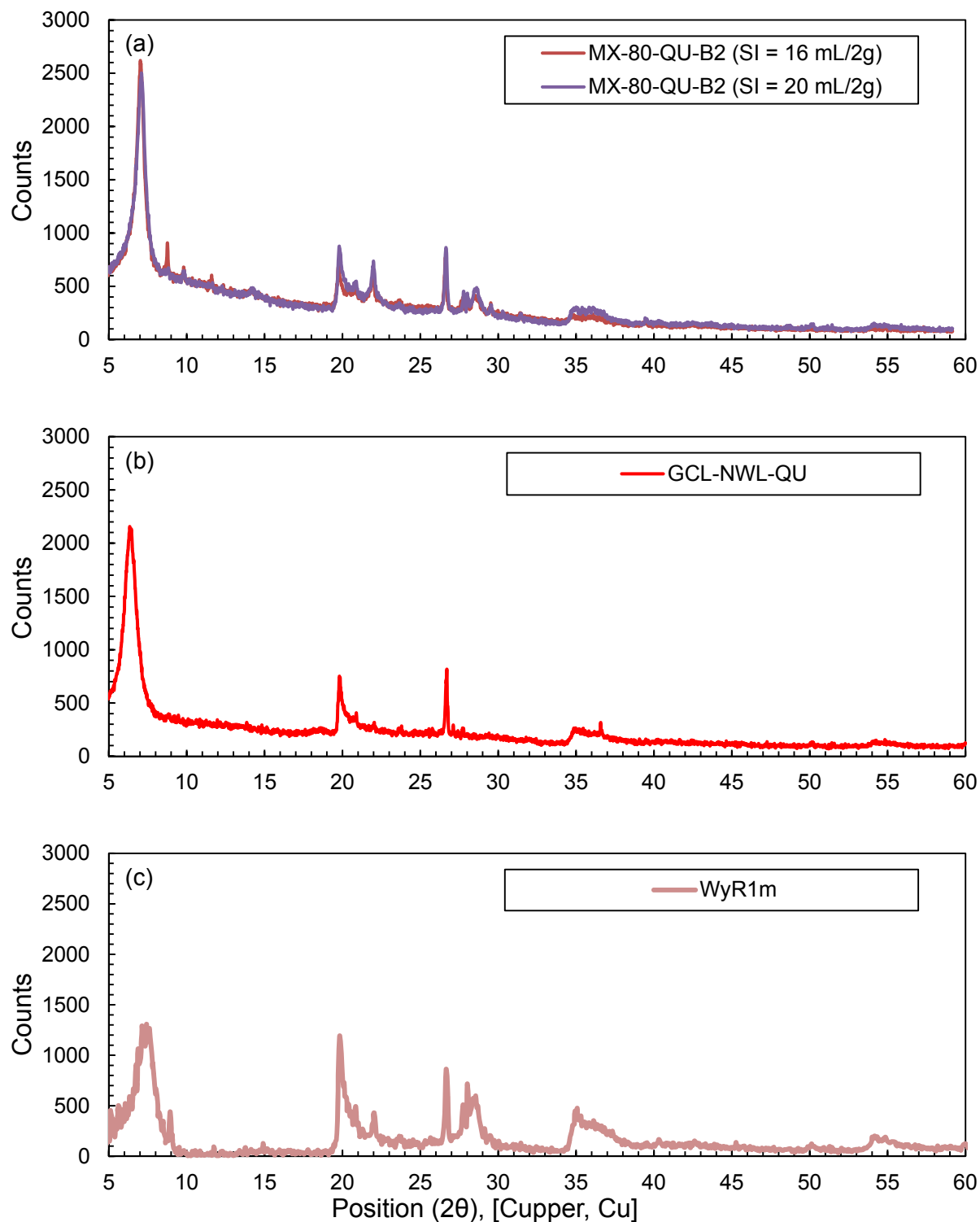


Fig. A1-3. XRD of: (a) MX-80-QU-B2 bentonite, (b) GCL-NWL-QU, and (c) MX-80-WyR1 bentonite (from Karland et al., 2006, p. 16, Fig. 3.7). XRD pattern for MX-80-QU-B2 and GCL-NWL-QU converted from K-beta filtered Co radiation ($\lambda=1.79 \text{ \AA}$) to K-beta filtered Cu radiation ($\lambda=1.54 \text{ \AA}$) to be able to compare them with WyR1. Position in degrees.

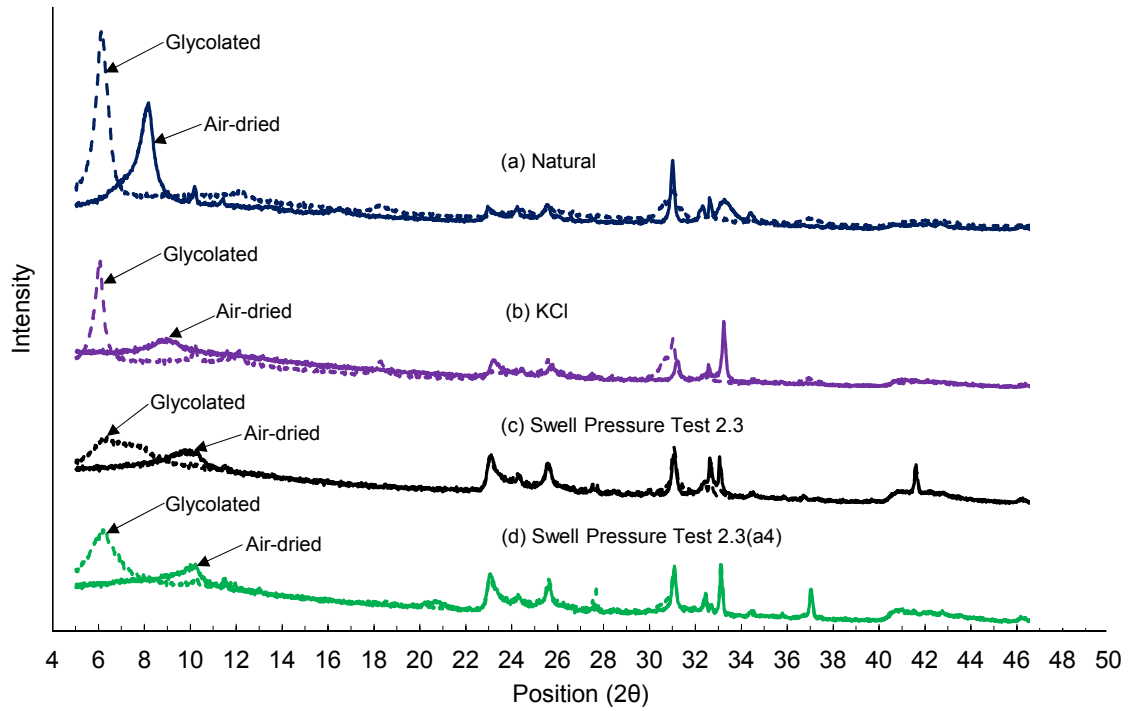


Fig. A1-4. Preferred orientation x-ray diffraction traces (soil fraction < 75 μm) for MX-80.

Appendix 2. Procedures

A2.1 Sample preparation for swell pressure, permeation and hydration tests

The procedures for preparing samples of bentonite and sand/bentonite mixtures for the swell pressure, permeation, and hydration experiments are documented in this Appendix.

1. The required amount of bentonite or bentonite-sand mixture required to achieve the target dry density was mixed with de-ionized (DI) water to achieve the desired initial bentonite water content. In most cases, and unless otherwise noted, the initial gravimetric bentonite water content was 11%. This sample (denoted herein as the soil sample) was then sealed in a container for one hour for conditioning.
2. The thickness of the porous stones and layers of filter paper to be used were measured with calipers to ± 0.1 mm.
3. An air-dried porous stone was placed into the base of the cell.
4. Two steel rings were placed on the base of the cell. The lower ring is used to contain the test sample. The upper ring is used to contain the uncompacted sample and will be removed after sample compaction. Both rings were fastened to the base with bolts.



Figure A2-1. Measurement of elevation of the top surface of the bottom porous stone with laser displacement transducer.

5. The test cell was placed under a laser beam to obtain Profile 1 that defines the elevation of the top surface of the bottom porous stone (L_1).
6. A layer of filter paper (Whatman, CAT No.1442-055, Pore size = $2.5 \mu\text{m}$, and nominal thickness of 0.15 mm) was placed on top of the porous stone.
7. The soil sample was placed inside the rings in three lightly-compacted layers of equal thickness. A 165 gm rammer falling from a height of 4 cm (± 1 cm) was used to compact each layer by imparting 15 blows per layer.
8. Another layer of filter paper was placed on top of the lightly-compacted soil sample. The upper porous stone was then placed.
9. The test cell was repositioned beneath the laser beam to obtain Profile 2 that defines the initial elevation of the top surface of the upper porous stone (L_2).

The initial soil sample thickness was calculated as $T_{\text{initial}} = L_2 - L_1$ - thickness of upper porous stone - thickness of two layers of filter paper.

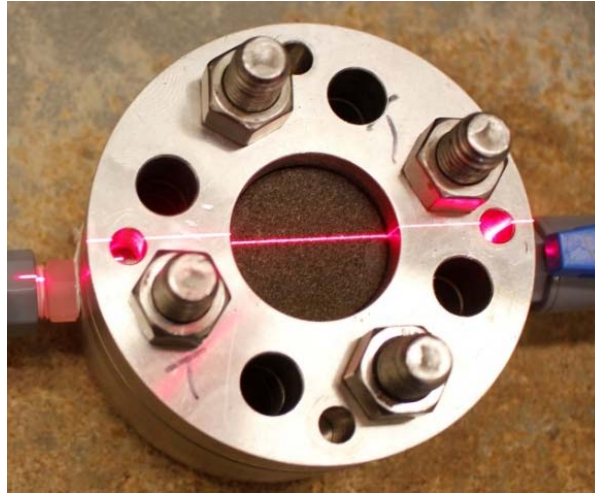


Figure M1-2. Measurement of elevation of the top surface of the upper porous stone with laser displacement transducer prior to static compaction.

10. The target compaction thickness (i.e. the thickness of the soil sample under the compaction stress) was the target final thickness of 10 mm plus an over-compression displacement. The over-compression displacement was to allow for elastic rebound of the compacted specimen upon removal of the compaction stress. Based upon trial and error, the over-compression displacement was:

Target Density (Mg/m ³)	Over compression displacement (mm)	
	MX-80/NWL	MX-80/SP
1.41	0.50-0.60	0.40-0.50
1.61	1.00-1.30	-
1.65	1.40-1.60	0.60-1.00
1.80	1.80-2.00	0.80-1.00

11. The soil sample was then statically compacted to the compaction thickness using a displacement controlled ram at a rate of 0.05 mm per minute. Once the compaction thickness was attained, the displacement was then held constant for 16 h. One of two load frames was used for static compaction. One was a 20 kN ZwickRoell (Model: MTMT1-FR020TH.A50); the other was a 50 kN GDS load frame (Model: GDSL50). Compaction force was measured with a 20 kN load cell (Model: TC-LC020KN.G02) for samples compacted with the Zwick frame. Compaction force was not measured for samples compacted with the GDS load frame.



Figure M1-3. Application of static compaction force using ZwickRoell frame.

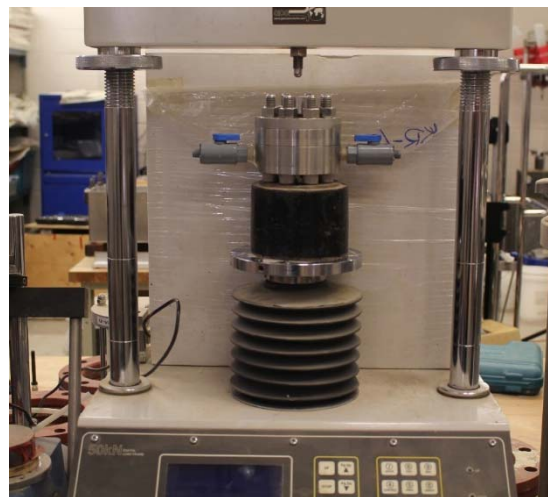


Figure M1-4. Application of static compaction force using GDS frame.

12. Following removal of the compaction stress, the test cell was repositioned beneath the laser beam to obtain Profile 3 that defines the post-compaction elevation of the top surface of the upper porous stone (L_3). The time elapsed between unloading and thickness measurement was approximately 10 minutes.

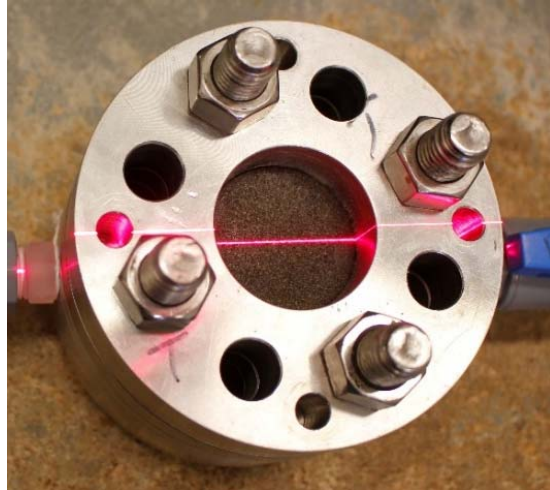


Figure M1-5. Measurement of elevation of the top surface of the upper porous stone with laser displacement transducer after static compaction.

13. Final sample thickness was taken as $T_f = L_3 - L_1$ - thickness of upper porous stone - thickness of two layers of filter paper.
14. The sample was used for testing provided that the absolute difference between the target and final sample thickness was no greater than 0.1 mm and the final sample thickness was used to compute the initial dry density. Otherwise, a new sample was prepared.

A2.2 Sample preparation for radial gap swell tests

The procedures for preparing samples of bentonite and sand/bentonite mixtures for the radial gap swell experiments were the same as detailed in Section A2.1, except for the creation of an initial radial gap as detailed in this Section.

1. Prior to placement of the soil sample in the assembled rings (Section A2.1, Step 7), a split-cylinder sleeve (outside diameter = 38 mm, inside diameter = 36.1 mm) was placed inside the apparatus.

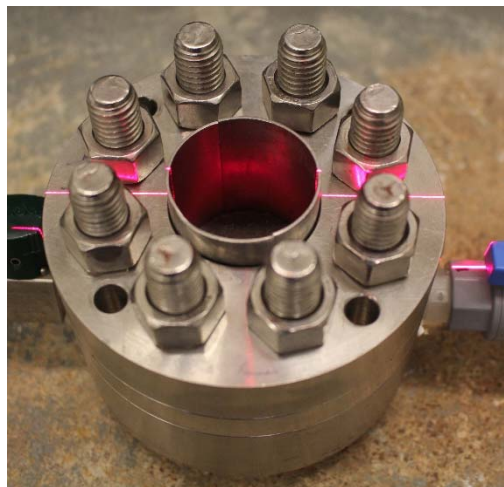


Figure A2-6. Removable sleeve placed inside rings prior to soil sample placement.

2. The soil sample was then compacted as detailed in Section A2.1. The only difference was that target final thickness was either 20 or 22.1 mm (depending on the size of rings used) as the radial gap swell tests were intended to be twice as thick as the swell pressure or permeability tests.
3. After sample compaction, and verification of acceptable final thickness (as detailed in Section A2.1) the sleeve and soil sample were extruded from the ring using the ZwickRoell ram by applying force only to the sleeve.

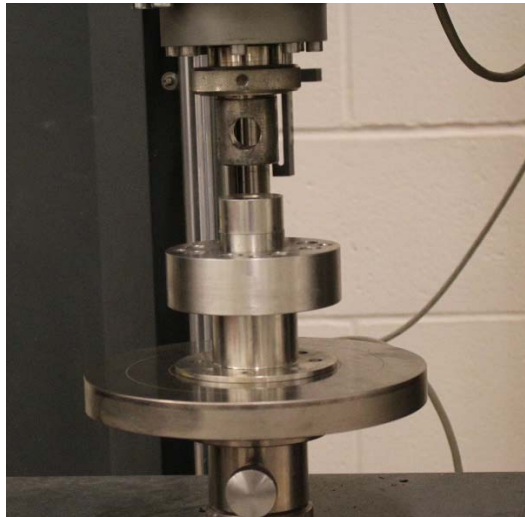


Figure A2-7. Removal of specimen and sleeve using Zwick load frame

4. The soil sample was then removed from the sleeve by separating the two halves of the split-sleeve. The soil sample was then placed back in the apparatus and positioned such that the radial gap was equal around the sample.



Figure A2-8. Soil sample with initial radial gap of 0.95 mm between exterior of soil sample and interior of apparatus.

A2.3 Post-compaction procedures for swell pressure tests

1. The compaction ring was removed, leaving the lower ring containing the soil sample.
2. The loading cap (with o-ring) and load cell were placed on top of the soil sample.



Figure A2-9. Prior to placement of top of cell. Load cell visible.

3. The top of the cell was then placed on top of the load cell and held in position while the bolts connecting the top and bottom of the cell were finger tightened.



Figure A2-10. Complete setup of swell pressure test.

4. The bottom inlet was connected to the hydrating liquid under fluid pressure of 15 kPa.
5. Air was removed from the bottom part of the cell through the purging valve.
6. Commence readings of force from load cell. At this point, approximately 20 minutes have elapsed between post and the start of hydration.
7. Purge the bottom valve once per month using the hydrating liquid under the head of 1.5 m.

A2.4 Post-compaction procedures for permeability and hydration tests

1. The compaction ring was removed, leaving the lower ring containing the soil sample.
2. Place the top cell on the cell containing specimen and tighten the bolts.



Figure A2-11. Complete setup of experiment for permeation test/hydration test

3. Connect the bottom inlet valve with the influent burette and remove air from the bottom part of the cell by opening the purging valve.
4. The time elapsed between post compaction and permeation start time is approximately 15 minutes.
5. Start measuring the inflow and outflow volume for permeation tests. For hydration tests, a standing water head of 1.5 m was maintained to hydrate the specimen from the bottom.
6. Purge the loading cap once per month using the hydrating liquid under head of 1.5 m.

Appendix ' . Additional swell pressure results

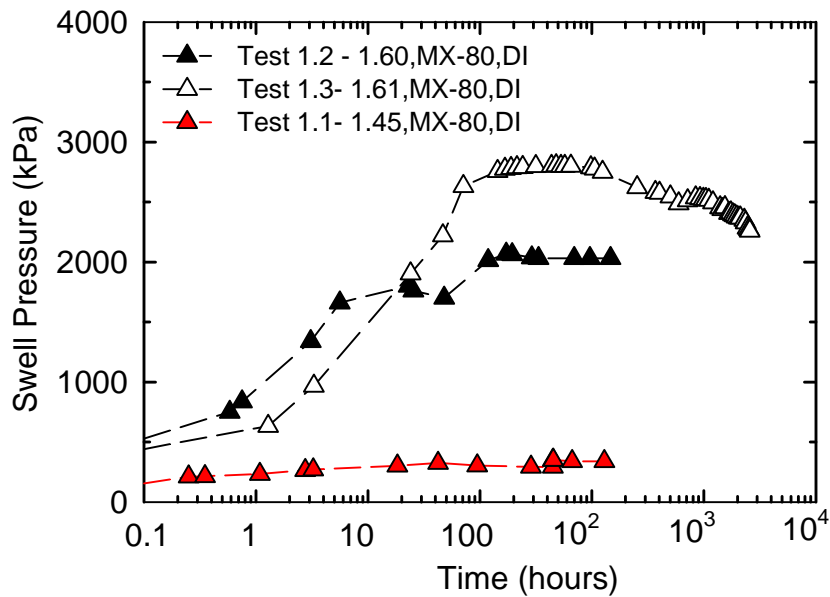
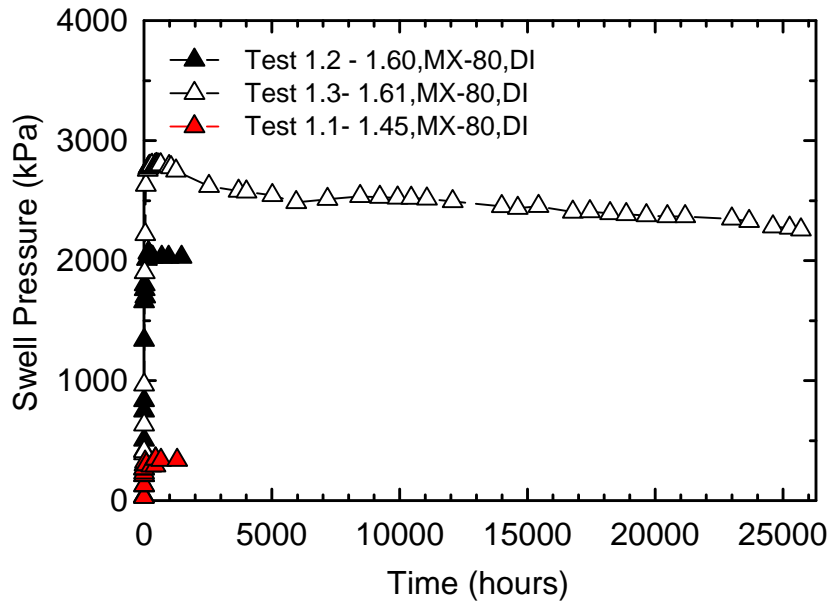


Figure A5-1. Swell pressure of MX-80 compacted at different initial dry density and hydrated with DI water. DI water head = 1.5 m except for Test 1.1 which started at water head of 0.3 m then the head increased to 1.5 m after 450 hrs.

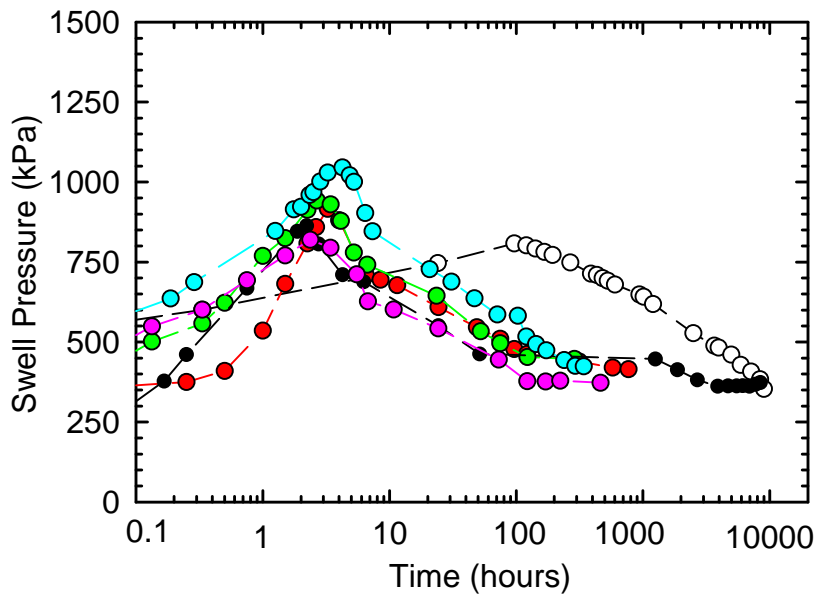
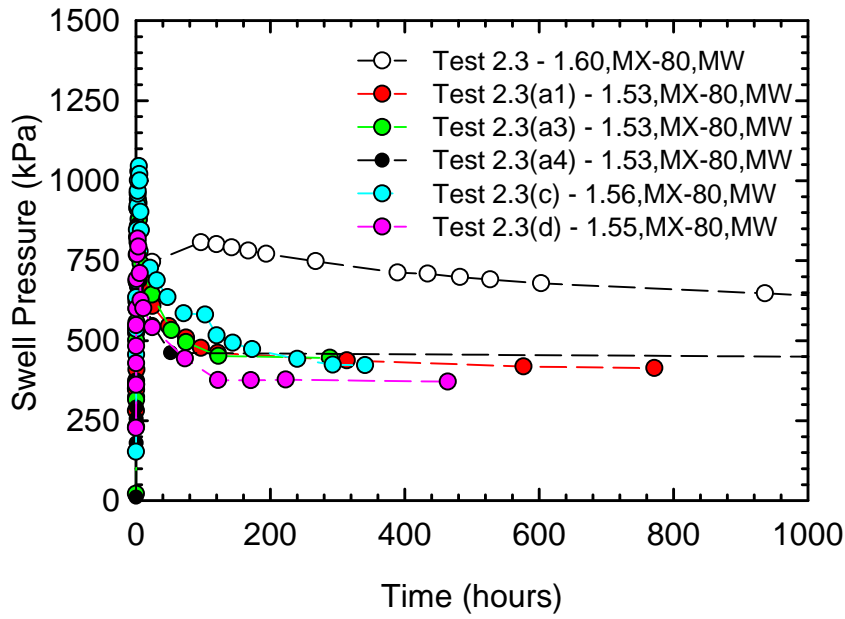


Figure A5-2. Swell pressure of MX-80 samples prepared at initial dry density of 1.53 to 1.60 Mg/m³ with single sided MW hydration. Note: Test 2.3 had a different initial recording frequency.

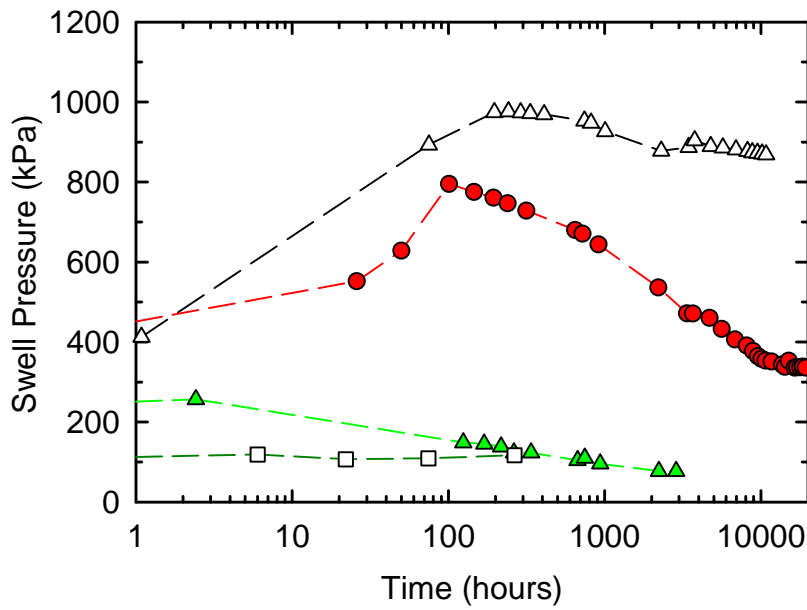
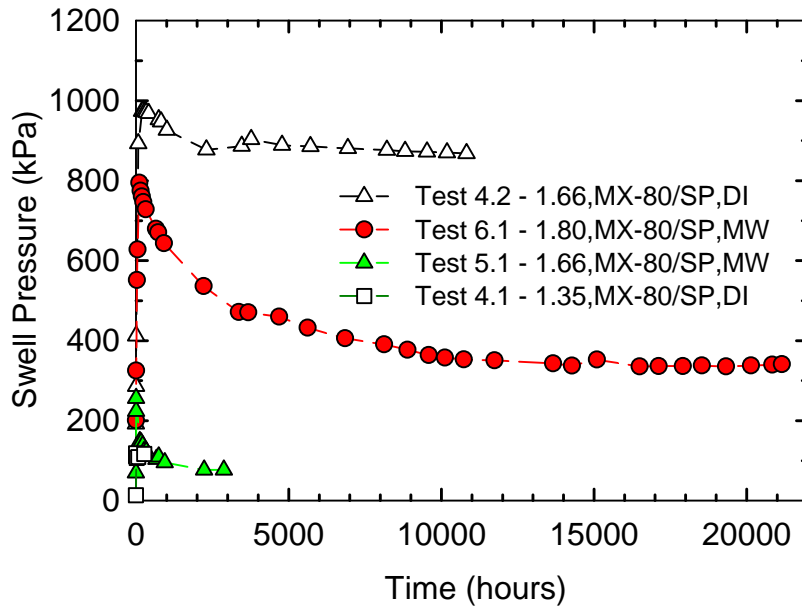


Figure A5-3. Swell pressure of MX-80/SP samples prepared at different initial dry densities when hydrated with either DI or MW.

Appendix (. Additional permeability results

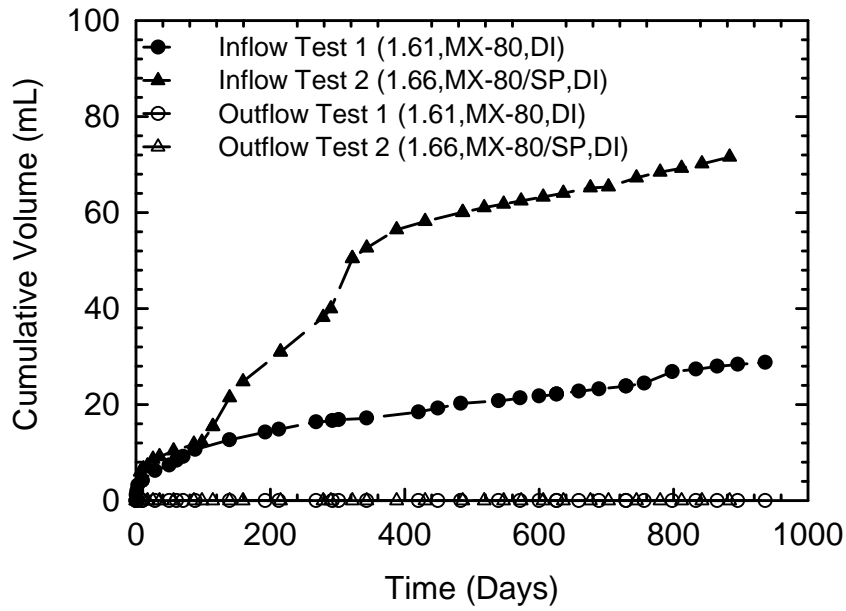


Figure A6-1. Cumulative inflow and outflow volume measured for on-going permeation test for MX-80 and MX-80/SP samples compacted at different dry density permeated with distilled water.

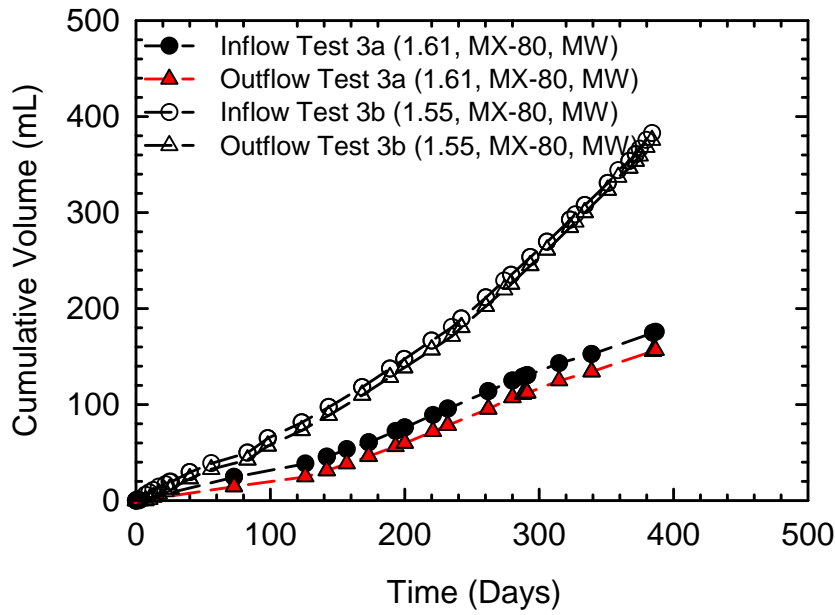


Figure A6-2. Cumulative inflow and outflow volume for MX-80 samples permeated with model water.

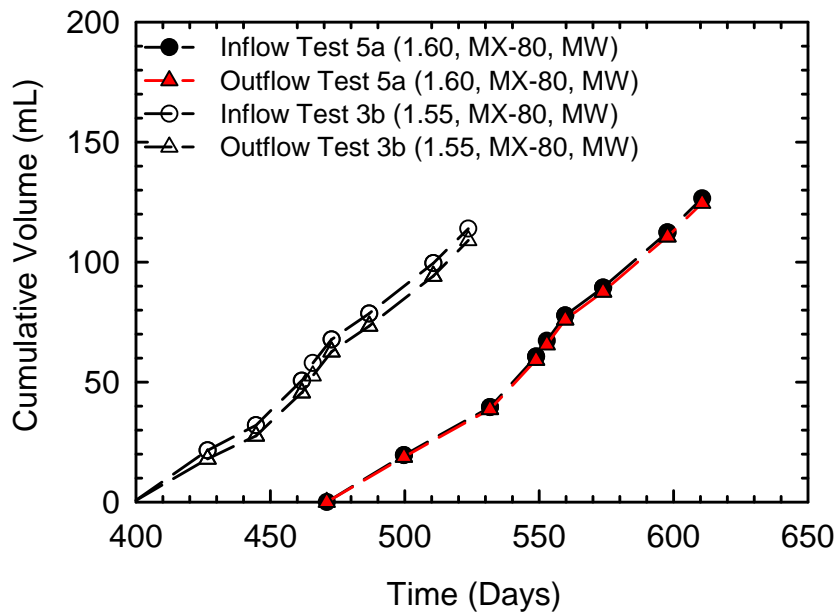


Figure A6-3. Cumulative inflow and outflow volume for MX-80 samples permeated with model water after one year of hydration.

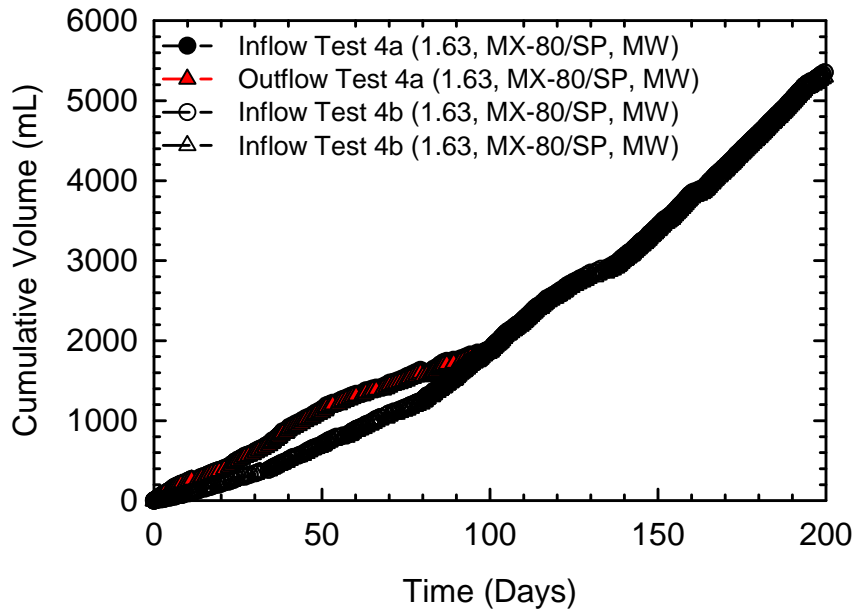


Figure A6-4. Cumulative inflow and outflow volume measured for permeation test of MX-80/SP permeated with model water with pressure head of 1.5m and 0.4 m for test 4a and 4b respectively.

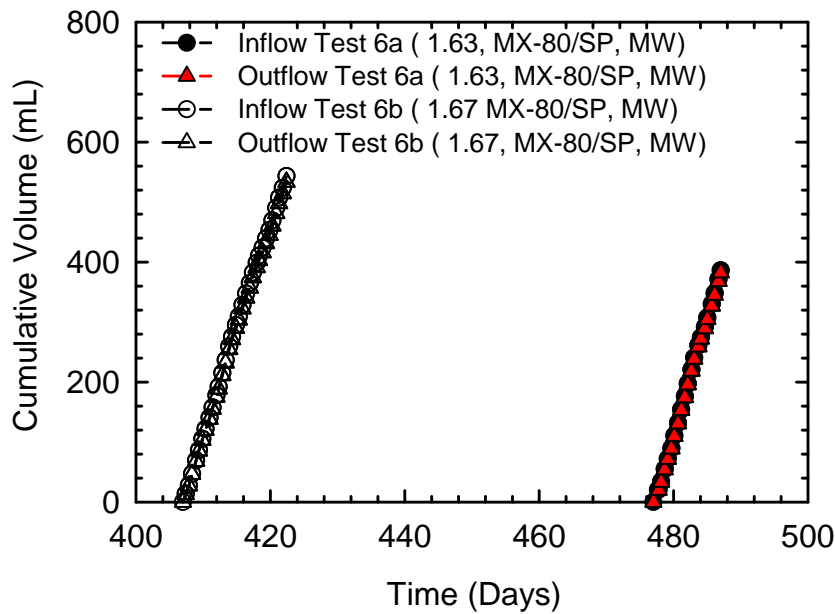


Figure A6-5. Cumulative inflow and outflow volume measured for permeation test of MX-80/SP after one year hydration with model water and pressure head of 0.4 m.

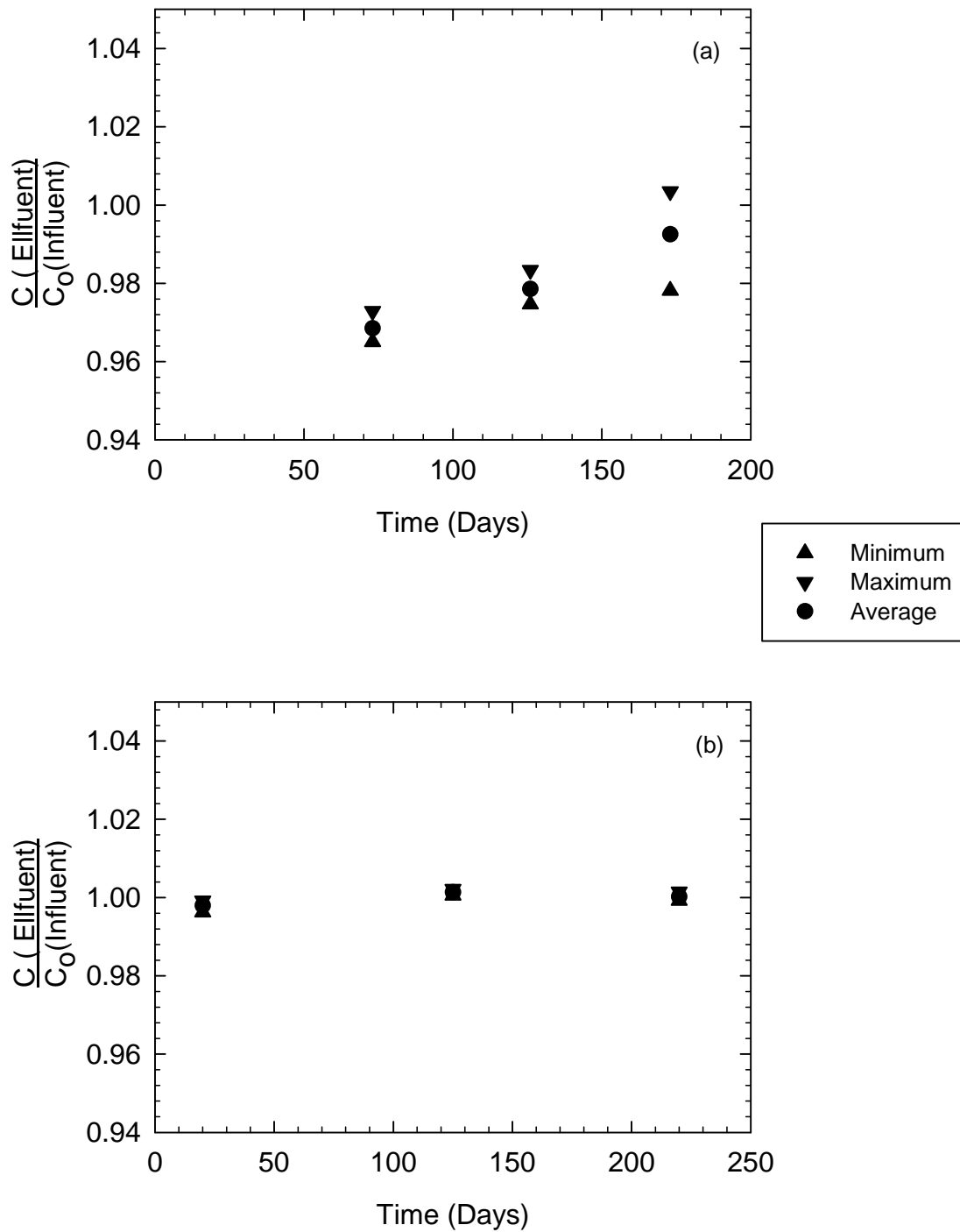


Figure A6-6. Concentration ratio measured for perm test pore fluid by electrical conductivity meter (a)- Test 3a: 1.61,MX-80, MW, (b) Test 3b:1.62,MX-80, MW

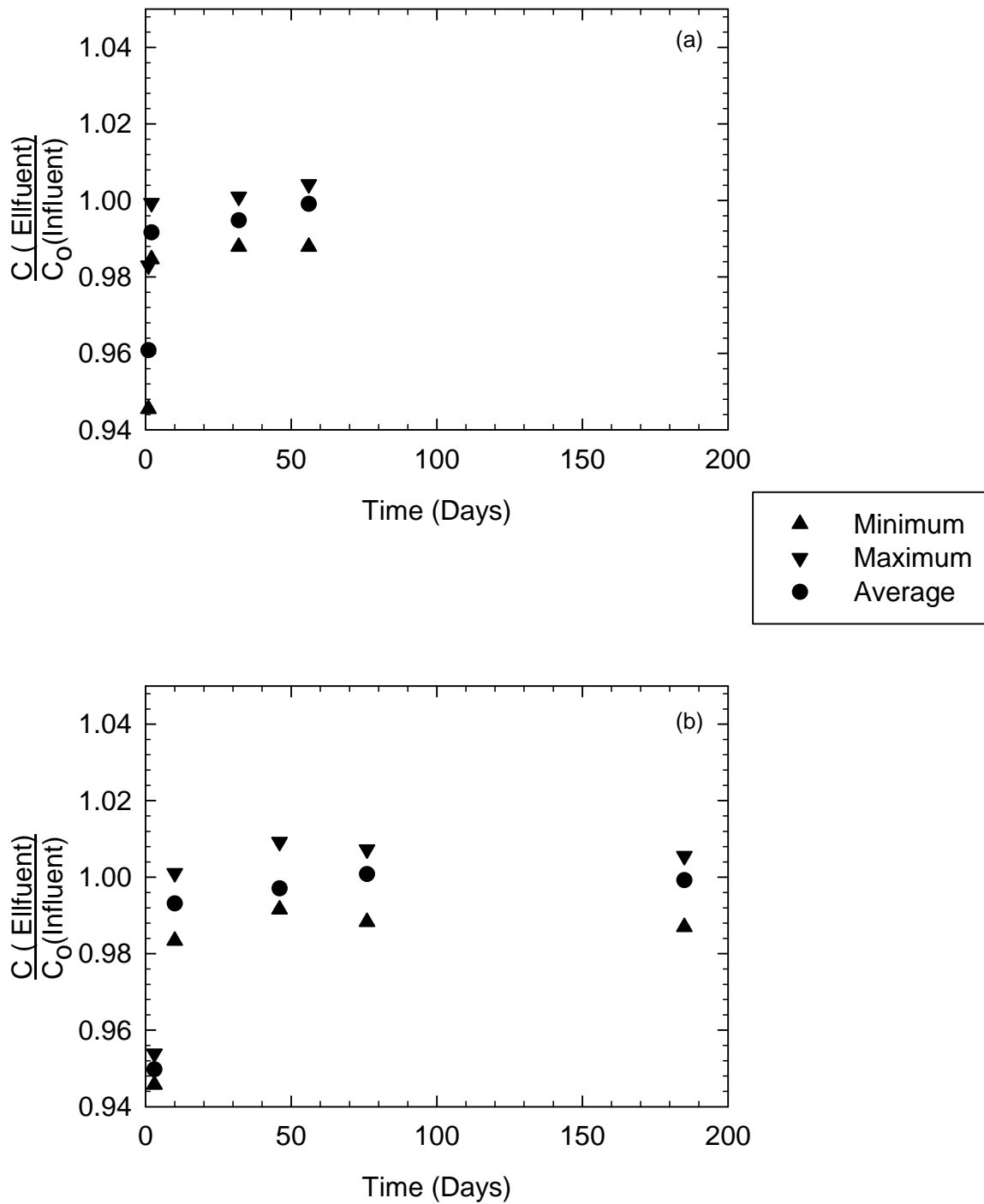


Figure A6-7. Concentration ratio measured for perm test pore fluid by electrical conductivity meter (a)- Test 4a: 1.66, MX-80/SP, MW, (b) Test 4b: 1.67, MX-80/SP, MW

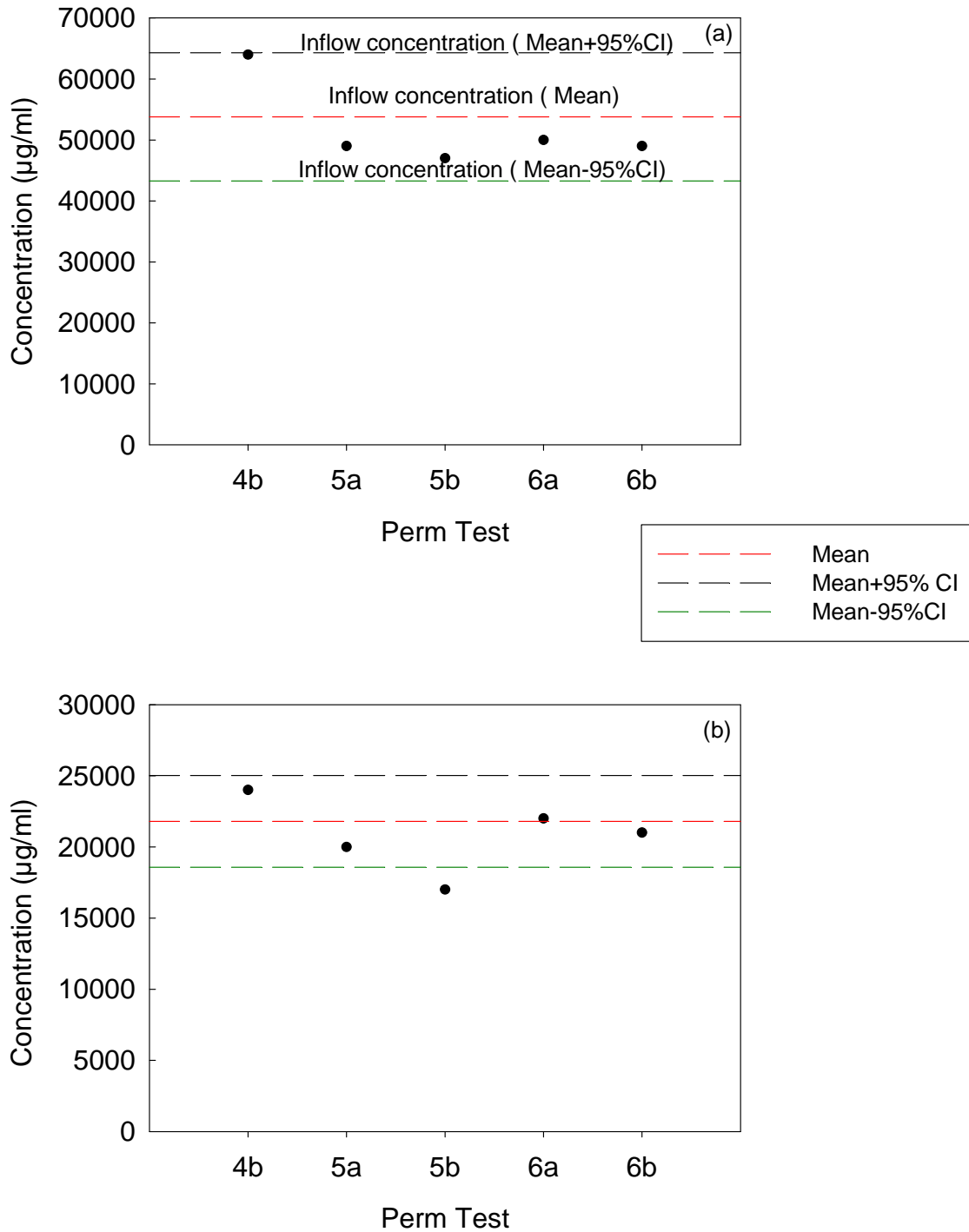


Figure A6-8. Concentration of major cations performed by Inductively Coupled Plasma (ICP) test (a) Na-ion and (b) Ca-ion for influent and effluent fluid.

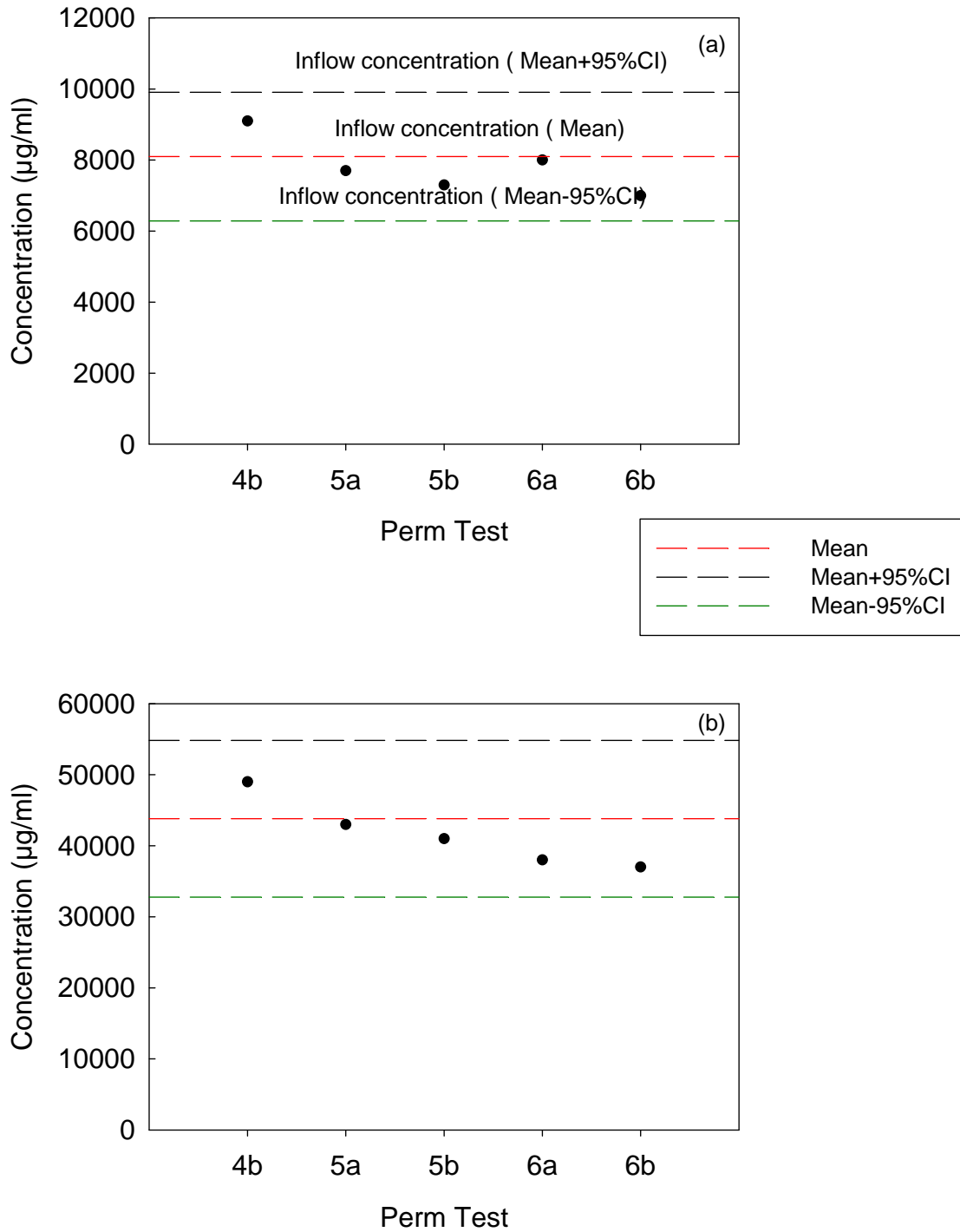


Figure A6-9. Concentration of major cations performed by Inductively Coupled Plasma (ICP) test (a) Mg-ion and (b) K-ion for influent and effluent fluid.

Appendix 5. Measured versus calculated water content with model water

According to ASTM-D2216 (2010), the gravimetric water content of soils are determined by Eq. [A5-1] after measuring the moist mass and the oven-dried (at 110 ± 5 °C) mass of the soil specimen.

$$w = (m_{ws} - m_{ods}) / m_{ods} \times 100 = m_w / m_{soil} \times 100 \quad [A5-1]$$

where, w is gravimetric water content, m_{ws} is mass of wet specimen, m_{ods} is mass of oven dried specimen, m_w is mass of water lost in the oven, and m_{soil} is the mass of soil.

In the case of suction measurement tests with a high salt concentration model water solution, while the salt was dissolved in the pore water during the suction measurement, this mass will remain and contribute to the dry mass of soil after oven drying. Furthermore, when CaCl_2 , MgCl_2 , MgSO_4 are crystalized they might have structural water in the salt crystals after oven drying at 105°C . So that, the structural water of salt crystals, which is a part of pore water when suction measurements are performed, may remain as a part of the dry mass. In this case, following the standard gravimetric water content determination procedure (ASTM-D2216, 2010), the measured water content of a specimen hydrated with high concentrated brine will be:

$$w_m = (m_{ws} - m_{ods}) / m_{ods} \times 100 = m_{w-OD} / (m_{soil} + m_{w-st} + m_{salt}) \times 100 \quad [A5-2]$$

$$m_{w-OD} = m_{w-total} - m_{w-st} \quad [A5-3]$$

where, w_m is the measured gravimetric water content, m_{ws} is mass of wet specimen, m_{ods} is mass of oven dried specimen, m_s is the mass of soil, m_{w-st} is the mass of structural water of salt crystals, m_{w-OD} is the mass of oven-dried water, $m_{w-total}$ is the total mass of water in the wet specimen, and m_{salt} is the mass of salt.

Theoretically, the actual water content of the water specimen may be calculated to be:

$$w_c = m_{w-total} / m_{soil} \quad [A5-4]$$

where, w_c is the calculated gravimetric water content by omitting the mass of crystals (salt and crystal water), $m_{w-total}$ is the total mass of water in the wet specimen, m_{soil} is mass of soil specimen.

Figure A5-1 shows a conceptual model of the phase diagram of an unsaturated soil specimen which was hydrated with DI water as well as hydrated and oven-dried phase diagrams of an unsaturated soil specimen which was hydrated with model water.

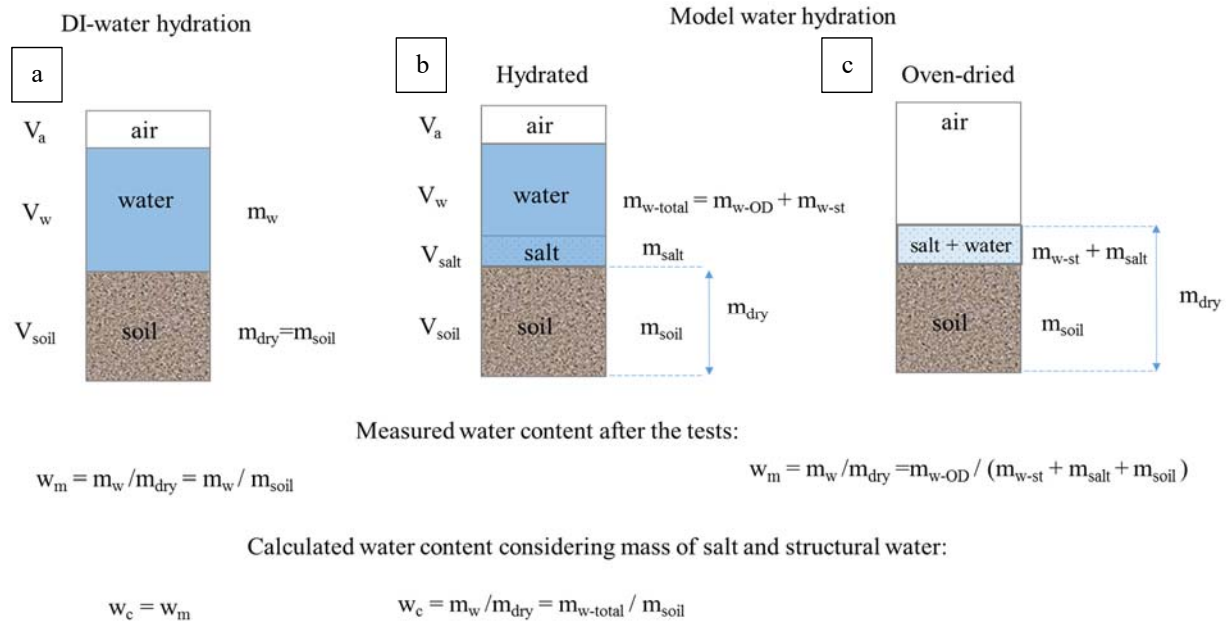


Fig. A5-1. A conceptual model of (a) the phase diagram of an unsaturated soil specimen which was hydrated with DI; (b) hydrated and (c) oven-dried phase diagrams of an unsaturated soil specimen which was hydrated with model water.

The mass of 1 L model water was measured as 1223.1 g. The total dissolved salt (TDS) of the MW2-supernatant was 328.9 g/L. In this case, the mass of DI water (894.2 g) was calculated as 73% of the mass of 1 L of MW2-supernatant. Furthermore, it was assumed that, the salts of CaCl₂, MgCl₂, and MgSO₄ will be in the form of CaCl₂·2H₂O, MgCl₂·6H₂O, and MgSO₄·7H₂O crystals after oven drying. It is worth to underline that, the possible losses of crystal water at 105°C was ignored in the calculations. After these assumptions, the mass of oven dried water was calculated as 68% of the mass of 1 L of model water supernatant after 5% of loss due to crystal water.

The gravimetric water contents w_m and w_c were calculated using the masses of MX80, SP and model water used for each water retention specimen. Calculations were performed considering the air-dried water content of MX80 as 8.7% and according to the assumption that the salts of

CaCl₂, MgCl₂, and MgSO₄ will be in the form of CaCl₂.2H₂O, MgCl₂.6H₂O, and MgSO₄.7H₂O crystals after oven drying. Table A5-1 shows the calculated w_m and w_c values according to Eqs [A5-2], [A5-3] and [A5-4] and compares the calculated w_m with the real measured water contents of the specimens according to ASTM-D2216 (2010). The table also shows the calculations of TDS values in the pore water of each water retention specimen.

Table A5-1. Gravimetric water contents of water retention specimens calculated with equations of conceptual model (Eqs [A5-2], [A5-3] and [A5-4]); the real water contents of each specimen determined according to ASTM-D2216 (2010); calculated TDS values of each specimen

1.61 Mg/m³, MX80

Suction MPa	w_m		w_c	TDS in the specimen
	equ. [2] and [3]	ASTM-D2216 (2010)	equ. [4]	(g/L)
44.1	21.6%	22.1%	24.3%	236
44.57	21.6%	21.8%	24.3%	236
43.48	20.2%	21.8%	22.5%	225
45.09	19.5%	19.9%	21.6%	219
45.08	18.8%	18.9%	20.7%	213
45.88	17.3%	17.6%	18.9%	198
49.15	15.8%	16.0%	17.1%	180
52.74	14.4%	14.9%	15.3%	158
59.19	13.6%	13.8%	14.4%	145
61.36	12.8%	13.0%	13.5%	130
67.85	11.3%	11.5%	11.7%	94
76.48	10.5%	10.7%	10.8%	71
77.04	9.7%	10.2%	9.9%	44
88.79	8.9%	9.3%	9.0%	11
96.95	8.7%	8.6%	8.7%	0

1.50 Mg/m³, MX80/SP

Suction MPa	W _m		W _c	TDS in the specimen (g/L)
	Eq. [2] and [3]	ASTM-D2216 (2010)	Eq. [4]	
42.550	24.2%	23.0%	27.6%	287
45.030	22.8%	22.1%	25.8%	281
44.520	21.4%	21.6%	24.0%	274
44.830	19.2%	19.7%	21.3%	263
41.880	17.0%	18.4%	18.6%	247
44.740	15.9%	15.4%	17.3%	238
44.210	14.8%	15.1%	15.9%	227
45.200	13.6%	13.7%	14.6%	214
44.710	12.4%	13.5%	13.2%	198
50.150	11.3%	11.2%	11.9%	179
56.060	10.1%	10.6%	10.5%	155
57.640	8.2%	9.2%	8.4%	102
68.480	7.2%	8.8%	7.4%	63
77.600	6.7%	7.2%	6.7%	35

1.65 Mg/m³, MX80/SP

Suction MPa	W _m		W _c	TDS in the specimen (g/L)
	Eq. [2] and [3]	ASTM-D2216 (2010)	Eq. [4]	
44.960	20.0%	20.0%	22.2%	267
44.500	18.5%	19.5%	20.4%	258
44.060	17.0%	18.1%	18.6%	247
44.830	16.3%	17.8%	17.7%	241
44.570	16.3%	15.6%	17.7%	241
44.190	15.5%	16.0%	16.8%	234
43.080	14.0%	14.8%	15.0%	218
45.860	13.2%	13.1%	14.1%	209
46.330	12.0%	12.9%	12.8%	192
50.970	10.9%	11.3%	11.4%	171
55.930	10.1%	10.1%	10.5%	155
64.600	9.3%	8.7%	9.6%	135
76.520	8.2%	7.6%	8.4%	102
82.280	7.1%	7.1%	7.2%	58
101.810	6.1%	5.7%	6.1%	0

According to Table A5-1, the w_m results calculated with Eqs [A5-2] & [A5-3] and determined according to ASTM-D2216 (2010) were very comparable, which supports the hypothesis presented in conceptual model (Figure 10). The w_c values calculated with Eq. [A5-4] shows that the mass of crystals (salt and crystal water) lowers the measured water content according to ASTM-D2216 (2010). The impact of the mass of salt crystals on the measured water content values as well as on the TDS values in the specimens increase with the increase in the water contents. Figure A5-2 compares the w_m values (ASTM-D2216, 2010) of the specimens with the w_c calculated with Eq. [A5-4]. According to Figure A2, the w_m and w_c values were very close up to ~13-14%, and for the water contents > 14% w_m values were lower than w_c values. The difference increases with the increase in TDS values in the pore water of each specimen.

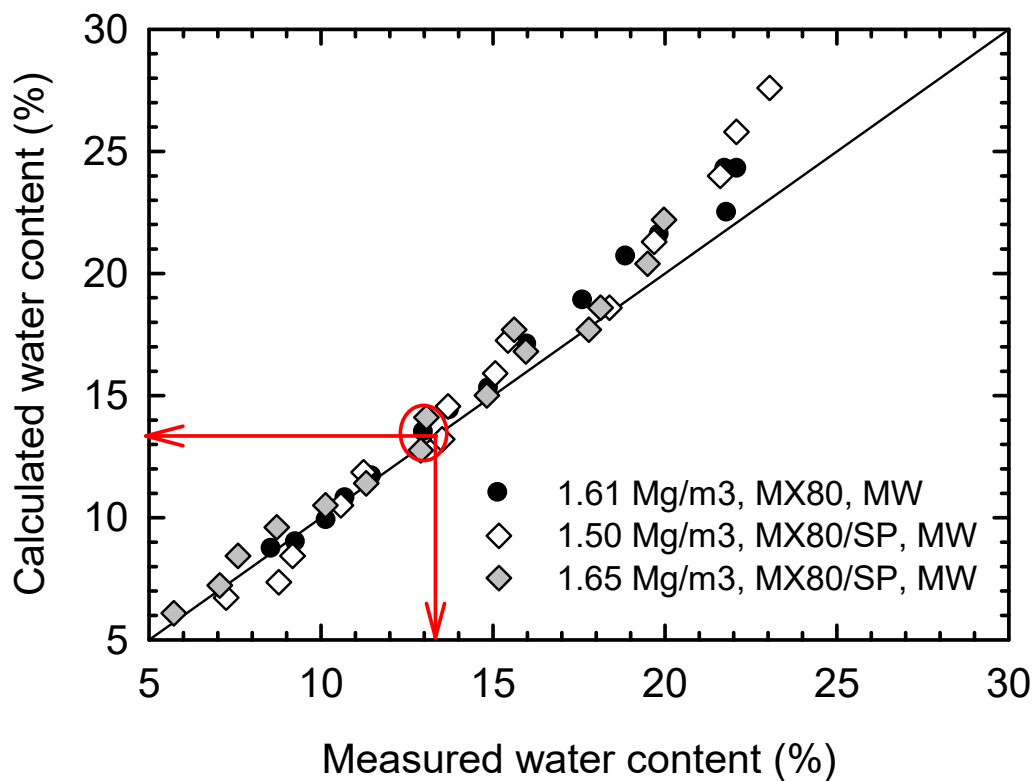


Fig. A5-2. Measured water contents (ASTM-D2216, 2010) versus calculated water contents (Eq. [A5-4])